NEGATIVE MOMENT REGION SHEAR STRENGTH OF LIGHTLY REINFORCED T-BEAMS

by

Carlos Pinto Rodrigues

David Darwin

A Report on Research Sponsored by

THE NATIONAL SCIENCE FOUNDATION

Research Grant

PFR 79-24696

UNIVERSITY OF KANSAS

LAWRENCE, KANSAS

June 1984

50272-101

REPORT DOCUMENTATION PAGE	1. REPORT NO.	2.	3. Recipient's Accession No.

4. Title and Subtitle
Negative Moment Region Shear Strength of Lightly Reinforced T-Beams

5. Report Date
June 1984

6.

7. Author(s)
Carlos P. Rodriques and David Darwin

8. Performing Organization Rept. No.
SM Report No. 13

9. Performing Organization Name and Address
University of Kansas Center for Research, Inc.
2291 Irving Hill Drive, West Campus
Lawrence, KS 66045

10. Project/Task/Work Unit No.

11. Contract(C) or Grant(G) No.
(C)
(G) NSF PFR 79-24696

12. Sponsoring Organization Name and Address
National Science Foundation
Washington, D.C. 20550

13. Type of Report & Period Covered

14.

15. Supplementary Notes

16. Abstract (Limit: 200 words)

The negative moment region shear strength of lightly reinforced concrete T-beams is studied. Nine restrained T-beams with and without web reinforcement were tested. The primary variables were the longitudinal reinforcement ratio (0.47 and 0.70 percent) and the nominal stirrup strength (0 to 84 psi). The test results are analyzed and compared with the shear design provisions of "Building Code Requirements for Reinforced Concrete (ACI 318-83)" and predictions of other investigators.

The tests indicate that both the concrete and stirrup contributions to shear strength are lower in negative moment regions than in positive moment regions. In both positive and negative moment regions, the cracking shear is lower than predicted by ACI 318-83, while the stirrup contribution exceeds that predicted by ACI 318-83. The current ACI shear provisions appear to be conservative for the positive moment regions of beams with longitudinal reinforcement ratios greater than or equal to 0.5 percent. The ACI shear provisions are also conservative for the negative moment regions of beams in which the factored shear is less than or equal to the design shear strength of the concrete. However, the ACI shear provisions appear to be unconservative for the negative moment regions of beams with longitudinal reinforcement ratios less than 0.85 percent and factored shears greater than the design shear strength of the concrete.

17. Document Analysis a. Descriptors
beams (supports); cracking (fracturing); diagonal tension; flexural strength; loads (forces); reinforced concrete; reinforcing steels; research; shear strength; stirrups; structural design; T-beams; web reinforcement.

b. Identifiers/Open-Ended Terms

c. COSATI Field/Group

18. Availability Statement	19. Security Class (This Report)	21. No. of Pages
Release unlimited	Unclassified	
	20. Security Class (This Page) Unclassified	22. Price

ACKNOWLEDGEMENTS

This report is based on a thesis submitted by Carlos Pinto Rodrigues in partial fulfillment of the requirements for the MSCE degree.

This research was supported by the National Science Foundation under NSF Grant PFR 79-24696. The reinforcing steel was donated by ARMCO, INC. and Sheffield Steel Corporation.

TABLE OF CONTENTS

TABLE OF CONTENTS (continued)

LIST OF TABLES

LIST OF FIGURES

LIST OF FIGURES (continued)

LIST OF FIGURES (continued)

Chapter 1

INTRODUCTION

1.1 General

The effect of the longitudinal reinforcement ratio on the shear cracking load of reinforced concrete beams is not accurately incorporated in the design requirements of the ACI Building Code (4). While the shear cracking loads in ACI 318-83 (4) are conservative for beams having longitudinal reinforcement ratios, ρ_w, greater than 1 percent, they are unconservative for beams with ρ_w less than 1 percent (5,6,12,14,20,21,22,23,24,26). In spite of this, the overall shear provisions have appeared to be satisfactory, since the Building Code underestimates the contribution of web reinforcement (5,9,11,20,21) and requires its use in beams with shears greater than one-half of the predicted cracking shear.

Most of what is known about shear strength is based on tests of simply supported beams subjected to positive bending, even though most reinforced concrete beams in practice are continuous. The test results obtained using these simply supported beams have been in turn applied to the design of continuous beams. This tacitly assumes that continuity, and therefore a negative bending moment, has no effect on shear strength. However, there is evidence that this assumption is not correct (11). Of particular concern is the shear strength of continuous reinforced concrete beams with low values of longitudinal reinforcement.

The purpose of this investigation is to experimentally study the shear strength in negative moment regions of reinforced concrete beams with low amounts of both flexure and shear reinforcement, and to compare these test results with the provisions of ACI 318-83 (4) and the predictive equations of other investigators (6,9,11,22,23,26).

1.2 Background

At low loads, shear is carried mainly by concrete. With the formation of diagonal tension cracks, a redistribution of internal forces takes place. The vertical shear is then carried by the concrete, shear reinforcement, aggregate interlock and dowel action. For design purposes, the assumption is usually made that shear is carried by the concrete and shear reinforcement alone (4).

A number of factors influence the shear strength of reinforced concrete beams. These factors include the size and shape of the beam, structural restraints, percentage, arrangement and yield strength of longitudinal and transverse reinforcement, degree of prestressing, load distribution, loading history, and concrete quality.

Investigators (5,6,12,13,14,20,21,22,23,25,26) have studied the effect of the longitudinal reinforcing ratio referenced to the area of the beam web, ρ_w, on the shear strength of reinforced concrete beams and found that shear strength increases with increasing ρ_w ($\rho_w = A_s/b_w d$ in which A_s = cross-sectional area of flexural steel, b_w = web width, and d = effective depth of beam). The longitudinal steel appears to contribute to shear strength both through dowel action and by

limiting the extent of cracking; as ρ_w increases (3), 1) the dowel shear increases, and 2) the flexural cracks become narrower and shorter, increasing both the shear capacity of the compression zone and the interface shear transfer.

The shear cracking load, V_c, calculated according to ACI 318-83 (4) is conservative for ρ_w greater than 1 percent (10,12,22,26), but is unconservative for ρ_w less than 1 percent (5,6,12,14,20,21,22,23,24,26)

Investigators have studied the contribution of web reinforcement to the shear strength of reinforced concrete beams (5,9,11,20,21). The ACI procedure for designing stirrups assumes that after diagonal tension cracking, the additional shear is resisted by stirrups only. Hence the stirrups are designed for the shear in excess of the value that causes shear cracking. The stirrups, apart from carrying the excess shear, also help to increase the shear capacity by restricting the diagonal tension crack widths, thus helping to maintain interface shear transfer, and supporting the longitudinal bars and increasing their dowel capacity. Investigators (5,9,11,20,21) have found that web reinforcement contributes more to shear strength than predicted by ACI 318-83 (4), even for beams with low values of ρ_w (5,20,21).

Most of these studies have been carried out using simply supported beams under positive moment. However, it is not clear that the test results apply to negative moment regions. Continuous beams with low reinforcing ratios that may be undergoing local flexural failure and inelastic moment redistribution are of special concern.

Although these beams are still intact, a shear strength in the negative moment region below that specified in the building codes may lead to a sudden failure. To help study this problem, an experimental study was carried out to determine the contribution of concrete and web reinforcement to the shear strength in negative moment regions of reinforced concrete T-beams with low values of ρ_w.

1.3 Previous Work

Previous work (6,12,13,14,20,21,22,23,26) indicates that reinforced concrete beams have a lower shear strength as the longitudinal reinforcing ratio, ρ_w, decreases. Krefeld and Thurston (14), Kani (12), Rajagopalan and Ferguson (23), and Batchelor and Kwun (6), have shown that the ACI shear design procedures are unconservative for reinforced concrete beams without stirrups and with ρ_w less than 1 percent. MacGregor and Gergely (16) have observed that a beam with ρ_w less than 1 percent and minimum web reinforcement may be understrength in shear, especially in regions away from points of maximum moment, where some of the longitudinal reinforcement has been terminated.

For beams without web reinforcement, the cracking shear is given by the following equation in ACI 318-83 (4).

$$v_c = (1.9\sqrt{f'_c} + 2500\rho_w V_u d/M_u)b_w d \leq 3.5\sqrt{f'_c} b_w d \qquad (1.1a)$$

in which f'_c = compressive strength of concrete, psi.

V_u = factored shear force at section, lb or kips.

M_u = factored bending moment at section, ft-lb or ft-kips.

or more conservatively,

$$V_c = 2\sqrt{f'_c} b_w d \tag{1.2a}$$

In terms of shear stress, v_c, Eq.(1.1a) and (1.2a) can be rewritten as

$$v_c = V_c/b_w d = 1.9\sqrt{f'_c} + 2500\rho_w V_u d/M_u \leq 3.5\sqrt{f'_c} \tag{1.1b}$$

$$v_c = V_c/b_w d = 2\sqrt{f'_c} \tag{1.2b}$$

These equations were originally derived using the test results of 194 rectangular beams without web reinforcement (1). Most of these beams were simply supported.

Rangan (24) suggested that Eq.(1.1) and (1.2) be multiplied by the factor $[(1 + 100\rho_w)/2]$ for ρ_w less than or equal to 1 percent in order to make the expression more conservative.

Zsutty (26), after carrying out a dimensional and regression analysis on shear test data obtained from various investigators, proposed the following equation for the shear cracking stress.

$$v_c = 59(f'_c \rho_w d/a)^{1/3} \tag{1.3}$$

in which a = shear-span from beam reaction to the first concentrated load point, in.

This equation was derived using the test results of 151 beams without web reinforcement, having ρ_w greater than 1.0 percent and a shear-span to depth ratio, a/d, greater than 2.5.

Placas and Regan (22) tested 63 simply supported beams with T, I, and rectangular sections. The a/d ratios were greater than 3.4 and ρ_w varied from 0.3 to 4.1 percent. They proposed the following equation for shear cracking stress.

$$v_c = 8(f'_c 100\rho_w)^{1/3} \tag{1.4}$$

Eq. (1.3) and (1.4) give the same prediction when a/d is about 4.

Rajagopalan and Ferguson (23) tested 10 rectangular beams without web reinforcement and with ρ_w ranging from 0.25 to 1.7 percent. 27 other beams with ρ_w less than 1.2 percent and without web reinforcement tested by other investigators were also considered in their analysis. All beams were simply supported and had a/d ratios greater than 2.75. To account for the effect of ρ_w, Rajagopalan and Ferguson proposed the following equation for the shear cracking stress.

$$v_c = (0.8 + 100\rho_w)\sqrt{f'_c} \leq 2\sqrt{f'_c} \tag{1.5}$$

After some study, ACI-ASCE Committee 426 (3) proposed an equation similar to Eq.(1.5) to account for the effect of low ρ_w.

$$\sqrt{f'_c} \leq v_b = (0.8 + 120\rho_w)\sqrt{f'_c} \leq 2.3\sqrt{f'_c} \qquad (1.6)$$

in which v_b = basic shear stress.

Batchelor and Kwun (6) conducted tests on 10 continuous and 4 simply supported, rectangular reinforced concrete beams without web reinforcement, with values of ρ_w as low as 0.17 percent. They also considered test results of 262 additional beams with rectangular and T-sections without shear reinforcement in their analysis. The 276 beams had a/d ratios greater than 2.0. Based on their analysis, Batchelor and Kwun proposed the following equation for the shear cracking stress.

$$v_c = 1.10\sqrt{f'_c} \leq (0.60 + 110\rho_w)\sqrt{f'_c} \leq 2.25\sqrt{f'_c} \qquad (1.7)$$

Batchelor and Kwun felt that Eq. (1.6), proposed by ACI-ASCE Committee 426 (3), was feasible; however, they pointed out that when compared to the data, Eq. (1.6) has a higher coefficient of variation and is not as conservative as Eq. (1.7).

For their continuous beams, Batchelor and Kwun (6) found the shear cracking stress, v_c, to be greater in the negative moment regions than in the positive moment regions.

Palaskas, Attiogbe and Darwin (5,20,21) tested 15 lightly reinforced concrete T-beams. The beams were simply supported with a/d ratios approximately equal to 4.0 and ρ_w ranging from 0.5 to 1.0 percent. Their test results also show that Eq. (1.1) and (1.2) are unconservative for predicting shear cracking for beams with ρ_w less than

1 percent. The ratio of the test shear cracking stress to the calculated shear cracking stress using Eq. (1.1) was equal to 0.82, with a coefficient of variation of 10 percent.

Haddadin, Hong and Mattock (11) tested 24 simply supported and 3 restrained T-beams with no axial force and with ρ_w in excess of 3.8 percent. Contrary to the observations of Batchelor and Kwun (7) for continuous rectangular sections, Haddadin, Hong and Mattock's (11) test results indicate that the shear cracking load, V_c, for T-beams is lower in the negative moment region than in the positive moment region.

Current ACI procedures for the shear design of beams with web reinforcement have appeared to be conservative (5,9,11,20,21) especially in positive moment regions. The shear force, V_c, resisted by the stirrups is calculated assuming that the inclined crack has a horizontal projection equal to the effective depth, d. The nominal shear stress resisted by the stirrups, v_s, is expressed as

$$v_s = V_s/b_w d = A_v f_{vy}(\mathrm{Sin}\alpha + \mathrm{Cos}\alpha)/b_w s \qquad (1.8a)$$

in which A_v = cross-sectional area of stirrup

f_{vy} = yield stress of stirrups

s = spacing of stirrups

α = angle of inclination of stirrup with horizontal.

For vertical stirrups,

$$v_s = V_s/b_w d = \rho_v f_{vy} \qquad (1.8b)$$

in which ρ_v =shear reinforcement ratio ($=A_v/b_w s$).

Bresler and Scordelis (9), and Haddadin, Hong and Mattock (11) observed that the contribution of web reinforcement to the shear capacity of the reinforced concrete beams is more than 75 percent greater than the strength calculated using Eq. (1.8) for low values of web reinforcement (up to about 200 psi). Beams in both studies had flexural reinforcement ratios, ρ_w, in excess of 1.8 percent.

In their tests of lightly reinforced T-beams, Palaskas, Attiogbe and Darwin (5,20,21) found that web reinforcement contributes about 50 percent more strength than that given by Eq.(1.8). For beams with stirrups and low values of ρ_w, the lower shear strength of the concrete is compensated by the higher effectiveness of the stirrups. A comparison with the work of Bresler and Scordelis (9) and Haddadin, Hong and Mattock (11) indicates that the stirrup contribution in excess of Eq.(1.8) appears to drop off with a reduced value of ρ_w. Palaskas, Attiogbe and Darwin (5,20,21) recommended that the present procedures in ACI 318-83 (3) for determining nominal shear strength be retained for beams with stirrups, until such time as the full strength of the stirrups is utilized in design.

1.4 Object and Scope

The object of this research is to study the negative moment region shear strength of lightly reinforced concrete T-beams. Nine restrained reinforced concrete T-beams with and without web reinforcement were tested. The primary variables in this investigation were longitudinal reinforcement ratio, ρ_w, and nominal stirrup strength, $\rho_v f_{vy}$.

The test results along with those of Palaskas, Attiogbe and Darwin (5,20,21) are analyzed and compared with the ACI Code provisions (4) and with the predictive equations of other investigators (3,6,9,11,22,23,26). Design recommendations are made.

Chapter 2

EXPERIMENTAL INVESTIGATION

2.1 General

In order to determine the shear cracking load and stirrup effectiveness in the negative moment region, nine reinforced concrete T-beams were tested, with flexural reinforcement ratios, ρ_w, of 0.70 and 0.47 percent and shear reinforcement, $v_s = \rho_v f_{vy}$, varying from 0 to 84 psi. All beams had shear-span to depth ratios, a/d, of about 4. The shear cracking load was determined using four criteria: 1) cracking patterns; 2) stirrup strain; 3) concrete strain; and 4) beam depth. Stirrup effectiveness was determined based on the difference between the failure load and the shear cracking load.

The beams failed by diagonal tension cracking. Six beams failed in the negative moment region and three in the positive moment region. The failure shear crack propagated towards the support in the negative moment region and towards the load point in the positive moment region. In the negative moment region, the failure shear crack was an extension of an initial shear crack, while in the positive moment region, the failure shear crack grew after and cut across earlier shear cracks.

2.2 Test Specimens

Nine restrained reinforced T-beams were tested to failure. The details and dimensions of the beams are shown in Fig. 2.1a and 2.1b, and Table 2.1. The flange width and thickness were 24 in. and 4 in., respectively. The web width was 7 1/2 in., and the total beam depth was 18 in. The beams had a 15 ft span, with a 5 ft cantilever on one side. 3 1/2 ft extensions were added on each end of the beams to increase the embedment and prevent slippage of the flexural steel, for a total length of 27 ft. The shear-span to depth ratio for the beams was approximately equal to 4, with the shear-span extending from the point of inflection to the maximum positive or negative moment sections. The moment and shear diagrams for the applied loads are shown in Fig. 2.2.

The beams were divided into two series, based on the longitudinal reinforcement ratio, ρ_w. The beams in series D and E had ρ_w (both top and bottom) equal to 0.70 and 0.47 percent, respectively. The longitudinal reinforcement consisted of non-prestressed, prestressing strands. The bottom and top longitudinal reinforcement consisted of five strands each. The five strands were placed in two layers as shown in Fig. 2.1a and 2.1b.

Strands were used to provide a low longitudinal reinforcement ratio and at the same time to insure flexural safety. The test specimens correspond to reinforced concrete beams with low values of ρ_w that have undergone local flexural failure but which remain intact due to moment redistribution; although the local flexural strength has been exceeded, the strength of these beams may be governed by shear strength.

Web reinforcement consisted of smooth low carbon wires. $\rho_v f_{vy}$ ranged from 0 to 84 psi. The smooth wires were used only in the test region, which extended from the load point within the span to the cantilever support. The test region consisted of one positive and one negative shear-span. To force failure within the test region, heavy web reinforcement was provided elsewhere.

The first beam tested, D-80(1), had smooth wire web reinforcement throughout its length. In order to prevent failure in the cantilever span, external stirrups were used. However, the beam failed in the positive moment region, outside the test region. Hence, a second beam D-80(2), as well as all subseqent beams, was built with the heavy web reinforcement outside the test region.

The flanges were reinforced transversely with #3 deformed bars.

2.3 Materials

2.3.1 Concrete

The concrete for all specimens was made with Type I portland cement and 3/4 in. maximum size coarse aggregate. The concrete was supplied by a ready-mix plant and delivered to the laboratory in transit mix trucks. During construction, air content and slump were measured. Twelve 6 x 12 in. compressive specimens and two 6 x 6 x 22 in. flexural specimens were cast along with each beam. Two 3 x 3 x 12 in. compressive prisms were also cast for beam D-80(2).

Concrete properties are presented in Table 2.2. A typical concrete stress-strain curve obtained from a prism specimen is shown in Fig. 2.3.

2.3.2 Steel

ASTM A 416 Grade 270, 1/2 in. diameter seven-wire low-relaxation strands and Grade 250, 7/16 in. diameter seven wire low-relaxation strands were used as the flexural steel in series D and E, respectively. Typical load-strain curves for these strands are shown in Fig. 2.4a and 2.4b.

The strands were flame-cut to the desired length of 26 ft 10 in., and stored outside of the laboratory, exposed to weather. This helped the strands to rust, which improved the bond and prevented slippage during the tests.

ASTM A 615 Grade 60 #3 deformed billet steel bars were used as transverse flange reinforcement, as well as web reinforcement outside the test region.

The stirrups used in the test region were low carbon smooth wires with diameters of 0.122, 0.179, and 0.245 in. for beams with $\rho_v f_{vy}$ of approximately 20, 40, and 80 psi, respectively. The wire arrived in coils. It was cut to the desired length of 40 in., straightened with a roller, and then preyielded to eliminate residual stresses which were introduced due to coiling and straightening.

Preyielding was required to give the wire a distinct yield point but also resulted in an increase in the yield strength of the wire with time, due to strain aging. To obtain the actual yield and ultimate loads of the wires on the day of the test, two wire specimens were tested after the failure of each beam. Typical stress-strain curves for the wires are shown in Fig. 2.5.

2.4 Specimen Preparation

To form the stirrups, the smooth wire and steel bars were bent into closed loops, using a specially prepared jig, and welded. #3 deformed bars for the flange were then welded to the stirrups. The strands and the stirrups were assembled to form a cage using commercially available ties. The stirrup spacing was 7 in.

Micro Measurements Type EA-06-031DE-120 strain gages were then installed on the stirrups and strands following the procedure used by Palaskas and Darwin (20). The 120 ohm strain gages were temperature compensated, polyimide encapsulated, and had a gage length of 0.031 in.

The strain gages were bonded to the stirrups at mid-height in the test region. The strain gages were also mounted on the strands at the two sections subjected to maximum moment and in the overhangs to detect any slip of the longitudinal reinforcement. The strain gage locations are shown in Fig. 2.6.

The beams were cast in a plywood form. The form was assembled using bolts and form ties; then it was cleaned and oiled. The reinforcing cage was secured in the form using commercially available steel chairs and form ties. The lead wires from the strain gages were carefully carried out of the form through holes provided in the sheathing at the level of the transformed neutral axis of the uncracked cross-section of the beam.

#4 deformed bars were bent into an inverted U-shape and embedded into the beam approximately 12 in. from each end to act as lifting devices. The concrete was placed in two layers, web and flange, with the help of a one cubic yard concrete bucket. Each layer was vibrated using internal vibrators. The same vibrating pattern was used for all beams. Beams were hand screeded along their length using a metal-edged screed. Two passes were made. Upon completion of screeding, the surface was floated using a magnesium bull float. The float travel was transverse to the beam.

After the concrete stopped bleeding (about two hours), the beams and the control specimens were covered with polyethylene sheets and wet cured until a compressive strength of 3000 psi was attained. At this point, the polyethylene sheets were removed and the forms stripped.

The beams were lifted to the test supports using a 3-ton capacity crane and two hydraulic lift tables. High strength gypsum cement (Hydrostone) was used to provide a uniform bearing at the beam supports. A thin coat of white latex paint was applied to one side and the locations of the longitudinal and shear reinforcement were

then marked on the beams. "Stirrup" locations were also marked on beams without web reinforcement for the purpose of comparison.

Paper-backed wire strain gages, Precision Type W240-120 (2.4 in. long), were then attached to the concrete on the top of the beams in the positive shear-span, and on the top bottom of the beams in the negative shear-span following the procedure used by Palaskas and Darwin (20). The locations of these gages are shown in Fig. 2.6.

2.5 Loading System

The test beams were supported by a bolster and a roller at the simple and cantilever supports, respectively. Two or three 1/32 in. teflon sheets were inserted between the bearing surfaces of the bolster to reduce friction.

Loads were applied to the test beam at two points, using a longitudinal loading beam (W21x62) (Fig. 2.7a and 2.7b). This loading arrangement was selected to develop equal maximum positive and negative moments and to provide a constant value of applied shear throughout the length of the beam.

The loads were applied by two hydraulic jacks located below the structural floor through two 1 in. diameter load rods. The load rods were strain gaged and calibrated as load cells. The load rods transferred the load to a short transverse loading beam (W14x43). The transverse loading beam rested on a bolster fixed to the longitudinal loading beam. The loads were transmitted from the longitudinal loading beam to the test beam by a bolster and a roller. The hydraulic jacks were powered by an Amsler hydraulic testing machine.

2.6 Instrumentation

The strain gages on the load rods and test specimen were connected to a Hewlett-Packard data acquisition system and to manually operated Vishay strain indicators.

The deflection at the load points was recorded using LVDTs connected to the data acquisition system and 0.001 in. dial gages (Fig. 2.7a).

Changes in the overall depth of the beam due to diagonal tension cracking were measured using 0.0001 in. dial gages attached to specially designed shear cracking frames (5,20,21). The frames were 28 inches square and were built using 1/2 in. square steel bars. Four frames were fixed in the negative shear-span for beams in series D, while two frames were fixed in positive and negative shear-spans in series E. The frames coincided with particular stirrup locations, as shown in Fig. 2.6. The frames were attached to the upper surface of the beams by bolting them to 1/4 in. steel plates, which were embedded in high strength gypsum cement.

2.7 Test Procedure

The beams were loaded to about one-third of the calculated flexural cracking load and then unloaded to check the equipment. Zero readings for all of the strain and dial gages were recorded. The load was then applied in increments of 2 1/2 kips until flexural cracking occurred in both the positive and negative moment regions. After flexural cracking, the load increments were increased to 5 kips until about two-thirds of the calculated shear cracking load was attained. The load increment was then reduced to 2 kips until failure.

At each increment, strain and dial gage readings were recorded, while the applied load was kept constant. Following the readings, cracks were marked, and the total applied load was inscribed at the end of each crack. Photographs of the beams were taken during and after the tests. All actions and observations during the tests were recorded. The time required for one test was about 1 hr. 15 min.

After failure, the remaining concrete cylinders, flexural specimens, and stirrup tension specimens were tested.

2.8 Test Observations

As the beams were subjected to increased loads, flexural cracks were observed at or near the maximum moment sections. As the load increased, these cracks extended vertically to about the centroid of the uncracked section. The crack patterns for the beams are shown in Fig. 2.8. The cracks curved towards the point of applied load in the positive shear-span and towards the cantilever support in the negative shear-span.

Six beams failed in the negative shear-span and three in the positive shear-span. The failure mode for all beams was diagonal tension. The critical shear crack in the positive moment region appeared after and cut across earlier shear cracks, while in the negative moment region, a initial shear crack grew to become the critical shear crack.

Shear cracking was accompanied by an increase in the stirrup strain and beam depth and a decrease in the concrete compressive strain. The shear cracks were extensions of flexural cracks and grew at inclinations equal to or flatter than 45 degrees.

In the negative shear-span, when the beams approached failure, a secondary crack developed and propagated along the intersection of the web and flange, usually cutting across two stirrups for the beams in series D and one stirrup in series E, as the bottom end of the critical shear crack neared the support. The bottom end of the critical shear crack extended until it reached the support.

The number and width of cracks seemed to depend on the amount of flexural reinforcement. The beams in series D exhibited a greater number of cracks of narrower width than the beams in the more lightly reinforced series E. No shear cracks were observed at or near the point of inflection.

A study of Fig. 2.8 shows that the negative moment regions exhibit fewer, more widely spaced cracks than the positive moment regions. This difference in the crack patterns is in all likelihood due to a lower bond strength for the top-cast flexural reinforcement, which controls flexural cracking in the negative moment regions, than for the bottom-cast flexural reinforcement, which controls flexural cracking in the positive moment regions. This difference in bond strength is commonly referred to as the "top bar" effect.

The deflections were always greater at the end of the cantilever than within the span, except for two beams that failed in the positive moment region, D-80(1) and E-40.

Stirrups intersected by a critical diagonal tension crack yielded prior to failure. The dial gages on the shear cracking frames began to record large readings once the vertical flexural cracks became inclined. For beams with stirrups, failure could be anticipated once the dial gage readings on the frames became unstable. For beams without stirrups, failure could not be anticipated since failure was abrupt.

2.9 Test Results

The nominal shear forces and stresses are given in Table 2.4. Typical curves of total applied load versus stirrup strain, concrete strain, and change in beam depth are shown in Fig. 2.9, 2.10 and 2.11, respectively. Typical curves of total applied load versus deflection are shown in Fig. 2.12. The crack patterns are reproduced in Fig. 2.8.

Chapter 3

ANALYSIS OF TEST RESULTS

3.1 General

In this chapter, the test results described in Chapter 2 are analyzed, and the shear cracking loads and stirrup effectiveness are determined. The contributions of dowel action and aggregate interlock to shear strength are estimated, and recommendations for design are made.

3.2 Determination of Shear Cracking Load

The shear cracking load is the load at which significant changes occur in the load carrying mechanism, resulting in the redistribution of stresses within a beam. The four techniques used to determine the load at which this change occurs are outlined in the following sections. A summary of the cracking loads and stresses is presented in Tables 3.1 and 3.2, respectively.

3.2.1 Crack Patterns

A number of different definitions have been used for the shear cracking load based on crack patterns. Haddadin, Hong and Mattock (11) defined the shear cracking load as the load at which a diagonal tension crack makes an angle of 45 degrees with the transformed neutral axis of the beam. According to Batchelor and Kwun (6), a shear crack is defined as an inclined crack extending from

longitudinal tension reinforcement into the compression zone and making a 45 degree angle with the flexural reinforcement. The shear cracking load is defined as the load at which a shear crack extends into the "compression zone".

Palaskas, Attiogbe and Darwin (5,20,21) defined the cracking load as the load at which a shear crack makes an angle of 45 degrees or flatter at or above the transformed neutral axis of the beam. In this study, the shear cracking load is defined in a similar manner as the load at which a diagonal tension crack first makes an angle of 45 degrees or flatter, at or above the neutral axis of the beam in the positive moment region, or at or below the neutral axis of the beam in the negative moment region. The crack patterns for the test specimens are shown in Fig. 2.8.

3.2.2 Stirrup Strain

The shear cracking load was obtained from load-stirrup strain curves, as illustrated in Fig. 2.9. Prior to cracking, the strain gages on the stirrups record little strain. Measureable strain readings are obtained when either a flexural crack or a shear crack crosses a stirrup. Flexural cracks lead to a gradual increase in stirrup strain, while diagonal cracks cause a sharp increase in stirrup strain. Therefore, the load at which a sharp increase in stirrup strain occurs is taken to be the shear cracking load.

In one beam, D-80(2), the stirrup strain data did not indicate any shear cracking, although cracking clearly occurred (Fig. 2.12). This may have been due to the stirrup being tightly bonded to the concrete in the vicinity of the strain gage. The stirrup strain gave a higher shear cracking stress than the crack patterns in 5 out of 7 cases in the positive moment region (Table 3.2). The stirrup strain gave the same or a higher value than obtained from the crack patterns in the negative moment region for all beams.

Palaskas, Attiogbe and Darwin (5,20,21) obtained the shear cracking load from load-strain data by extending back the portion of the curve that showed a marked increase in strain until it intersected the load axis. The point of intersection was defined as the shear cracking load. The extension of the curve was done in order to eliminate the effect of flexural cracking on the shear cracking load. In the current study, the results obtained by this method did not appear to be realistic because in some cases no shear cracks had yet crossed the stirrup at loads defined in this way. This was observed very clearly in the negative moment regions which contained very few inclined cracks.

3.2.3 Concrete Gages

A typical load-concrete strain curve is shown in Fig. 2.10. As the load increases, the concrete compressive strain increases until shear cracking occurs. When the load carrying mechanisms change due to shear cracking, the compressive strain in the cracked zone may decrease and even become tensile. The shear cracking load is taken as the load at which a reduction in compressive strain occurs.

3.2.4 Depth Increase

A typical load-depth increase curve is shown in Fig. 2.11. The dial gages on the depth frames began recording strain when the flexural cracks started inclining towards the load point in the positive moment region, and towards the support in the negative moment region. The initial portion of the curve shows a gradual increase in depth due to the presence of flexural cracks. A sharp increase in depth marks the shear cracking load.

Palaskas, Attiogbe and Darwin (5,20,21) defined the shear cracking load in a like manner to that obtained from stirrup strain as the intercept with the load axis of the portion of the curve that showed a sharp increase in depth. However, also like the stirrup strain results, it was observed in this study that the value of V_c obtained using this method represented loads prior to the formation of a shear crack.

3.3 Discussion of Test Results

Although this study was limited in scope, when combined with the earlier work of Palaskas, Attiogbe and Darwin (5,20,21) and other investigators (9,11), a number of clear trends appear. The results should, however, be viewed with the following limitations in mind: (1) nine beams were tested in this study, only six of which failed in the negative moment region. Therefore, the behavior of beams proportioned differently from the test beams may not be predicted with accuracy; and (2) the bond between the reinforcement and the concrete in this study is likely to be less than is obtained in actual structures

due to the use of strands for flexural reinforcement and smooth wires for shear reinforcement. Hence, the test results should be conservative.

3.3.1 Techniques for Determining the Shear Cracking Load

As shown in Table 3.2, the shear cracking stresses obtained from the crack patterns in the negative moment region are in most cases equal to or lower than those obtained using the other three methods. The greater relative sensitivity of the crack patterns is likely due to the following reasons: 1) stirrup strain will show a significant increase only after the shear crack intercepts the stirrup; 2) concrete strain is a function of crack length and since the rate of crack growth is a function of both ρ_w and $\rho_v f_{vy}$, it is possible that the concrete gages will detect a change in strain only well after the diagonal crack has formed; and 3) depth increase depends upon the width of the crack, which is also a function of both ρ_w and $\rho_v f_{vy}$.

The calculated shear cracking stresses obtained using equations proposed by other investigators (3,4,6,23,26) are given in Table 3.3. The shear cracking stresses obtained using each of the four techniques are compared to the calculated cracking stresses obtained using Eq. (1.2) through (1.7) in Tables 3.4 through 3.7. The equations given by Zsutty (26) and Placas and Regan (22) are the same for $a/d = 4$, the shear-span to depth ratio used in this study.

3.3.2 Sign of Bending Moment

The shear cracking stress obtained from crack patterns is higher in the positive moment region than in the negative moment region in 5 out of 8 cases (Table 3.2). On an average, the shear cracking stress is 18 percent greater in the positive moment region. This should be expected since a T-beam is effectively a rectangular beam in a negative moment region. In the positive moment region, however, the compressive stresses are distributed over the area of the flange, which affects the total stress distribution. It is also likely that the lower bond strength of the top-cast reinforcement contributes to the lower relative shear strength of the negative moment region. The greater shear cracking stresses obtained in positive bending compare favorably with the findings of Placas and Regan (22), who found that beams with 12 in. or wider flanges had about 20 percent more shear strength than rectangular beams.

3.3.2.1 Shear Cracking - Positive Moment Region

Tables 3.4 through 3.7 show the shear cracking stresses obtained using all four techniques. The shear cracking stresses obtained from the crack patterns are on the average 13 percent lower than the values predicted by Eq. (1.2) given in ACI 318-83(4), with a coefficient of variation of 17 percent (Table 3.4). The shear cracking stresses from crack patterns are higher than Eq. (1.3), (1.5), (1.6), and (1.7), predicted by Zsutty (26), Rajagopalan and Ferguson (23), ACI-ASCE Committee 426 (3), and Batchelor and Kwun (6) by 4, 25,15 and 38 percent, respectively. These trends are also shown

in Fig. 3.1 through 3.4 where $v_c/\sqrt{f'_c}$ is plotted versus the longitudinal reinforcement ratio, ρ_w, and in Fig. 3.5 through 3.8 where $v_c/\sqrt[3]{f'_c}$ is plotted versus ρ_w.

3.3.2.2 Shear Cracking - Negative Moment Region

The shear cracking stresses obtained from the crack patterns are on the average 29 percent lower than Eq. (1.2), with a coefficient of variation of 21 percent. The shear cracking stresses from crack patterns are lower than the Eq. (1.3) and (1.6) predicted by Zsutty (26) and ACI-ASCE Committee 426 (3) by 16 and 8 percent, respectively, and higher than the Eq. (1.5) and (1.7), predicted by Rajagopalan and Ferguson (23) and Batchelor and Kwun (6), by 1 and 12 percent, respectively. These trends are also shown in Fig. 3.9 through 3.12 where $v_c/\sqrt{f'_c}$ is plotted versus ρ_w and in Fig. 3.13 through 3.16 where $v_c/\sqrt[3]{f'_c}$ is plotted versus ρ_w.

3.3.3 Stirrup Effectiveness

The increase in the shear stress, v_n-v_c, above the shear cracking stress, v_c, can be considered to be a measure of the effectiveness of the web reinforcement. v_n-v_c includes the shear carried by stirrups as well as the shear carried by dowel action and aggregate interlock. The increment of stress, v_n-v_c, is given in Table 3.8.

3.3.3.1 Stirrup Effectiveness - Positive Moment Region

The test results for beams with stirrups that failed in the positive moment region, D-80(1) and E-40, are combined with the results of the simply supported T-beams tested by Palaskas, Attiogbe and Darwin (5,20,21). The increment of shear stress ($v_n - v_c$) based on the crack patterns is plotted against $\rho_v f_{vy}$, the nominal shear stress resisted by stirrups in Fig. 3.17. Using a regression analysis, the following relationship is obtained.

$$v_n - v_c = 1.59\rho_v f_{vy} + 1.4 \qquad (3.1)$$

Correlation Coefficient, r = 0.96

Hence, the contribution of the web reinforcement in the positive moment region is on the average $1.59\rho_v f_{vy}$, which is 59 percent more effective than predicted by ACI 318-83 (4) in Eq. (1.8).

A high contribution by web reinforcement to shear capacity was also observed by Bresler and Scordelis (9) who found the contribution to be $1.8\rho_v f_{vy}$. Haddadin, Hong and Mattock (11) found the contribution to be at least $1.75\rho_v f_{vy}$ for values of $\rho_v f_{vy}$ less than 200 psi. These values may be higher than obtained in the current study because the values of ρ_w were in excess of 1.8 percent, as compared to the values of ρ_w used in this study of less than 1 percent. In addition, these investigators used reinforcing bars instead of strands and smooth wires. The higher bond strength obtained using reinforcing bars could also have contributed to these higher values of stirrup effectiveness.

3.3.3.2 Stirrup Effectiveness - Negative Moment Region

The increment of stress, $(v_n - v_c)$, based on the crack patterns is plotted against the nominal shear stress resisted by the stirrups, $\rho_v f_{vy}$, in the negative moment region in Fig. 3.18. Using a regression analysis, the following equation is obtained.

$$v_n - v_c = 1.19\rho_v f_{vy} + 4.70 \qquad (3.2)$$

Correlation Coefficient, r = 0.96

This equation indicates that the web reinforcement is about 1.2 times as effective as predicted by the modified truss analogy, which assumes that the horizontal crack projection is equal to the effective depth, d. This also demonstrates that the stirrup contribution to shear strength is considerably less in the negative moment region than in the positive moment region. Although Haddadin, Hong and Mattock (11) had very limited data in the negative moment region, they also obtained a lower "stirrup contribution" to shear strength in the negative moment region than in the positive moment region, at least for low values of $\rho_v f_{vy}$.

The following equations are obtained for the other techniques used in this study.

$$v_n - v_c = 1.05\rho_v f_{vy} + 5.40 \quad \text{(stirrup strain)} \qquad (3.3)$$

Correlation Coefficient, r = 0.88

$$v_n - v_c = 0.77\rho_v f_{vy} + 22 \qquad \text{(depth increase)} \qquad (3.4)$$

Correlation Coefficient, r = 0.93

$$v_n - v_c = 0.78\rho_v f_{vy} + 14 \qquad \text{(concrete strain)} \qquad (3.5)$$

Correlation Coefficient, r = 0.75

These equations may not accurately represent stirrup effectiveness, due to the weaknesses of these techniques in predicting the shear cracking load, as discussed in Section 3.3.1.

3.3.4 Horizontal Crack Projection

An explanation for the observed differences in stirrup effectiveness can be obtained by studying the horizontal crack projections. The horizontal projections of the critical shear cracks are greater in positive moment regions than in negative moment regions: The horizontal projections averaged 1.7d, ranging from 1.4d to 2.2d, in the positive moment regions, and averaged 1.0d, ranging from 0.9d to 1.1d, in the negative moment regions, with the exception of one beam, E-20, that had a horizontal crack projection of 1.4d in the negative moment region (Fig. 2.8).

The beams tested by Haddadin, Hong and Mattock (11) also show that the horizontal projections of the critical shear cracks are greater in positive moment regions (1.9d to 2.3d) than in negative moment regions (1.5d to 1.7d). These projections are on the average longer in both regions than obtained for the more lightly reinforced beams in this study, strongly suggesting that the horizontal crack projection will increase with increased ρ_w.

The positive moment region has a longer horizontal crack projection due to a shallower crack angle and because the crack propagates along the intersection of web and flange before it enters the flange. Due to the longer horizontal crack projection in the positive moment region, the number of stirrups intercepted by the critical crack is larger. Hence, the shear taken by the stirrups is larger, explaining why the stirrup effectiveness, $v_n - v_c$, is greater in the positive moment region, as observed in Section 3.3.3.

The increase in shear stress above the shear cracking stress, $v_n - v_c$, measures not only the shear carried by the stirrups, but also the shear carried by dowel action and aggregate interlock. The shear stress carried by the stirrups alone can be expressed as

$$v_{si} = nA_v f_{vy}/b_w d \tag{3.6}$$

in which n = number of stirrups intercepted by the critical shear crack.

Hence, by knowing the number of stirrups intercepted by the critical crack, the shear carried by stirrups, v_{si}, can be calculated (Table 3.9). v_{si} is plotted versus the nominal shear stress resisted by the stirrups, $\rho_v f_{vy}$, in Fig. 3.19 and 3.20. Using regression analysis, the following equations are obtained:

$$v_{si} = 1.41\rho_v f_{vy} - 4.2 \quad \text{(positive moment region)} \tag{3.7}$$

Correlation Coefficient, r = 0.99

$$v_{si} = 1.00\rho_v f_{vy} - 6.0 \quad \text{(negative moment region)} \qquad (3.8)$$

Correlation Coefficient, r = 0.96

These relationships mean that about 40 percent more stirrups were intercepted by the critical shear crack than predicted by Eq. (1.8) (ACI 318-83 (4) in the positive moment regions, while about the same number of stirrups were intercepted as predicted by Eq. (1.8) in the negative moment regions. Eq. (3.8) and (1.8) agree because the horizontal crack projections in the negative moment regions happened to be approximately equal to beam effective depth, d, which agrees with the assumption made in deriving Eq. (1.8).

3.3.5 Dowel Action and Aggregate Interlock

The shear stress carried by dowel action and aggregate interlock can be estimated by substracting the shear stress carried by stirrups only, v_{si}, from v_n-v_c. $(v_n-v_c)-v_{si}$ is compared to $\rho_v f_{vy}$ in Table 3.9 and Fig. 3.21 and 3.22. The test data of Palaskas, Attiogbe and Darwin (5,20,21) are also included. Using a regression analysis, the following equation is obtained in the positive moment region.

$$(v_n - v_c) - v_{si} = 0.22\rho_v f_{vy} + 5.2 \qquad (3.9)$$

Correlation Coefficient, r = 0.50

A similar equation was derived for the negative moment region.

$$(v_n - v_c) - v_{si} = 0.22\rho_v f_{vy} + 10.7 \qquad (3.10)$$

Correlation Coefficient, r = 0.76

Hence, the contribution of dowel action and aggregate interlock to shear strength appears to be about $0.2\rho_v f_{vy}$ for this series of tests. The wide scatter in the data is clearly indicated by the low correlation coefficients. The similiarities between Eq. (3.9) and (3.10) suggest that the presence of a flange in the positive moment region does not effect dowel action and aggregate interlock.

3.3.6 Nominal Shear Stress

The measured nominal shear stresses are compared with the nominal shear stresses predicted by ACI 318-83 (4) in Table 3.10 and Fig. 3.23 for the current series as well as the 15 beams tested by Palaskas et al. (5,20,21). The ACI provisions are conservative for 12 out of the 18 beams, both with and without stirrups, that failed in the positive moment region. The average value of $v_n(\text{test})/v_n(\text{ACI})$ in the positive moment region for all beams is 1.04, with extreme values of 1.26 and 0.88, and a coefficient of variation of 9.3 percent. The ACI provisions are conservative for 11 out of the 14 beams with stirrups that failed in the positive moment region. The average value of $v_n(\text{test})/v_n(\text{ACI})$ in the positive moment region for beams with stirrups is 1.07, with extreme values of 1.26 and 0.99, and a coefficient of variation of 8.4 percent.

The ACI provisions are unconservative for 4 out of the 6 beams, both with and without stirrups, that failed in the negative moment region. The average value of $v_n(test)/v_n(ACI)$ in the negative moment region for all beams is 0.91, with extreme values of 1.02 and 0.76, and a coefficient of variation of 8.4 percent. The ACI provisions are unconservative for 4 out of 5 beams with stirrups that failed in the negative moment region. The average value of $v_n(test)/v_n(ACI)$ for the beams with stirrups is 0.89, with extreme values of 1.0 and 0.76, and a coefficient of variation of 11.0 percent.

On an average, the nominal shear strength was 14.3 percent greater in positive moment regions than in negative moment regions. For beams with stirrups, the nominal shear strength was 20.2 percent greater in positive moment regions than in negative moment regions.

In the positive moment regions, the relatively small drop in the concrete contribution, combined with the higher stirrup contribution to shear strength makes the ACI Code provisions (4) conservative for nominal shear strength. Therefore, in positive moment regions, even though the concrete contribution to shear strength is less than predicted by Eq. (1.1) and (1.2), the lower concrete strength is more than compensated by the higher effectiveness of the stirrups.

However, in negative moment regions, although the stirrup contribution is $1.2\rho_v f_{vy}$, it is not high enough to adequately compensate for the low concrete contribution to shear strength. Therefore for low values of ρ_w, the nominal shear stress remains less than predicted by the ACI Code (4).

3.3.7 Other Observations

To help visualize the combined effects of ρ_w and moment on the shear capacity of reinforced concrete beams, v_n is plotted versus $\rho_v f_{vy}$ in Fig. 3.24 (low ρ_w) and 3.25 (low and high ρ_w). In these figures, v_n is "normalized" in order to help eliminate the effect of concrete strength.

$$v_n(\text{norm}) = v_c(\text{test})\sqrt{(4000/f'_c)} + [v_n(\text{test}) - v_c(\text{test})] \quad (3.11)$$

The lines for values of $\rho_v f_{vy} \leq 200$ psi represent a least squares fit of the data.

Fig. 3.24 and 3.25 illustrate that 1) v_n and stirrup effectiveness (slope of the lines) increase with ρ_w; 2) v_n and stirrup effectiveness are higher in positive moment regions than in negative moment regions; 3) web steel is incrementally less effective as more is added (11); and 4) v_n increases with decreasing a/d ratio (11). Bresler and Scordelis (9) obtained higher values of v_n than Haddadin et al. (11), even though they had lower values of ρ_w and used rectangular rather than T-beams. This apparent deviation from the trend may be due to the greater relative beam widths used by Bresler and Scordelis (b/d = 0.67) compared to that used by Haddadin et al. (b_w/d = 0.50). Increased web widths have been shown to increase v_n, all other things being equal (15).

Fig. 3.26 compares $v_n(\text{norm})/\sqrt{4000}$ versus $\rho_v f_{vy}$. Fig. 3.26 is used to evaluate the ability of the ACI minimum shear reinforcement ($\rho_v f_{vy}$ = 50 psi) to insure that the shear capacity equals the code value of $v_c = 2\sqrt{f'_c}$ for beams with a factored shear, V_u, greater than

one half of the design shear strength of the concrete alone, $\phi V_c/2$ (4).

Fig. 3.26 illustrates, as discussed previously, that beams without web reinforcement have a lower shear capacity than that predicted by ACI 318-83 (4). But in all cases, the use of the minimum web reinforcement allows the beams to develop a nominal shear stress in excess of $2\sqrt{f'_c}$. These limited results indicate that as little as 26 psi of web steel will be sufficient to raise the nominal shear capacity, v_c, to $2\sqrt{f'_c}$ for beams with $\rho_w \geq 0.5$ percent, even in the negative moment region. Hence, if minimum web reinforcement $\rho_v f_{vy}$ = 50 psi is used, the nominal shear capacity of the concrete, v_c, predicted by ACI 318-83 (4) is safe. Since all tests have indicated that v_c is in excess of $\sqrt{f'_c}$, the effective usable shear strength for beams without stirrups, the current provisions remain satisfactory.

A somewhat more conservative approach to the question of minimum steel effectiveness leads to a similar conclusion. As an alternate to Fig. 3.26 in which best fit lines are used, Fig. 3.27 shows the same data, but with the nominal shear strength represented by the sum of the average experimental shear cracking stress plus the apparent stirrup effectiveness, from Eq. (3.1) and (3.2). The lines plotted in Fig. 3.27 are based on the following.

$$v_n(\text{avg and norm})/\sqrt{4000} = [v_c(\text{avg and norm}) + A\rho_v f_{vy}]/\sqrt{4000} \tag{3.12}$$

in which $v_c(\text{avg and norm}) = \frac{1}{n}\Sigma v_c\sqrt{(4000/f'_c)}$

$A = 1.59$ for positive moment regions

A = 1.19 for negative moment regions

The curves in Fig. 3.27 attain a value of 2.0 ($v_c = 2\sqrt{f'_c}$) at a higher value of $\rho_v f_{vy}$ than in Fig. 3.26. However, these results also show that in all cases, the minimum web reinforcement (4), $\rho_v f_{vy}$ = 50 psi, will provide a total shear capacity of at least $2\sqrt{f'_c}$, indicating that the current minimum is satisfactory, as long as the strength of the stirrups is not used to compute shear capacity.

To help establish over which ranges of ρ_w and $\rho_v f_{vy}$ the current provisions are conservative when including stirrup strength, the "normalized" data obtained with Eq. (3.11) and the curves obtained using Eq. (3.12) are compared to the ACI predicted capacity ($2\sqrt{f'_c}$ + $\rho_v f_{vy}$, f'_c = 4000 psi) in Fig. 3.28. This figure shows that for positive moment regions, v_n is greater than v_n (ACI) if $\rho_v f_{vy}$ is greater than 50 psi. The shear capacity is actually about 2 percent less than predicted (4) for beams with ρ_w = 0.5 percent and $\rho_v f_{vy}$ = 50 psi in the positive moment region ($\rho_v f_{vy}$ must be greater than 55 psi to reach v_n(ACI) for ρ_w = 0.5 percent).

However, for negative moment regions, v_n is lower than v_n(ACI), even for values of $\rho_v f_{vy}$ much greater than 50 psi. The shear capacity is 6 and 22 percent less than predicted by ACI 318-83 (4) for beams with $\rho_v f_{vy}$ = 50 psi and ρ_w = 0.7 and 0.5 percent, respectively. v_n only equals v_n(ACI) for values of $\rho_v f_{vy}$ greater than 100 psi for ρ_w = 0.7 percent and values of $\rho_v f_{vy}$ greater than 245 psi for ρ_w = 0.5 percent.

Hence, while the minimum shear reinforcement provisions remain satisfactory, the safety of beams in negative moment regions with low amounts of flexural and web reinforcing is in doubt. If the strength of the stirrups is used to compute shear capacity, the minimum web reinforcement ($\rho_v f_{vy}$ = 50 psi) will clearly not provide the predicted (4) shear capacity in these beams.

3.4 Recommendations

3.4.1 Beams with stirrups

The test results illustrate that the positive moment region has a higher shear capacity, v_n, than the negative moment region. The ACI provisions (4) appear to be generally conservative in positive moment regions. However, they appear to be unconservative in negative moment regions for beams with stirrups and ρ_w less than about 0.7 percent.

One possibility to improve the safety of beams with low values of ρ_w would be to adopt one of the recommended expressions for v_c presented in Chapter 1 (3,6,23,26). The use of this expressions is illustrated in Fig. 3.29 for the normalized curves developed using Eq. (3.12). As seen in Fig. 3.29, Eq. (1.4) and (1.6) developed by Rajagopalan and Ferguson (23) and Batchelor and Kwun (6), respectively, become overconservative when the actual strength of the stirrups is utilized. Eq. (1.5) by ACI-ASCE Committee 426 (3) is slightly unconservative for low values of $\rho_v f_{vy}$ and ρ_w = 0.5 percent. Eq. (1.3) by Zsutty (26) is unconservative for values of $\rho_v f_{vy}$ up to 109 psi for beams with ρ_w = 0.5 percent.

To help provide a more consistent margin of safety, the following expression is proposed for v_c in negative moment regions for beams with $\rho_w \leq 0.85$ percent, when the strength of the stirrups is utilized.

$$v_c = (0.3 + 200\rho_w)\sqrt{f'_c} \tag{3.13}$$

Eq. (3.13) should be applied using the value of ρ_w at the point of the maximum negative moment. Only fully developed steel should be included. Although in typical construction ρ_w will be reduced as steel is terminated, the a/d ratio will also decrease, resulting in an increase in the shear capacity of the concrete. Application of Eq. (3.13) in this manner will improve safety with a minimum impact on the required design effort.

Eq. (3.13) is applied to normalized data obtained with Eq. (3.11) and the curves obtained using Eq. (3.12) in Fig. 3.30. Eq. (3.13) has two principal advantages over the other expressions of its type (3,6,23,26): (1) Since it is applicable to beams with values of $\rho_w \leq 0.85$ percent rather than 1 percent, it must be applied to fewer beams in practice. (2) It provides a more uniform margin of safety than the other expressions and does not result in either a large excess capacity or understrength.

Eq. (3.13) is offered with one caveat: It was derived using the test results of only 6 beams and more tests would be desirable to determine the complete suitability of this expression, especially for ranges of variables not checked in this study. Certainly, a better appreciation of the magnitude of this problem is necessary.

3.4.2 Beams without stirrups

The test results again illustrate that the shear cracking stress of beams with ρ_w < 1.0 percent is much lower than that predicted by the ACI Code (4). But they also illustrate that the ACI provisions for minimum web reinforcement ($\rho_v f_{vy}$ = 50 psi for beams with v_u greater than $\phi\sqrt{f'_c}$) raise the nominal shear capacity to a value greater than $2\sqrt{f'_c}$. The test results also indicate that v_c is always greater than $\sqrt{f'_c}$. Hence, the current ACI provisions (4) may be safely retained for the shear design of beams without web reinforcement.

Chapter 4

SUMMARY AND CONCLUSIONS

4.1 Summary

The object of this research is to study the negative moment region shear strength of lightly reinforced concrete T-beams. Nine restrained reinforced concrete T-beams with and without web reinforcement were tested. The primary variables in this investigation were the longitudinal reinforcement ratio, ρ_w (= 0.70 and 0.47 percent), and the nominal stirrup strength, $\rho_v f_{vy}$ (= 0 to 84 psi). Shear cracking loads were determined using four techniques based on crack patterns, stirrup strain, depth increase and concrete strain. Stirrup effectiveness, taken as the increase in load from shear cracking to ultimate, is obtained using linear regression analysis. The contribution of dowel action and aggregate interlock on shear capacity is also estimated.

The test results, along with those of Palaskas, Attiogbe and Darwin (5,20,21), are analyzed and compared with the shear provisions of the ACI Code (4) and with the predictive equations of other investigators (3,6,9,11,22,23,26). Design recommendations are made for beams with and without stirrups.

4.2 Conclusions

The following conclusions can be made based on the test results and analyses described in this report.

1. For the same longitudinal reinforcement ratio, ρ_w, diagonal cracks form at a higher shear stress in positive moment regions than in negative moment regions for reinforced concrete T-beams. This lower relative negative moment region shear strength appears to be the result of a smaller effective concrete section due to cracking of the flanges, and a lower bond strength for the negative longitudinal reinforcement, due to the "top bar" effect.

2. Negative moment regions exhibit fewer cracks at a wider spacing than positive moment regions, also due to the top bar effect.

3. For lower values of shear reinforcement (up to about 200 psi), the stirrup contribution to shear strength is greater in positive moment regions than in negative moment regions. This appears to be largely due to a greater horizontal crack projection, which results in a greater number of stirrups intersected by the critical shear crack.

4. In both moment regions, the stirrup contribution exceeds that predicted by ACI 318-83 (4).

5. The contribution of dowel action and aggregate interlock to shear capacity, which is treated as a portion of the stirrup contribution, is about $0.2\rho_v f_{vy}$ in both moment regions for the lightly reinforced T-beams tested.

6. The current ACI shear provisions (4) appear to be conservative for the positive moment regions of beams with $\rho_w \geq 0.5$ percent.

7. The ACI shear provisions (4) are also conservative for the negative moment regions of beams in which $V_u \leq \phi V_c$.

8. However, the ACI shear provisions (4) appear to be unconservative for the negative moment regions of beams with $\rho_w \leq 0.85$ percent and $V_u \geq \phi V_c$.

9. To improve the safety of the shear provisions of ACI 318-83 (4), the following expression is proposed for V_c in negative moment regions.

$$V_c = (0.3 + 200\rho_w)\sqrt{f'_c}b_w d \qquad (4.1)$$

The expression applies to beams with reinforcement ratios ≤ 0.85 percent, for which stirrups are required to satisfy strength requirements, rather minimum reinforcement requirements. The value of ρ_w is based on the fully developed reinforcement at the point of the maximum negative moment.

4.3 Future Work

The current test series represents the only existing data for the negative moment region shear strength of beams with low values of both flexural and shear reinforcement. The number of variables considered were therefore limited, and additional information is needed.

True continuous beams with different shear-span to depth ratios, concrete strengths, reinforcement ratios, mild reinforcement and perhaps deformed bars for stirrups need to be tested. Reinforced concrete joist construction deserves special consideration. In addition, the effect of reinforcement ratio on the shear capacity of beams in which longitudinal reinforcement is terminated remains completely open to study.

REFERENCES

1. ACI-ASCE Commitee 326, "Shear and Diagonal Tension," ACI Journal, Proceedings V. 59, No. 1, Jan. 1962, pp. 1-30; No. 2, Feb. 1962, pp. 277-333; No. 3, Mar. 1962, pp. 353-395.

2. ACI-ASCE Commitee 426, "The Shear Strength of Reinforced Concrete Members," Journal of the Structural Division, ASCE, V. 99, No. ST6, June 1973, pp. 1091-1176.

3. ACI-ASCE Commitee 426, "Suggested Revisions to Shear Provisions of ACI Code 318-71," ACI Journal, Proceedings V. 74, No. 9, Sep. 1977, pp. 458-469.

4. American Concrete Institute, Building Code Requirements for Reinforced Concrete (ACI 318-83), Detroit, Michigan, 1983, 111 pp.

5. Attiogbe, E. K., Palaskas, M. N. and Darwin, D., "Shear Cracking and Stirrup Effectiveness of Lightly Reinforced Concrete Beams," Structural Engineering and Engineering Materials SM Report No. 1, University of Kansas Center for Research, Inc., Lawrence, July 1980, 138 pp.

6. Batchelor, B. deV. and Kwun, M. K., "Shear in RC Beams without Web Reinforcement," Journal of the Structural Division, ASCE, V. 107, No. ST5, May 1981, pp. 907-921.

7. Bower, J. E. and Viest, I. M., "Shear Strength of Reinforced Concrete Beams without Web reinforcement," ACI Journal, Proceedings V. 57, No. 1, July 1960, pp. 73-98.

8. Bresler, B. and MacGregor, J. G., "Review of Concrete Beams Failing in Shear," ACI Journal, Proceedings V. 93, No. 1, Feb. 1967, pp. 343-372.

9. Bresler, B. and Scordelis, A. C., "Shear Strength of Reinforced Concrete Beams," ACI Journal, Proceedings V. 60, No. 1, Jan. 1963, pp. 51-72.

10. Diaz de Cossio, Roger and Leora, Santiago, Discussion of "Basic Facts Concerning Shear Failure," by G. N. J. Kani, ACI Journal, Proceedings V. 63, No. 12, Dec. 1966, pp. 1511-1514.

11. Haddadin, M. J., Hong, S. and Mattock, A. H., "Stirrup Effectiveness in Reinforced Concrete Beams with Axial Force," Journal of the Structural Division, ASCE, V. 97, No. ST9, Sep. 1971, pp. 2277-2297.

12. Kani, G. N. J., "Basic Facts Concerning Shear Failure," ACI Journal, Proceedings V. 63, No. 6, June 1966, pp. 675-692.

13. Kani, M. W., Huggins, M. W. and Wittkop, R. R., ed., Kani on Shear in Reinforced Concrete, University of Toronto Press, Toronto, Ontario, Canada, 1979, 225 pp.

14. Krefeld, W. J. and Thurston, C. W., "Studies of the Shear and Diagonal Tension Strength of Simply Supported Reinforced Concrete Beams," Report, Columbia University, New York, N. Y., June 1962, 96 pp.

15. Leornard, F., and Walther, R., "The Stuttgart Shear Tests, 1961," Translations No. 111, Cement and Concrete Association, London, England, 1964.

16. MacGregor, J. G. and Gergely, P., "Suggested Revisions to ACI Building Code Clauses Dealing with Shear in Beams," ACI Journal, Proceedings V. 74, No. 10, Oct. 1977, pp. 493-500.

17. Mathey, R. G. and Watstein, G. "Strains in Beams Having Diagonal Cracks," ACI Journal, Proceedings V. 55, No. 6, Dec., 1958, pp. 717-728.

18. Mathey, R. G. and Watstein, G., "Shear Strength of Beams without Web Reinforcement Containing Deformed Bars of Different Yield Strengths," ACI Journal, Proceedings V. 60, No. 2, Feb. 1963, pp. 183-208.

19. Moody, K. G., Viest, I. M., Elstner, R. C. and Hognestad, E., "Shear Strength of Reinforced Concrete Beams," ACI Journal, Proceedings V. 51, No. 1, Dec. 1954, pp. 317-332; No. 2, Feb. 1955, pp. 525-539; No. 3, Mar. 1955, pp. 697-732.

20. Palaskas, M. N. and Darwin, D., "Shear Strength of Lightly Reinforced Concrete Beams," Structural Engineering and Engineering Materials SM Report No. 3, University of Kansas Center for Research, Inc., Lawrence, Sep. 1980, 198 pp.

21. Palaskas, M. N., Attiogbe, E. K. and Darwin, D., "Shear Strength of Lightly Reinforced T-Beams," ACI Journal, Proceedings V. 78, No. 6, Nov.-Dec. 1981, pp. 447-455.

22. Placas, A. and Regan, P. E., "Shear Failures of Reinforced Concrete Beams," ACI Journal, Proceedings V. 68, Oct. 1971, pp. 763-773.

23. Rajagopalan, K. S. and Ferguson, P. M., "Exploratory Shear Tests Emphasizing Percentage of Longitudinal Steel," ACI Journal, Proceedings V. 65, No. 8, Aug. 1968, pp. 634-638.

24. Rangan, B. V., " A Comparison of Code Requirements for Shear Strength of Reinforced Concrete Beams," Shear in Reinforced Concrete, SP - 42 Vol 1, American Concrete Institute, Detroit, Mich., 1974, pp. 285-293.

25. Rodriguez, J. J., Bianchini, A. C., Viest, I. M. and Kesler, C. E., "Shear Strength of Two Span Continuous Reinforced Concrete Beams," ACI Journal, Proceedings V. 55. No. 19, Apr. 1959, pp. 1089-1130.

26. Zsutty, T. C., "Beam Shear Strength Prediction by Analysis of Existing Data," ACI Journal, Proceedings V. 65, No. 11, Nov. 1968, pp. 943-951.

Table 2.1 Beam Properties

All beams - b_w = 24 in., a = 60 in., s = 7 in.
Group D - A_s: 5 - 1/2 in. dia strands = 0.805 in.
Group E - A_s: 5 - 7/16 in. dia strands = 0.540 in.

Positive Moment Region

Beam	d in.	a/d	b_w in.	$\rho_w = A_s/b_w d$	$\rho_v = A_v/b_w s$	$\rho_v f_{yy}$ psi
D-80(1)	15.44	3.89	7.58	0.0069	0.0018	82.9
D-80(2)	14.87	4.03	7.52	0.0072	0.0018	73.0
D-40	14.69	4.08	7.50	0.0073	0.0010	37.0
D-20	14.58	4.11	7.52	0.0073	0.0004	21.6
D-0	14.69	4.08	7.53	0.0073	0.0000	0.0
E-80	14.78	4.06	7.51	0.0049	0.0018	73.5
E-40	15.14	3.96	7.50	0.0048	0.0010	36.8
E-20	15.46	3.88	7.51	0.0047	0.0004	22.2
E-0	15.43	3.89	7.50	0.0047	0.0000	0.0

Negative Moment Region

Beam	d in.	a/d	b_w in.	$\rho_w = A_s/b_w d$	$\rho_v = A_s/b_w s$	$\rho_v f_{yy}$ psi
D-80(1)	15.18	3.95	7.52	0.0071	0.0018	83.6
D-80(2)	15.32	3.92	7.51	0.0070	0.0018	73.1
D-40	15.39	3.90	7.52	0.0070	0.0010	37.0
D-20	15.21	3.94	7.51	0.0071	0.0004	21.6
D-0	15.76	3.81	7.51	0.0068	0.0000	0.0
E-80	15.04	3.99	7.51	0.0048	0.0018	73.5
E-40	15.54	3.86	7.50	0.0046	0.0010	36.8
E-20	15.42	3.89	7.50	0.0047	0.0005	22.2
E-0	16.13	3.72	7.52	0.0045	0.0000	0.0

Table 2.2 Concrete Properties

Beam	Mix proportions by weight[1]	Slump in.	Air %	Concrete temp. F	f'_c[2] psi	f_t[3] psi	Age at test(days)
D-80(1)	1:0.44:2.58:2.52	2 3/4	3.0	65	5380	445	21
D-80(2)	1:0.50:2.89:2.89	2	9.5	63	4070	435	28
D-40	1:0.50:2.89:2.89	2 1/2	5.0	80	4200	500	6
D-20	1:0.50:2.89:2.89	1	3.0	52	4290	515	4
D-0	1:0.50:2.89:2.89	2 3/4	4.5	55	4540	440	14
E-80	1:0.50:2.89:2.89	2 1/4	3.0	73	4010	500	6
E-40	1:0.50:2.89:2.89	2 1/4	3.5	74	4550	560	5
E-20	1:0.50:2.89:2.89	3 1/4	6.0	70	4210	475	9
E-0	1:0.50:2.89:2.89	1 1/2	3.5	62	4500	565	6

1 Cement:water:fine aggregate:coarse aggregate
2 Compressive strength obtained using 6 x 12 in. cast in cylinders molds.
3 Modulus of rupture from 6 x 6 x 22 in. flexural specimens, third point loading on an 18 in. span.

Table 2.3 Reinforcement Properties

Beam	Bar size diam. in.	Bar area in.	Yield force kips	Yield stress ksi	Ult. stress ksi
Group D	1/2" strand	0.161	39.30	244.0	268.9
Group E	7/16" strand	0.108	25.90	239.8	267.6
	#3 reinf. bar	0.110	7.80	70.9	
D-80(1)	0.245" stirrup	0.047	2.20	46.7	
D-80(2)	0.245" stirrup	0.047	1.92	40.7	
D-40	0.179" stirrup	0.025	0.97	38.5	
D-20	0.122" stirrup	0.012	0.57	48.8	
E-80	0.245" stirrup	0.047	1.93	41.0	
E-40	0.179" stirrup	0.025	0.97	38.5	
E-20	0.122" stirrup	0.012	0.58	49.9	

Table 2.4 Measured Nominal Shear Strength

	Beam	V_n(test) (kips)	v_n(test) (psi)
*	D-80(1)	27.8	238
	D-80(2)	23.0	200
	D-40	16.8	146
	D-20	17.0	148
	D-0	16.3	138
	E-80	17.2	152
*	E-40	20.6	181
	E-20	14.7	127
*	E-0	15.4	133

* Positive moment region failure

Table 3.1 Shear Cracking Loads, V_c (kips)

Positive Moment Region

Beam	Crack patterns	Stirrup strain	Depth increase	Concrete strain
D-80(1)	12.1	15.0	xx	15.4
D-80(2)	15.5	15.0	xx	15.0
D-40	11.0	12.3	xx	12.1
D-20	15.9	9.4	xx	13.1
D-0	12.6	--	xx	10.6
E-80	12.6	14.3	14.3	14.3
E-40	14.4	15.2	14.4	12.4
E-20	10.3	10.8	--	10.3
E-0	13.2	--	11.2	11.9

Negative Moment Region

Beam	Crack patterns	Stirrup strain	Depth increase	Concrete strain
D-80(1)	11.5	16.1	15.4	12.8
D-80(2)	11.5	--	15.2	16.2
D-40	12.2	13.5	10.5	13.5
D-20	12.7	12.7	12.0	14.1
D-0	14.1	--	14.1	14.1
E-80	7.2	7.2	7.2	7.2
E-40	--	--	--	--
E-20	10.7	10.7	10.7	8.7
E-0	8.2	--	8.2	11.5

-- Method did not produce any results
xx Frames were not used

Table 3.2 Shear Cracking Stresses, v_c (psi)

Positive Moment Region

Beam	Crack patterns	Stirrup strain	Depth increase	Concrete strain
D-80(1)	103.4	125.6	xx	131.6
D-80(2)	138.7	134.2	xx	134.2
D-40	99.8	111.6	xx	111.6
D-20	144.9	85.4	xx	119.4
D-0	113.9	--	xx	95.8
E-80	113.9	129.3	129.3	109.3
E-40	126.7	133.9	126.7	109.2
E-20	88.7	93.0	--	88.7
E-0	114.1	--	96.8	102.8

Negative Moment Region

Beam	Crack patterns	Stirrup strain	Depth increase	Concrete strain
D-80(1)	100.8	141.1	135.0	112.2
D-80(2)	100.0	--	132.1	140.8
D-40	110.9	122.7	95.3	122.7
D-20	111.2	111.2	105.1	123.5
D-0	119.3	--	119.3	119.3
E-80	63.7	63.7	63.7	63.7
E-40	--	--	--	--
E-20	92.8	92.8	92.8	75.5
E-0	67.6	--	67.6	94.8

-- Method did not produce any results
xx Frames were not used

Table 3.3 Calculated Shear Cracking Stresses, v_c (psi)

Positive Moment Region

Beam	Eq. (1.2)[1]	Eq. (1.3)[2]	Eq. (1.5)[3]	Eq. (1.6)[4]	Eq. (1.7)[5]
D-80(1)	146.7	125.0	109.3	119.4	99.7
D-80(2)	127.6	114.2	97.0	106.2	88.8
D-40	129.6	115.4	99.2	108.6	90.9
D-20	131.0	116.0	100.2	109.8	91.9
D-0	134.8	118.5	103.1	112.9	94.5
E-80	126.6	99.1	81.1	87.1	71.4
E-40	134.9	104.2	86.3	92.8	76.1
E-20	129.8	101.5	82.4	88.5	72.5
E-0	134.2	103.7	85.2	91.5	74.9

Negative Moment Region

Beam	Eq. (1.2)[1]	Eq. (1.3)[2]	Eq. (1.5)[3]	Eq. (1.6)[4]	Eq. (1.7)[5]
D-80(1)	146.7	125.6	110.8	121.2	101.3
D-80(2)	127.6	114.2	95.7	104.6	87.4
D-40	129.6	115.6	97.2	106.3	88.8
D-20	131.0	116.5	98.9	108.2	90.5
D-0	134.8	118.5	99.7	108.9	90.8
E-80	126.6	98.9	80.4	86.4	70.7
E-40	134.9	103.6	85.0	91.2	74.6
E-20	129.8	100.7	81.8	87.7	71.8
E-0	134.2	103.7	83.9	89.9	73.5

1. $v_c = 2\sqrt{f'_c}$ ACI 318-83 (4)
2. $v_c = 59(f'_c d/a)$ Zsutty (25)
3. $v_c = (0.8 + 100\rho_w)\sqrt{f'_c}$ Rajagopalan and Ferguson (22)
4. $v_c = (0.8 + 120\rho_w)\sqrt{f'_c}$ ACI-ASCE 426 (3)
5. $v_c = (0.6 + 110\rho_w)\sqrt{f'_c}$ Batchelor and Kwun (6)

Table 3.4 Comparison of Test and Calculated Shear Cracking Stresses

Measured v_c from Crack Patterns (psi)

Positive Moment Region

Beam	$\frac{v_c(\text{test})}{v_c(\text{Eq.1.2})}$[1]	$\frac{v_c(\text{test})}{v_c(\text{Eq.1.3})}$[2]	$\frac{v_c(\text{test})}{v_c(\text{Eq.1.5})}$[3]	$\frac{v_c(\text{test})}{v_c(\text{Eq.1.6})}$[4]	$\frac{v_c(\text{test})}{v_c(\text{Eq.1.7})}$[5]
D-80(1)	0.70	0.83	0.95	0.87	1.04
D-80(2)	1.09	1.21	1.53	1.31	1.56
D-40	0.77	0.86	1.01	0.92	1.10
D-20	1.11	1.25	1.45	1.32	1.58
D-0	0.84	0.94	1.08	0.98	1.18
E-80	0.90	1.15	1.40	1.31	1.59
E-40	0.94	1.22	1.47	1.37	1.67
E-20	0.68	0.87	1.08	1.00	1.22
E-0	0.85	1.10	1.34	1.25	1.52
Mean	0.87	1.04	1.25	1.15	1.38
Standard deviation	0.15	0.17	0.21	0.20	0.24
Coeff. of variation	17.2	16.3	16.8	17.4	17.4

Negative Moment Region

Beam	$\frac{v_c(\text{test})}{v_c(\text{Eq.1.2})}$[1]	$\frac{v_c(\text{test})}{v_c(\text{Eq.1.3})}$[2]	$\frac{v_c(\text{test})}{v_c(\text{Eq.1.5})}$[3]	$\frac{v_c(\text{test})}{v_c(\text{Eq.1.6})}$[4]	$\frac{v_c(\text{test})}{v_c(\text{Eq.1.7})}$[5]
D-80(1)	0.69	0.80	0.91	0.83	1.00
D-80(2)	0.78	0.88	1.04	0.96	1.14
D-40	0.86	0.96	1.14	1.04	1.25
D-20	0.84	0.95	1.12	1.03	1.23
D-0	0.89	0.94	1.12	1.02	1.22
E-80	0.51	0.64	0.79	0.74	0.90
E-40	--	--	--	--	--
E-20	0.71	0.92	1.11	1.06	1.29
E-0	0.50	0.65	0.81	0.71	0.92
Mean	0.71	0.84	1.01	0.92	1.12
Standard deviation	0.15	0.13	0.15	0.14	0.16
Coeff. of variation	21.1	15.5	14.9	15.2	14.3

1. $v_c = 2\sqrt{f'_c}$ ACI 318-83 (4)
2. $v_c = 59(f'_c d/a)$ Zsutty (25)
3. $v_c = (0.8 + 100\rho_w)\sqrt{f'_c}$ Rajagopalan and Ferguson (22)
4. $v_c = (0.8 + 120\rho_w)\sqrt{f'_c}$ ACI-ASCE 426 (3)
5. $v_c = (0.6 + 110\rho_w)\sqrt{f'_c}$ Batchelor and Kwun (6)

Table 3.5 Comparison of Test and Calculated Shear Cracking Stresses

Measured v_c from Stirrup Strain (psi)

Positive Moment Region

Beam	$\frac{v_c(\text{test})}{v_c(\text{Eq.1.2})}$[1]	$\frac{v(\text{test})}{v_c(\text{Eq.1.3})}$[2]	$\frac{v_c(\text{test})}{v_c(\text{Eq.1.5})}$[3]	$\frac{v_c(\text{test})}{v_c(\text{Eq.1.6})}$[4]	$\frac{v_c(\text{test})}{v_c(\text{Eq.1.7})}$[5]
D-80(1)	0.86	1.00	1.15	1.05	1.26
D-80(2)	1.05	1.18	1.38	1.26	1.51
D-40	0.86	0.97	1.13	1.03	1.13
D-20	0.65	0.74	0.85	0.78	0.93
E-80	1.03	1.30	1.59	1.48	1.81
E-40	0.99	1.29	1.55	1.44	1.76
E-20	0.72	0.92	1.13	1.05	1.28
Mean	0.88	1.06	1.25	1.16	1.40
Standard deviation	0.15	0.21	0.26	0.25	0.30
Coeff. of variation	17.0	19.8	20.8	21.6	22.0

Negative Moment Region

Beam	$\frac{v_c(\text{test})}{v_c(\text{Eq.1.2})}$[1]	$\frac{v_c(\text{test})}{v_c(\text{Eq.1.3})}$[2]	$\frac{v_c(\text{test})}{v_c(\text{Eq.1.5})}$[3]	$\frac{v_c(\text{test})}{v_c(\text{Eq.1.6})}$[4]	$\frac{v_c(\text{test})}{v_c(\text{Eq.1.7})}$[5]
D-80(1)	0.69	0.80	0.91	0.83	1.00
D-80(1)	0.96	1.12	1.27	1.16	1.39
D-80(2)	—	—	—	—	—
D-40	0.95	1.06	1.26	1.15	1.38
D-20	0.85	0.95	1.12	1.03	1.23
E-80	0.51	0.64	0.79	0.79	0.90
E-40	—	—	—	—	—
E-20	0.71	0.92	1.11	1.06	1.29
Mean	0.80	0.94	1.11	1.04	1.24
Standard deviation	0.19	0.19	0.19	0.15	0.20
Coeff. of variation	23.8	20.2	17.1	14.4	16.1

1. $v_c = 2\sqrt{f'_c}$ ACI 318-83 (4)
2. $v_c = 59(f'_c d/a)$ Zsutty (25)
3. $v_c = (0.8 + 100\rho_w)\sqrt{f'_c}$ Rajagopalan and Ferguson (22)
4. $v_c = (0.8 + 120\rho_w)\sqrt{f'_c}$ ACI-ASCE 426 (3)
5. $v_c = (0.6 + 110\rho_w)\sqrt{f'_c}$ Batchelor and Kwun (6)

Table 3.6 Comparison of Test and Calculated Shear Cracking Stresses

Measured v_c from Depth Increase (psi)

Positive Moment Region

Beam	$\frac{v_c(\text{test})}{v_c(\text{Eq.1.2})}$[1]	$\frac{v_c(\text{test})}{v_c(\text{Eq.1.3})}$[2]	$\frac{v_c(\text{test})}{v_c(\text{Eq.1.5})}$[3]	$\frac{v_c(\text{test})}{v_c(\text{Eq. .6})}$[4]	$\frac{v_c(\text{test})}{v_c(\text{Eq.1.7})}$[5]
D-80(1)	0.86	1.00	1.15	1.05	1.26
D-80(1)	--	--	--	--	--
D-80(2)	--	--	--	--	--
D-40	--	--	--	--	--
D-20	--	--	--	--	--
D-0	--	--	--	--	--
E-80	1.03	1.30	1.59	1.48	1.81
E-40	0.94	1.22	1.47	1.37	1.67
E-20	--	--	--	--	--
E-0	0.72	0.93	1.14	1.06	1.29
Mean	0.90	1.15	1.40	1.34	1.59
Standard deviation	0.16	0.19	0.23	0.22	0.27
Coeff. of variation	17.8	16.5	16.4	16.4	17.0

Negative Moment Region

Beam	$\frac{v_c(\text{test})}{v_c(\text{Eq.1.2})}$[1]	$\frac{v_c(\text{test})}{v_c(\text{Eq.1.3})}$[2]	$\frac{v_c(\text{test})}{v_c(\text{Eq.1.5})}$[3]	$\frac{v_c(\text{test})}{v_c(\text{Eq.1.6})}$[4]	$\frac{v_c(\text{test})}{v_c(\text{Eq.1.7})}$[5]
D-80(1)	0.92	1.08	1.22	1.11	1.33
D-80(2)	1.04	1.16	1.38	1.26	1.51
D-40	0.74	0.82	0.98	0.90	1.07
D-20	0.80	0.90	1.06	0.97	1.16
D-0	0.89	1.01	1.20	1.10	1.31
E-80	0.51	0.64	0.79	0.79	0.90
E-40	--	--	--	--	--
E-20	0.71	0.92	1.11	1.06	1.29
E-0	0.71	0.84	1.01	0.92	1.12
Mean	0.79	0.92	1.09	1.01	1.21
Standard deviation	0.15	0.16	0.18	0.15	0.19
Coeff. of variation	19.0	17.4	16.5	14.9	15.5

1. $v_c = 2\sqrt{f'_c}$ ACI 318-83 (4)

2. $v_c = 59(f'_c d/a)$ Zsutty (25)

3. $v_c = (0.8 + 100\rho_w)\sqrt{f'_c}$ Rajagopalan and Ferguson (22)

4. $v_c = (0.8 + 120\rho_w)\sqrt{f'_c}$ ACI-ASCE 426 (3)

5. $v_c = (0.6 + 110\rho_w)\sqrt{f'_c}$ Batchelor and Kwun (6)

Table 3.7 Comparison of Test and Calculated Shear Cracking Stresses

Measured v_c from Concrete Strain (psi)

Positive Moment Region

Beam	$\frac{v_c(test)}{v_c(Eq.1.2)}^1$	$\frac{v_c(test)}{v_c(Eq.1.3)}^2$	$\frac{v_c(test)}{v_c(Eq.1.5)}^3$	$\frac{v_c(test)}{v_c(Eq.1.6)}^4$	$\frac{v_c(test)}{v_c(Eq.1.7)}^5$
D-80(1)	0.86	1.00	1.15	1.05	1.26
D-80(1)	0.90	1.05	1.20	1.10	1.32
D-80(2)	1.05	1.18	1.38	1.26	1.51
D-40	0.86	0.97	1.13	1.03	1.23
D-20	0.91	1.03	1.19	1.09	1.30
D-0	0.71	0.81	0.93	0.85	1.01
E-80	1.03	1.30	1.59	1.48	1.81
E-40	0.81	1.05	1.27	1.18	1.43
E-20	0.68	0.87	1.08	1.00	1.22
E-0	0.77	0.99	1.21	1.12	1.37
Mean	0.86	1.03	1.22	1.12	1.36
Standard deviation	0.13	0.15	0.19	0.18	0.22
Coeff. of variation	15.1	14.6	15.6	16.1	16.2

Negative Moment Region

Beam	$\frac{v_c(test)}{v_c(Eq.1.2)}^1$	$\frac{v_c(test)}{v_c(Eq.1.3)}^2$	$\frac{v_c(test)}{v_c(Eq.1.5)}^3$	$\frac{v_c(test)}{v_c(Eq.1.6)}^4$	$\frac{v_c(test)}{v_c(Eq.1.7)}^5$
D-80(1)	0.69	0.80	0.91	0.83	1.00
D-80(1)	0.76	0.89	1.01	0.93	1.11
D-80(2)	1.10	1.23	1.47	1.35	1.61
D-40	0.95	1.06	1.26	1.15	1.38
D-20	0.94	1.06	1.25	1.14	1.36
D-0	0.82	0.94	1.12	1.02	1.22
E-80	0.51	0.64	0.79	0.79	0.90
E-40	--	--	--	--	--
E-20	0.58	0.75	0.92	0.86	1.05
E-0	0.71	0.91	1.13	1.05	1.29
Mean	0.80	0.94	1.12	1.04	1.24
Standard deviation	0.21	0.19	0.21	0.17	0.22
Coeff. of variation	26.3	20.2	18.8	16.3	17.7

1. $v_c = 2\sqrt{f'_c}$ ACI 318-83 (4)
2. $v_c = 59(f'_c d/a)$ Zsutty (25)
3. $v_c = (0.8 + 100\rho_w)\sqrt{f'_c}$ Rajagopalan and Ferguson (22)
4. $v_c = (0.8 + 120\rho_w)\sqrt{f'_c}$ ACI-ASCE 426 (3)
5. $v_c = (0.6 + 110\rho_w)\sqrt{f'_c}$ Batchelor and Kwun (6)

Table 3.8 Stirrup Effectiveness, $v_n - v_c$ (psi)

Current Study

Beam	Crack patterns	Stirrup strain	Depth increase	Concrete strain
* D-80(1)	134.6	--	--	--
D-80(2)	99.9	--	67.8	59.1
D-40	34.7	22.9	50.3	22.9
D-20	37.0	37.0	43.1	24.5
D-0	18.4	--	18.4	18.4
E-80	88.6	88.6	88.6	88.6
* E-40	54.7	47.5	54.7	72.2
E-20	34.6	34.6	34.6	51.9
* E-0	19.0	--	36.3	30.3

* Positive moment region failure

Palaskas, Attiogbe and Darwin (5,20,21)

Beam	$v_n - v_c$ (psi)
A-0	13.9
A-25	55.1
A-25a	67.5
A-50	103.0
A-50a	98.3
A-75	164.0
B-0	47.1
B-25	49.1
B-50	110.4
C-0	18.8
C-25	52.0
C-50	146.0
C-75	172.0

Table 3.9 Horizontal Crack Projection and Shear Stress carried by Stirrups alone and by Dowel Action and Aggregate Interlock

Positive Moment Region

Beam	Horizontal crack projection	# of stirrups intercepted	$v_{si}=\frac{nA_v f_{vy}}{b_w d}$ psi	$(v_n-v_c)-v_{si}$ psi	$\rho_v f_{vy}$ psi
D-80(1)	1.4d	3	116.0	18.6	82.9
E-40	1.6d	3	49.7	5.0	36.8
* A-25	1.7d	3	43.4	11.7	31.8
* A-25a	2.2d	3	43.8	23.7	31.8
* A-50	1.8d	3	100.6	2.4	74.0
* A-50a	2.0d	3	101.7	0.0	75.0
* A-75	1.8d	3	131.1	32.9	97.0
* B-25	1.8d	2	29.2	19.9	32.4
* B-50	1.5d	3	104.0	6.4	76.2
* C-25	1.7d	3	44.4	7.6	32.4
* C-50	1.7d	3	103.4	42.6	76.2
* C-75	1.7d	3	139.0	33.0	103.0

Negative Moment Region

Beam	Horizontal crack projection	# of stirrups intercepted	$v_{si}=\frac{nA_v f_{vy}}{b_w d}$ psi	$(v_n-v_c)-v_{si}$ psi	$\rho_v f_{vy}$ psi
D-80(2)	1.1d	2	66.8	33.1	73.1
D-40	0.9d	1	16.8	17.9	37.0
D-20	1.1d	2	20.0	17.0	21.6
E-80	0.9d	2	68.3	20.3	73.5
E-20	1.4d	2	20.2	14.4	22.2

* Test results of Palaskas, Attiogbe and Darwin (5,20,21)

Table 3.10 Comparison of Test and Calculated Nominal Shear Stresses

Positive Moment Region

Beam	v_n (test) psi	v_n (ACI)** psi	$\frac{v_n \text{ (test)}}{v_n \text{ (ACI)}}$
D-80(1)	238	230	1.03
E-40	181	172	1.05
E-0	133	134	1.00
* #2	147	138	1.10
* A-00	126	138	0.91
* A-25	167	169	0.99
* A-25a	182	170	1.10
* A-50	225	198	1.14
* A-50(a)	213	202	1.05
* A-75	275	234	1.18
* #1	286	259	1.10
* B-00	136	136	1.00
* B-25	153	166	0.92
* B-50	208	209	1.00
* C-00	115	131	0.88
* C-25	166	161	1.03
* C-50	261	207	1.26
* C-75	266	234	1.14
Mean (all beams)			1.04
Coeff. of variation			9.3%
Mean (beams with stirrups)			1.07
Coeff. of variation			8.4%

Negative Moment Region

Beam	v_n (test) psi	v_n (ACI)** psi	$\frac{v_n \text{ (test)}}{v_n \text{ (ACI)}}$
D-80(2)	200	201	1.00
D-40	146	167	0.82
D-20	148	153	0.97
D-0	138	135	1.02
E-80	152	200	0.76
E-20	127	152	0.84
Mean (all beams)			0.91
Coeff. of variation			8.4%
Mean (beams with stirrups)			0.89
Coeff. of variation			11.0%

* Test results of Palaskas, Attiogbe and Darwin (5,20,21)

** $v_n = v_c + 2\sqrt{f'_c}$

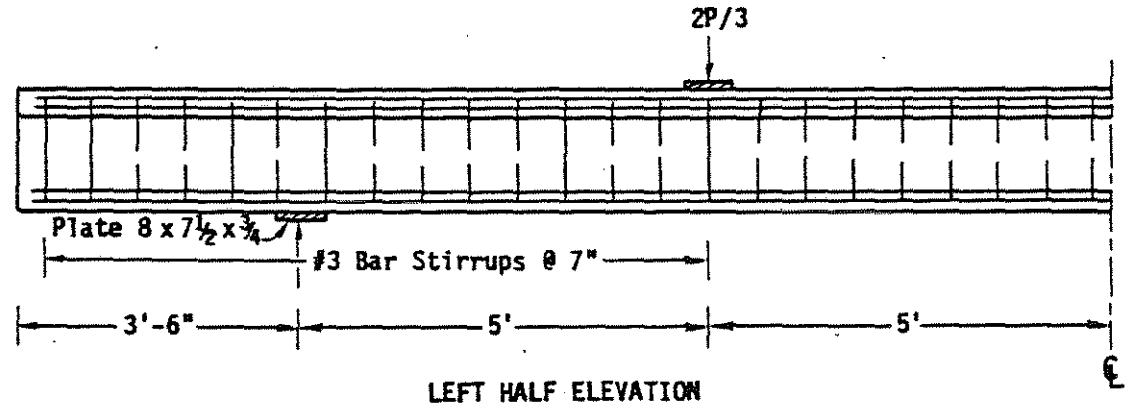

LEFT HALF ELEVATION
(Positive Moment Region)

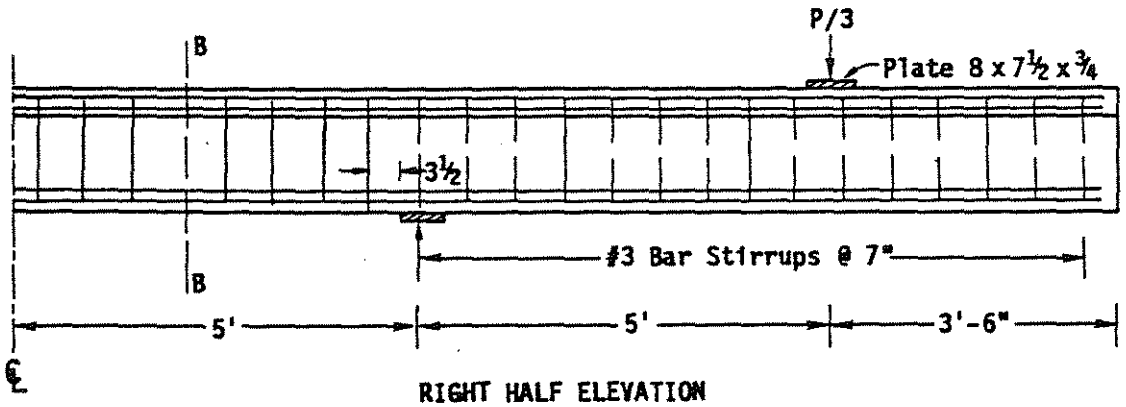

RIGHT HALF ELEVATION
(Negative Moment Region)

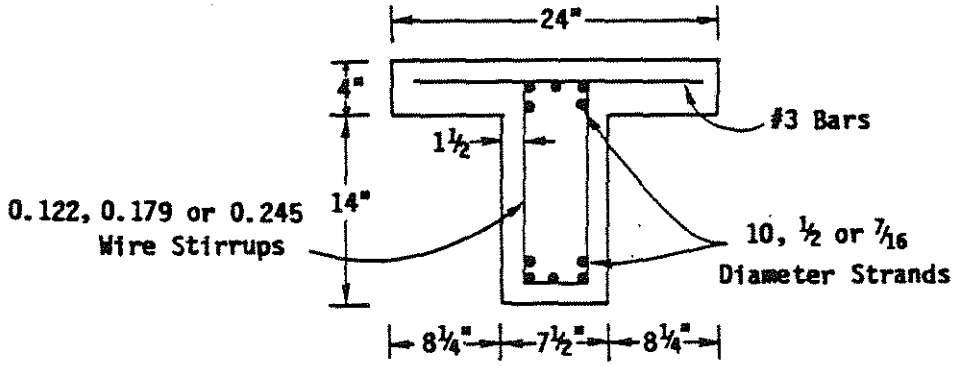

SECTION B-B

Fig. 2.1a Beams with Stirrups

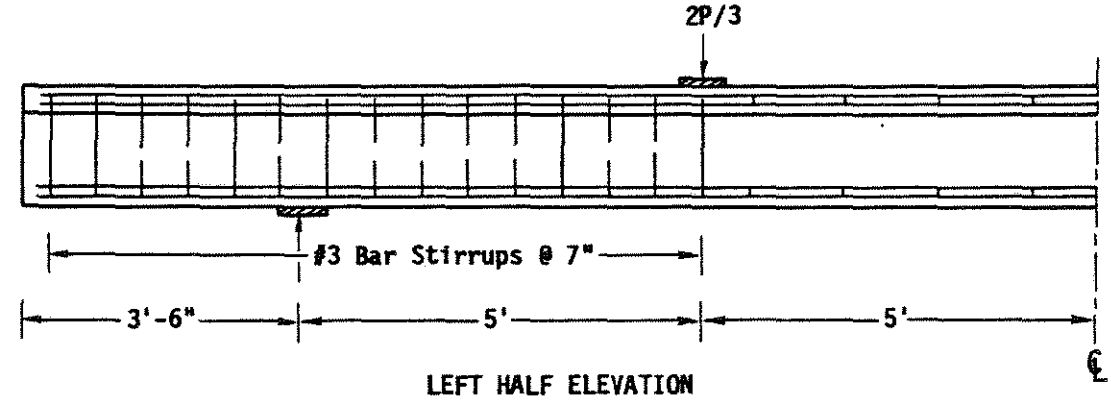

LEFT HALF ELEVATION
(Positive Moment Region)

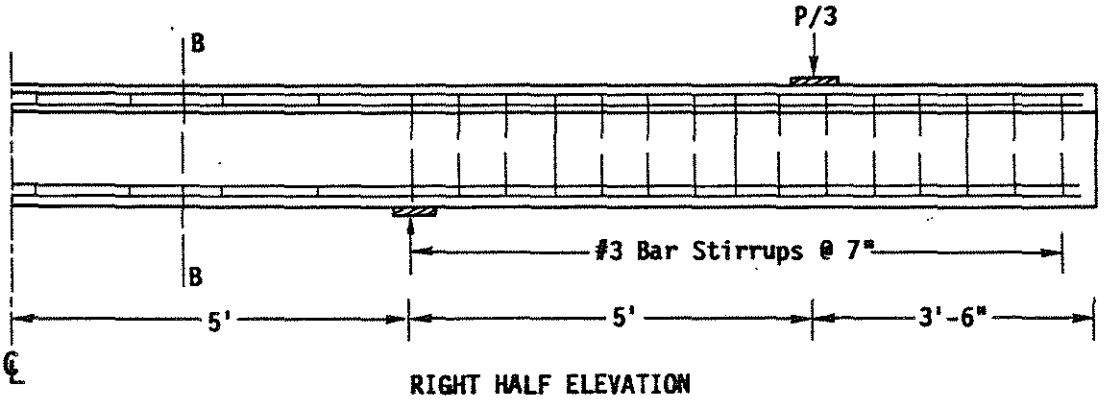

RIGHT HALF ELEVATION
(Negative Moment Region)

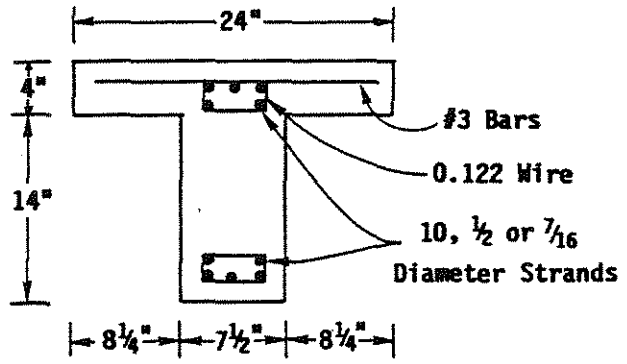

SECTION B-B

Fig. 2.1b Beams without Stirrups

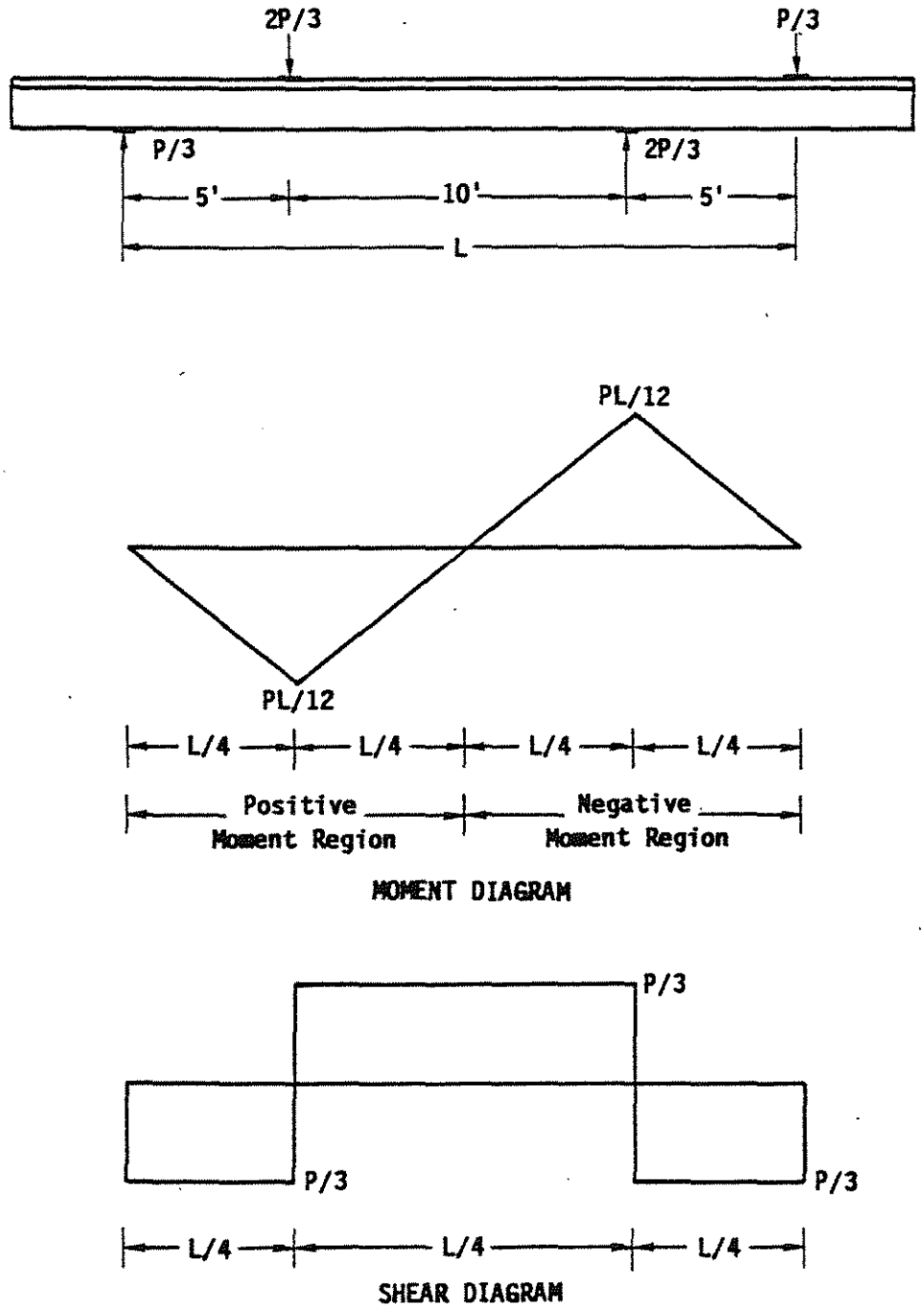

Fig. 2.2 Moment and Shear Diagrams due to Loading

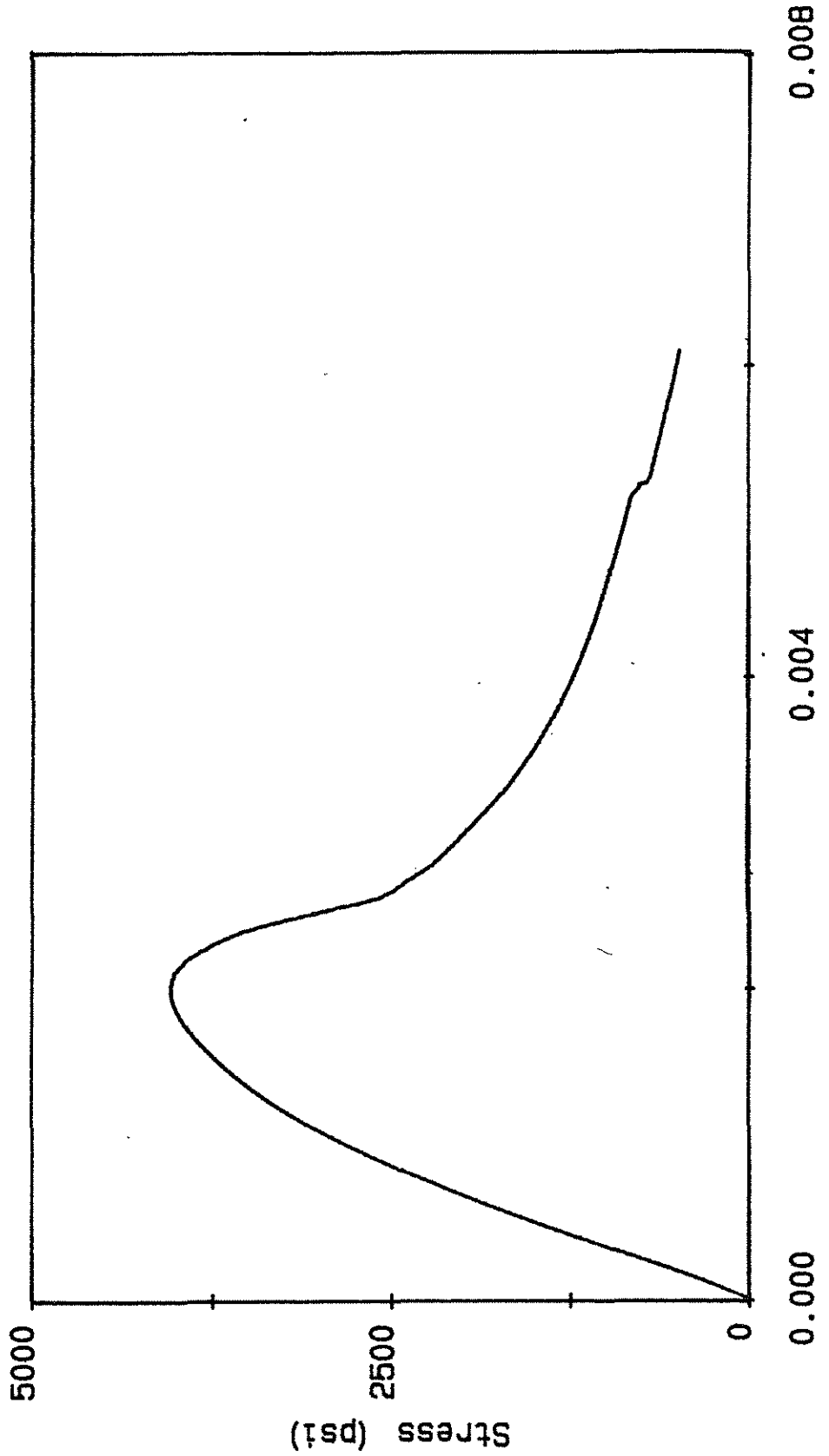

Fig. 2.3 Stress-Strain Curve for Concrete

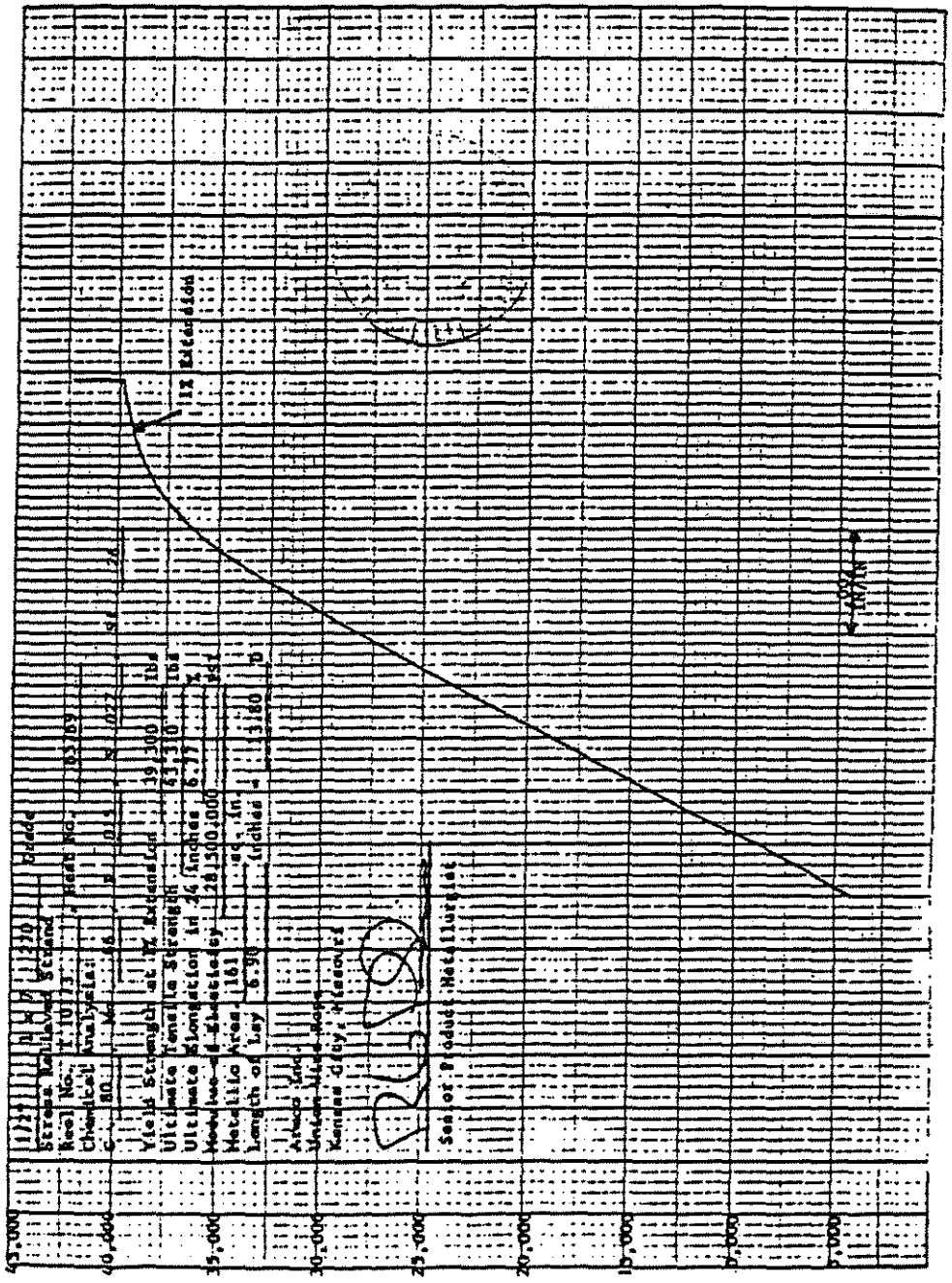

Fig. 2.4a Load-Strain Curve for 1/2 in. Strand

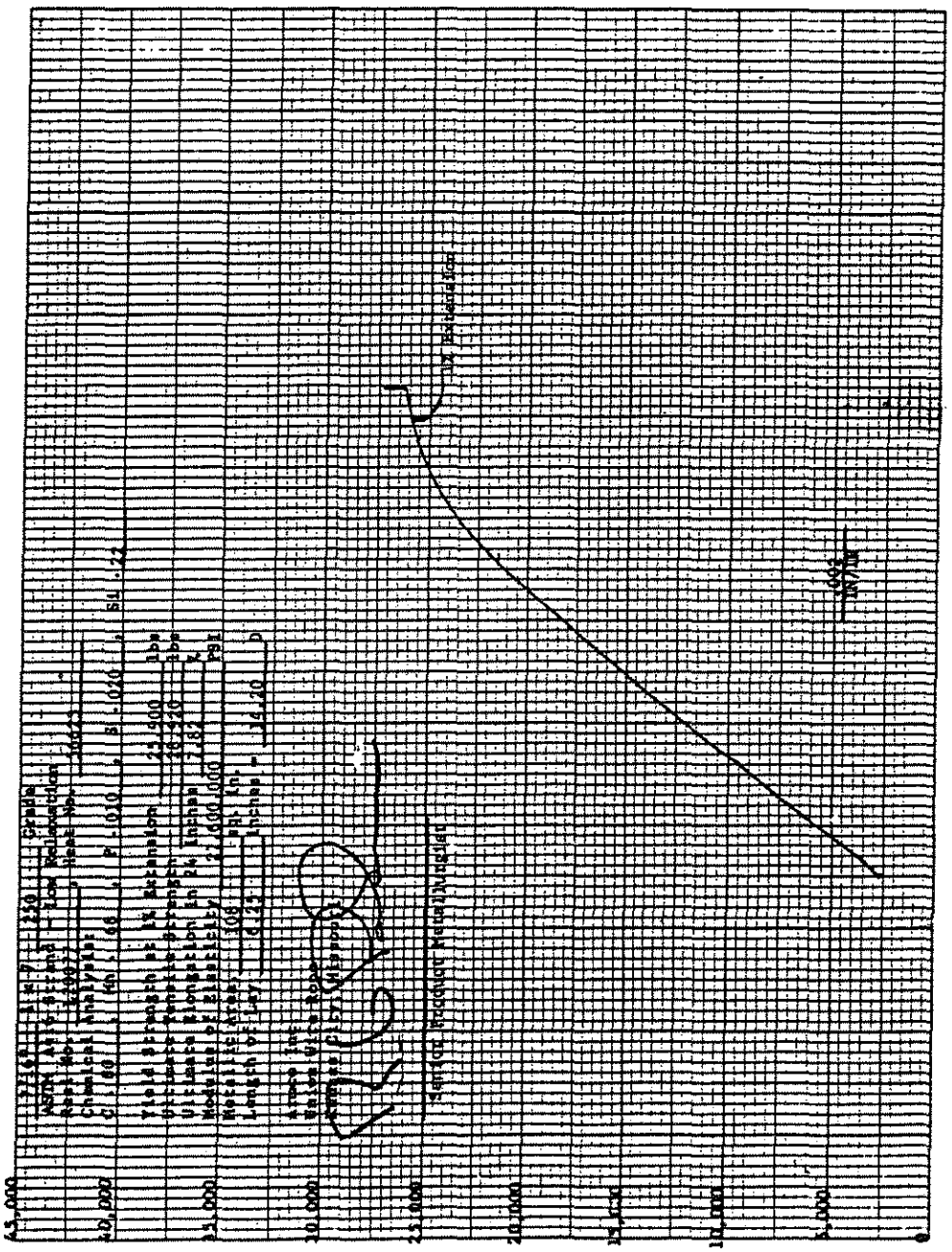

Fig. 2.4b Load-Strain Curve for 7/16 in. Strand

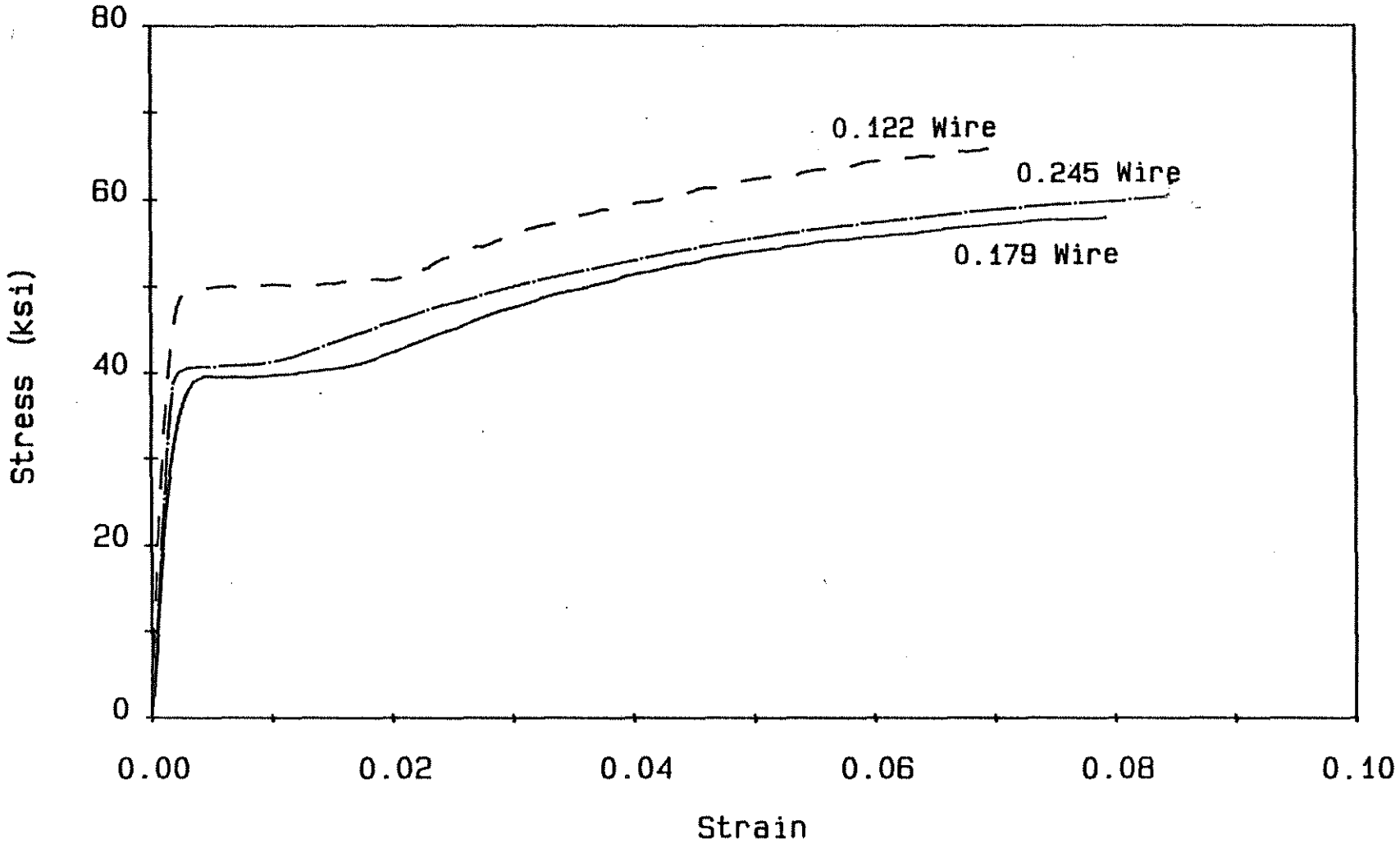

Fig. 2.5 Stress-Strain Curves for Wires

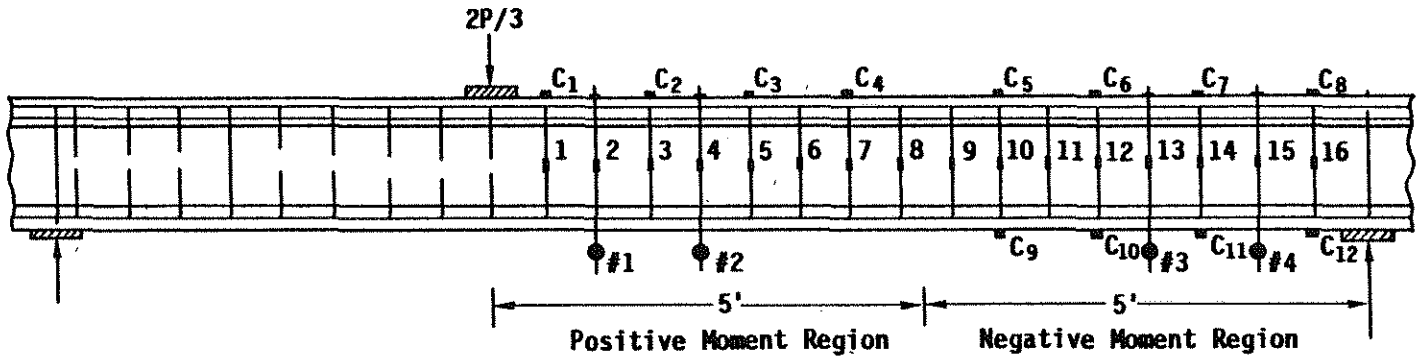

$C_1 - C_4$; $C_9 - C_{12}$ Concrete Compressive Gages

$C_5 - C_8$ Concrete Tensile Gages

1 - 16 Stirrup Gages

#1 - #4 Depth Frames

Fig. 2.6 Strain Gage Locations

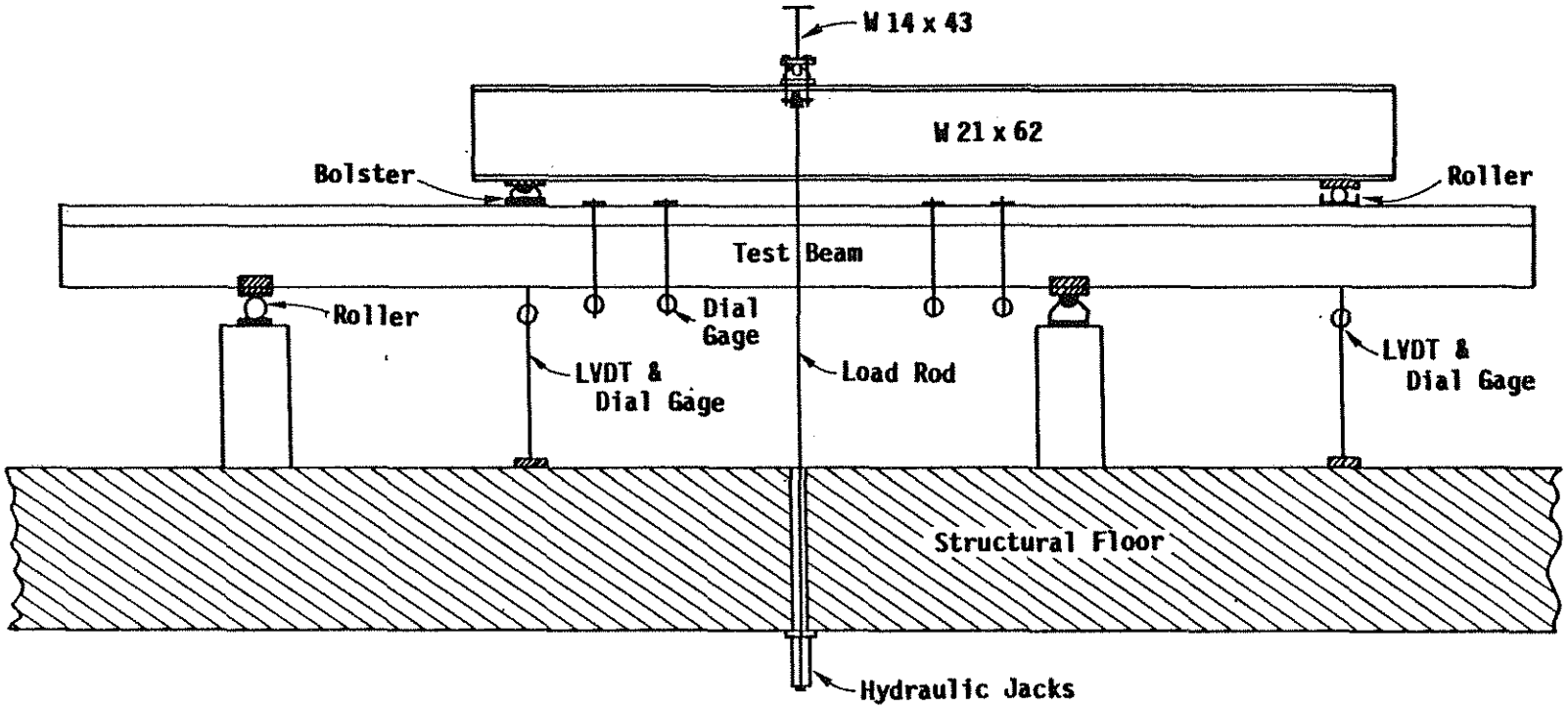

Fig. 2.7a Loading System - Side View

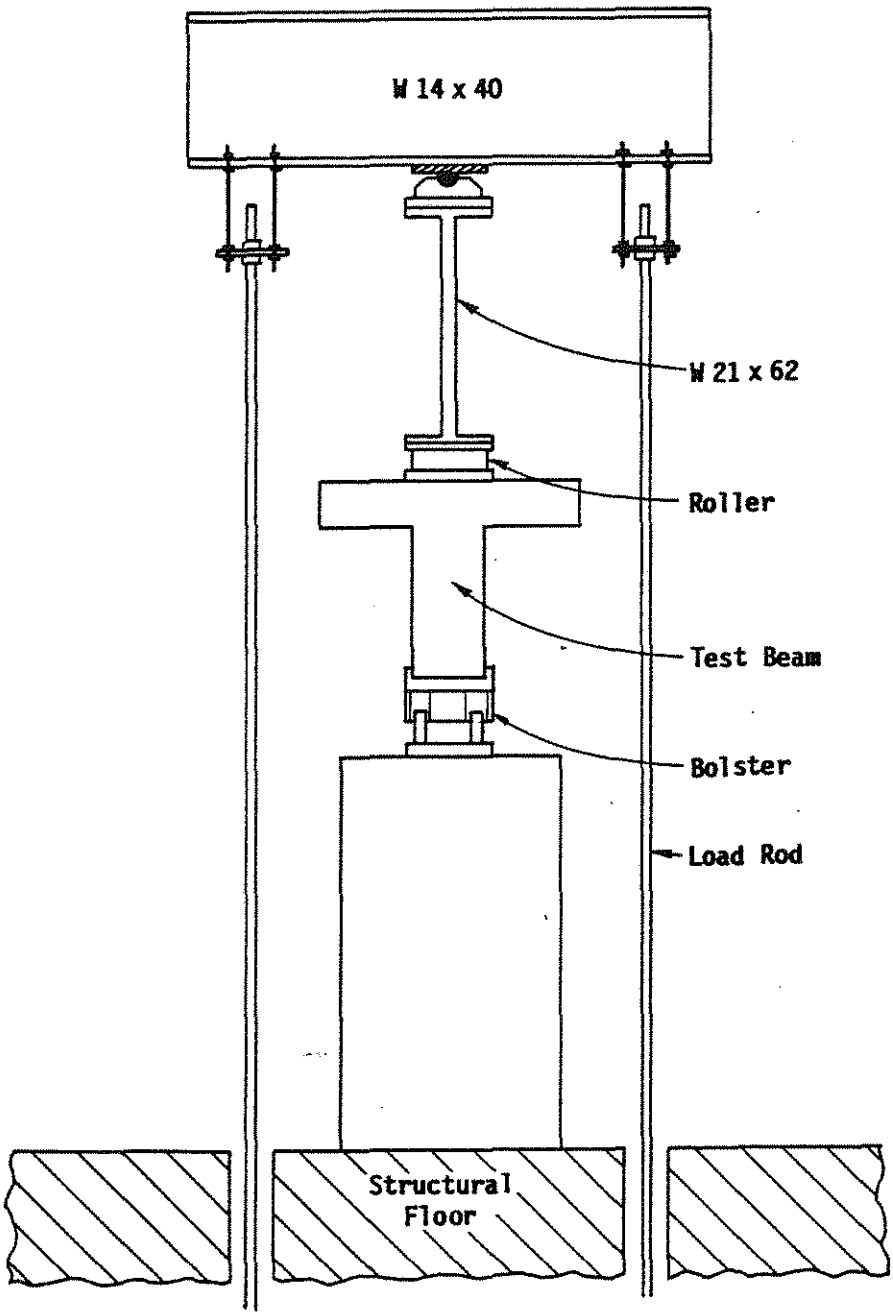

Fig. 2.7b Loading System - End View

Beam D-80(1)

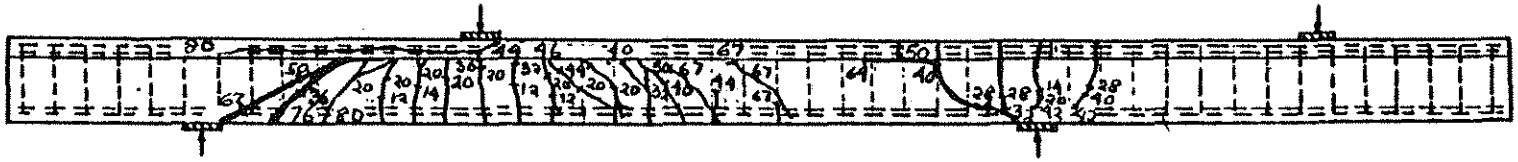

Beam D-80(2)

Beam D-40

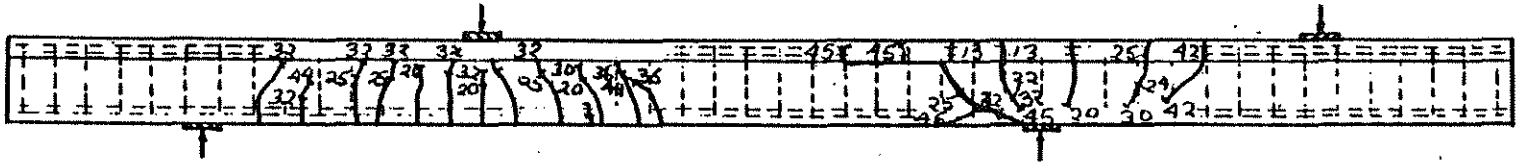

Fig. 2.8 Crack Patterns

Beam D-20

Beam D-0

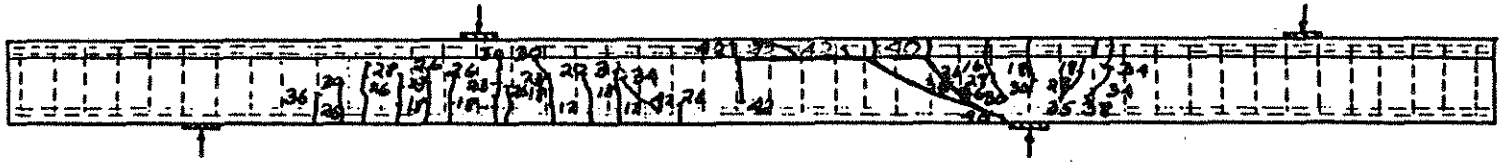

Beam E-80

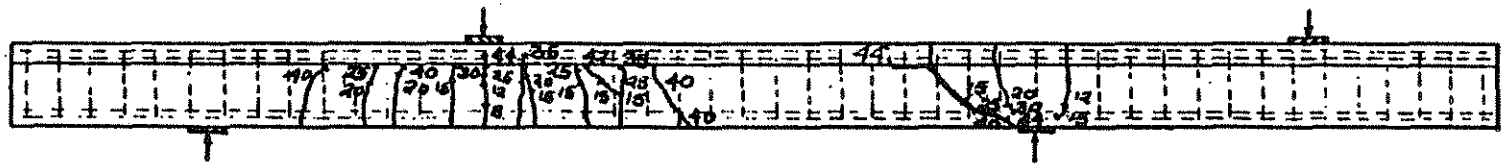

Fig. 2.8, Continued

Beam E-40

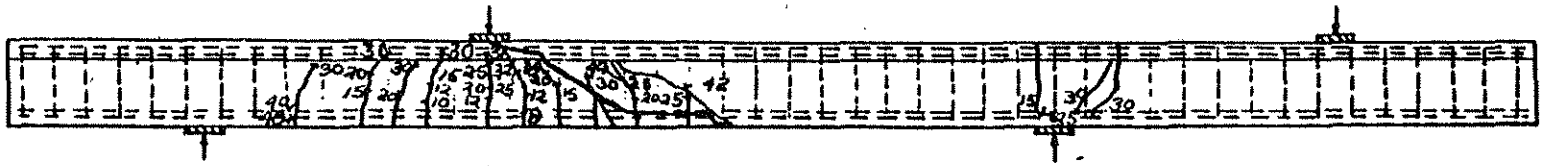

Beam E-20

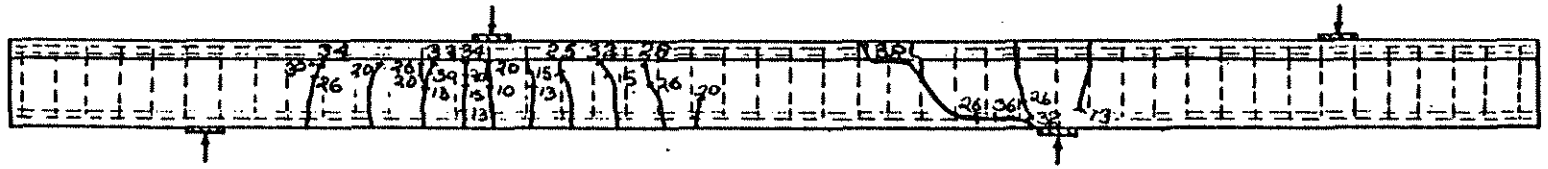

Beam E-0

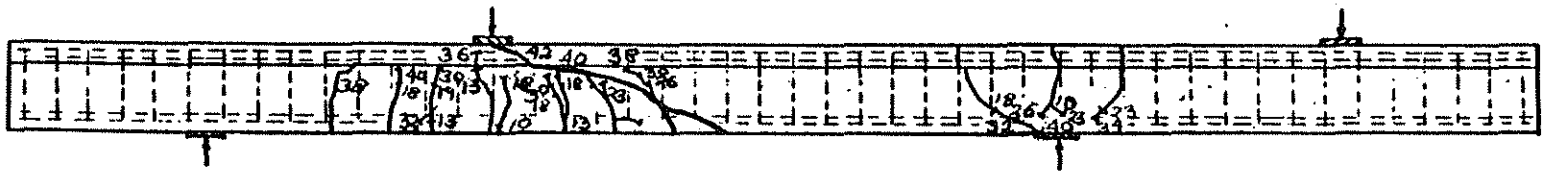

Fig. 2.8, Continued

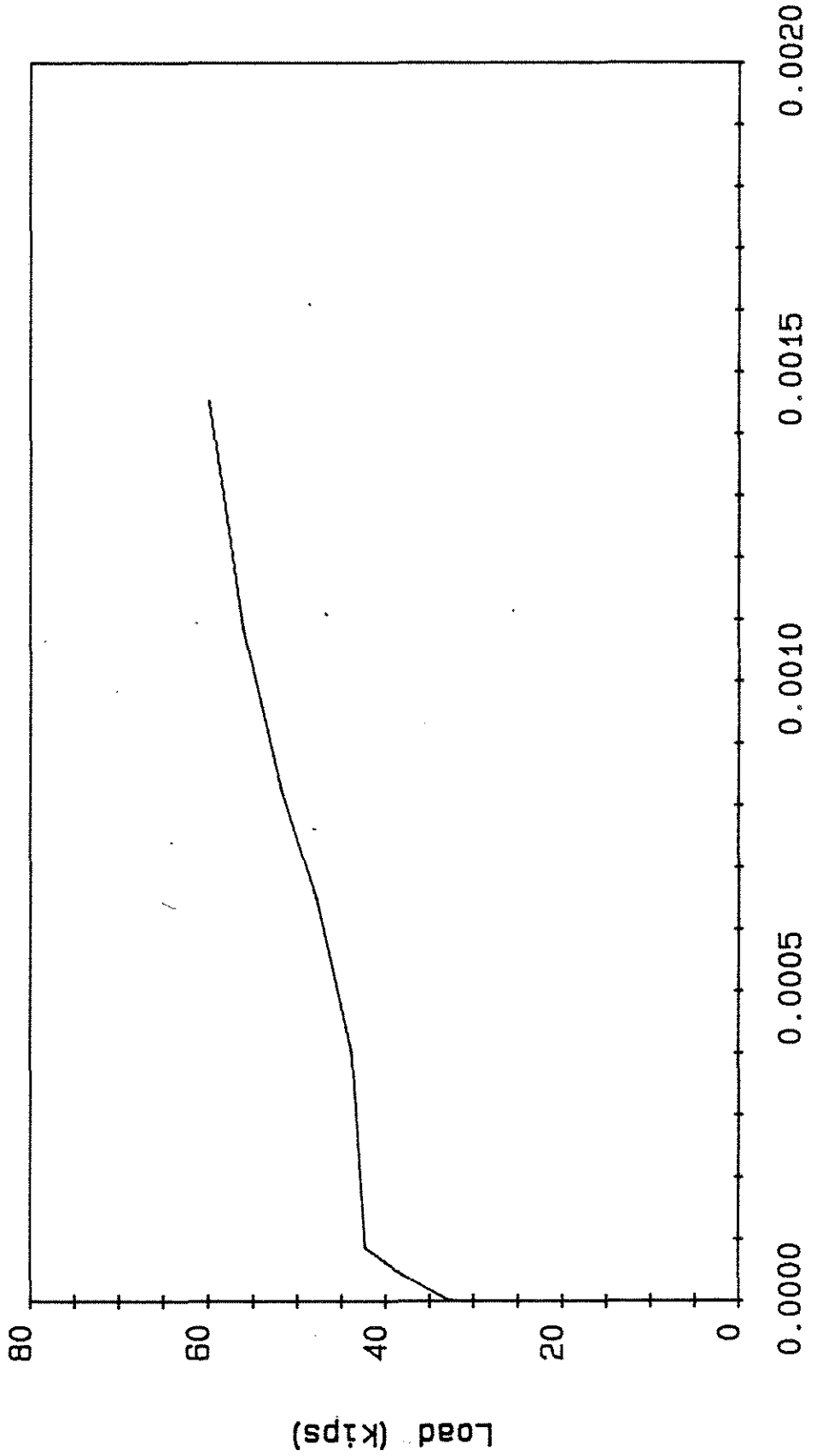

Fig. 2.9 Typical Load-Stirrup Strain Curve

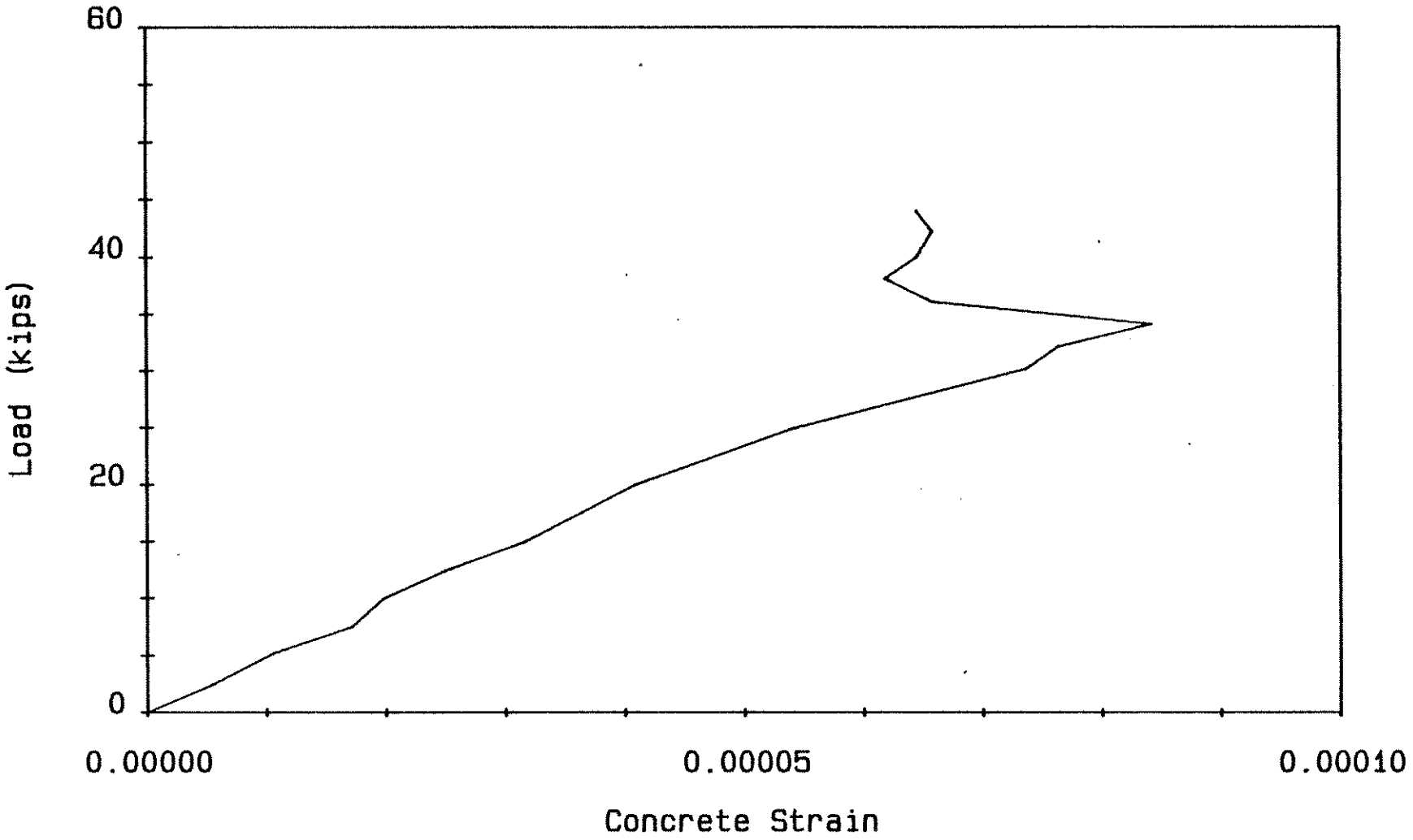

Fig. 2.10 Typical Load-Concrete Strain Curve

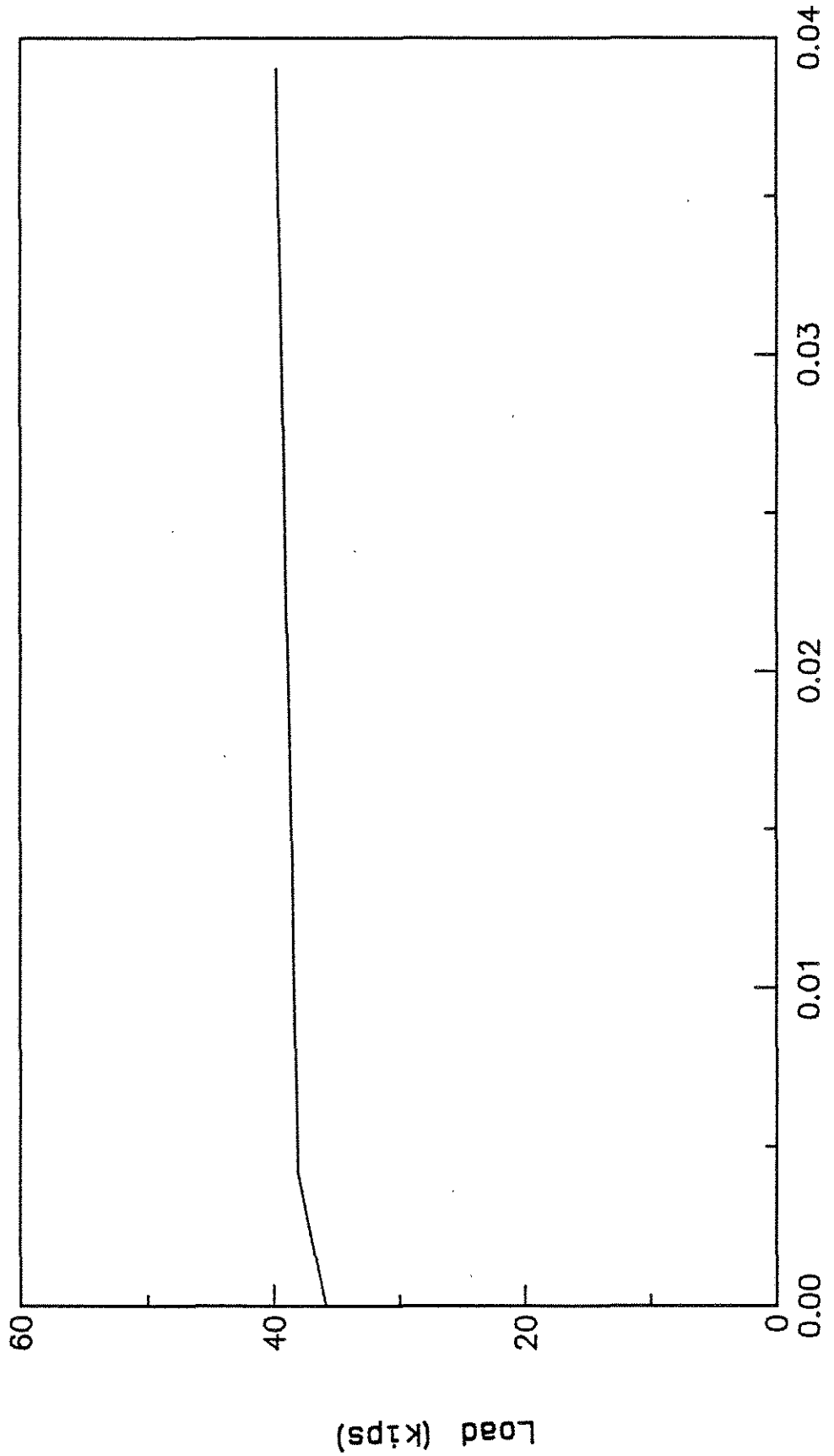

Fig. 2.11 Typical Load-Change in Beam Depth Curve

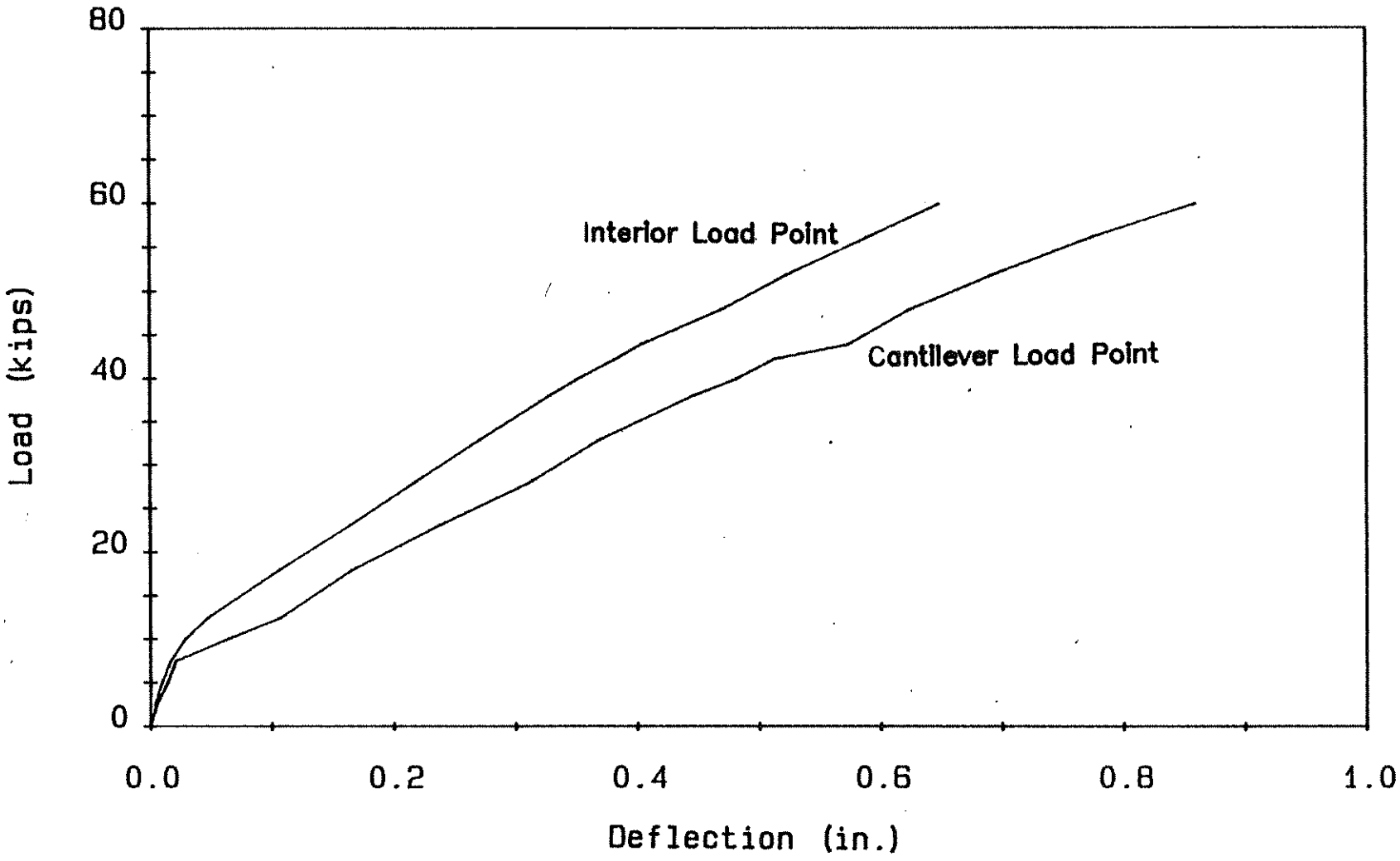

Fig. 2.12 Typical Load-Deflection Curve

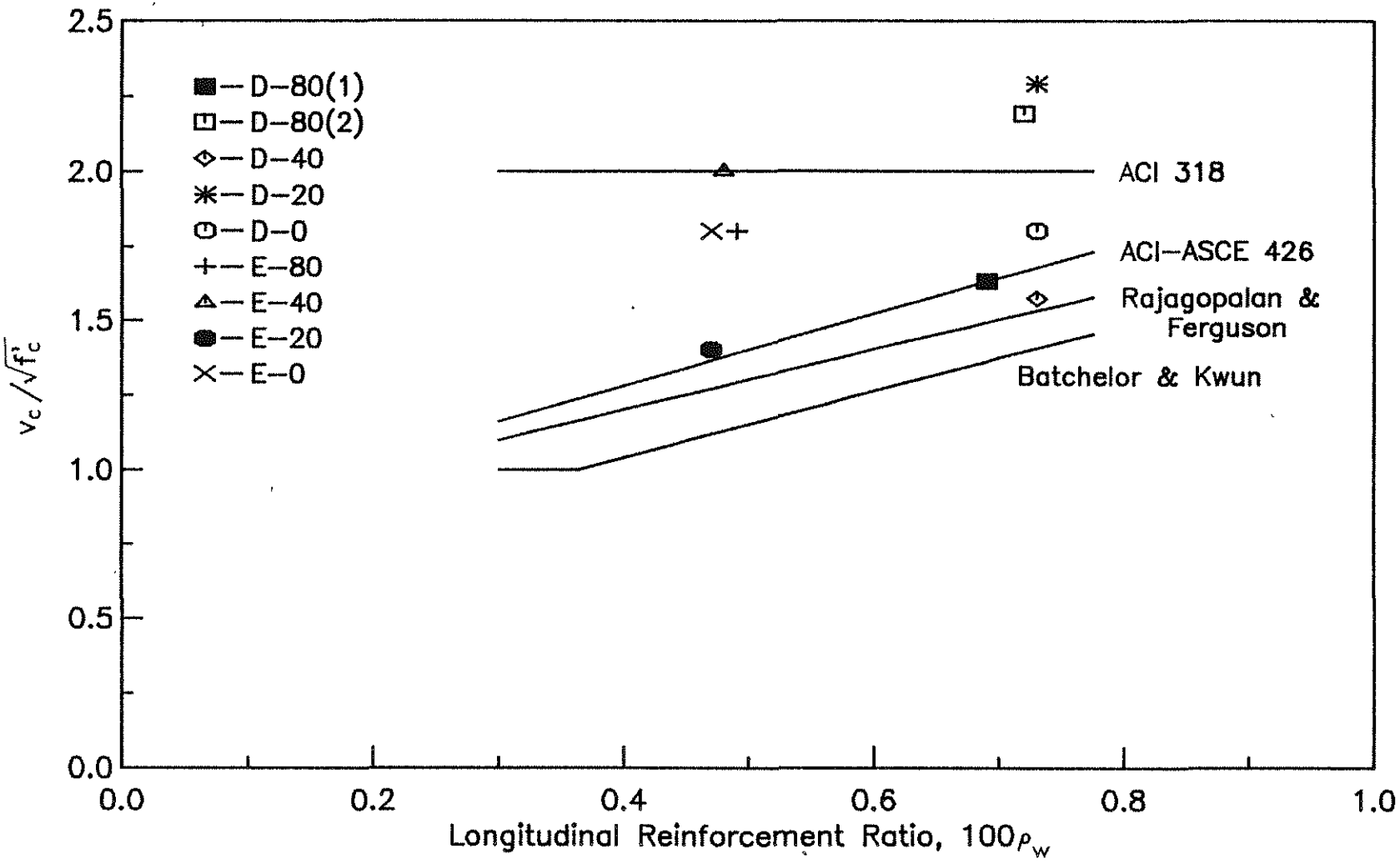

Fig. 3.1 Shear Cracking Stress from Crack Patterns in the Positive Moment Region

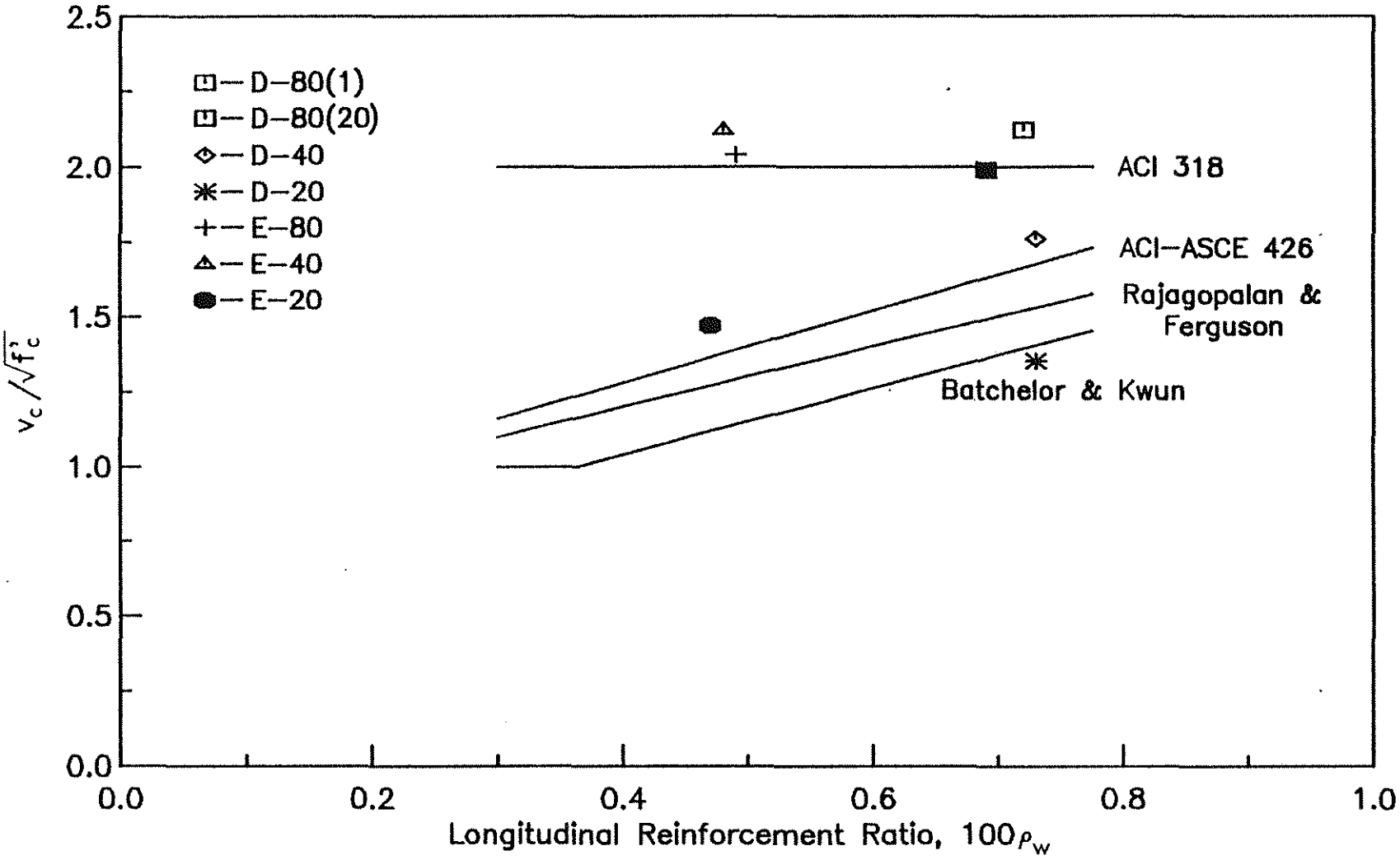

Fig. 3.2 Shear Cracking Stress from Stirrup Strain in the Positive Moment Region

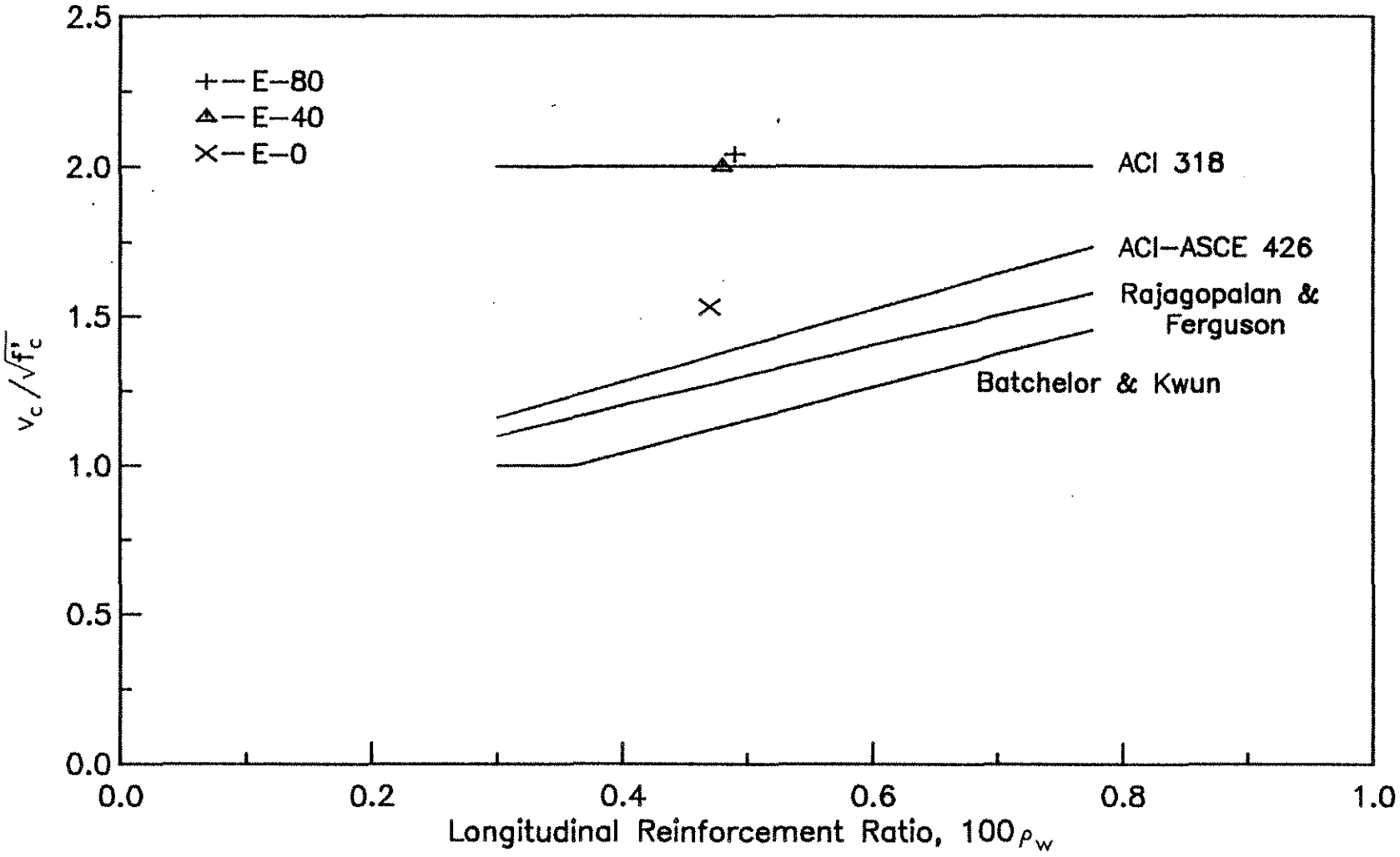

Fig. 3.3 Shear Cracking Stress from Depth Increase in the Positive Moment Region

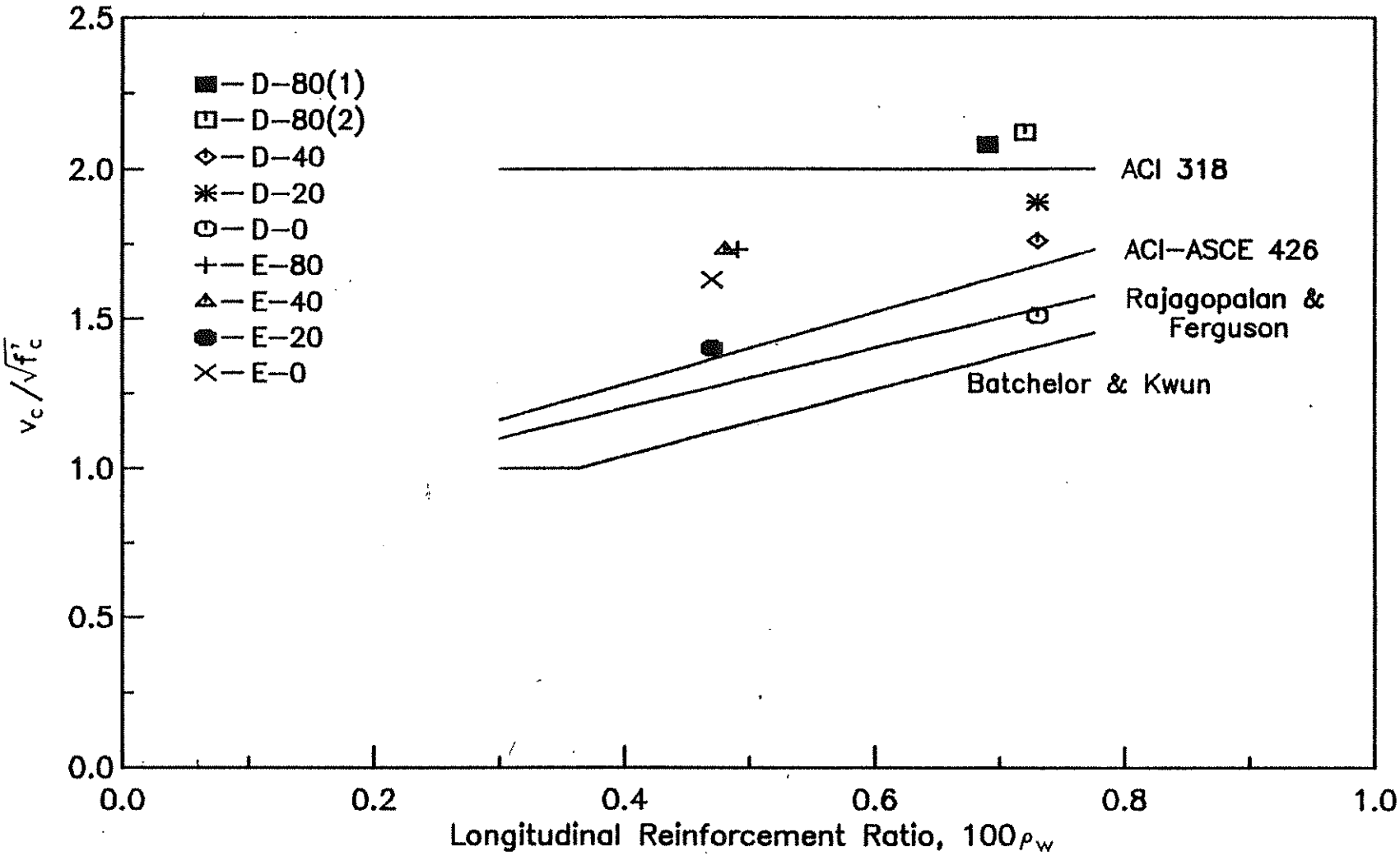

Fig. 3.4 Shear Cracking Stress from Concrete Strain in the Positive Moment Region

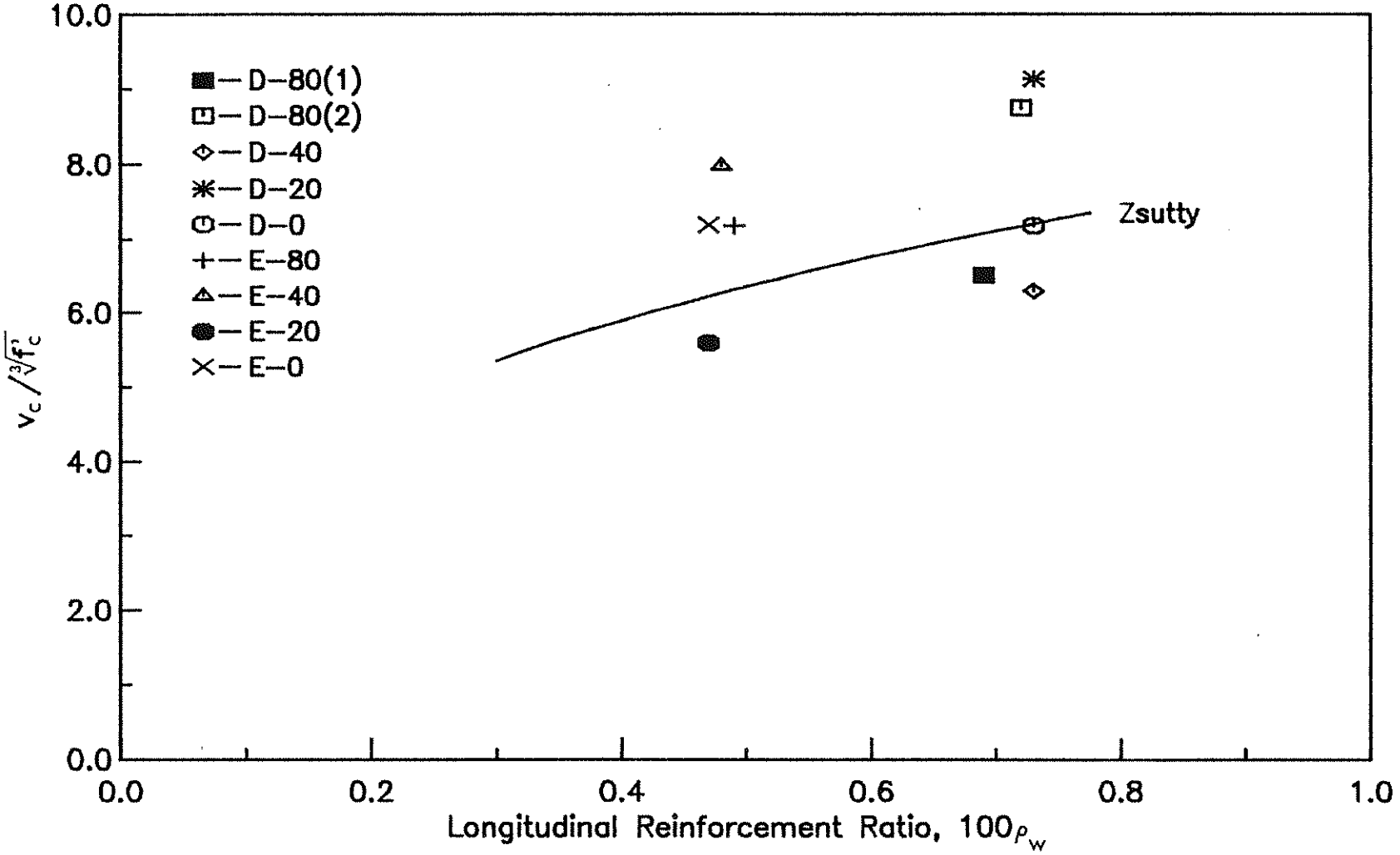

Fig. 3.5 Shear Cracking Stress from Crack Pattern in the Positive Moment Region

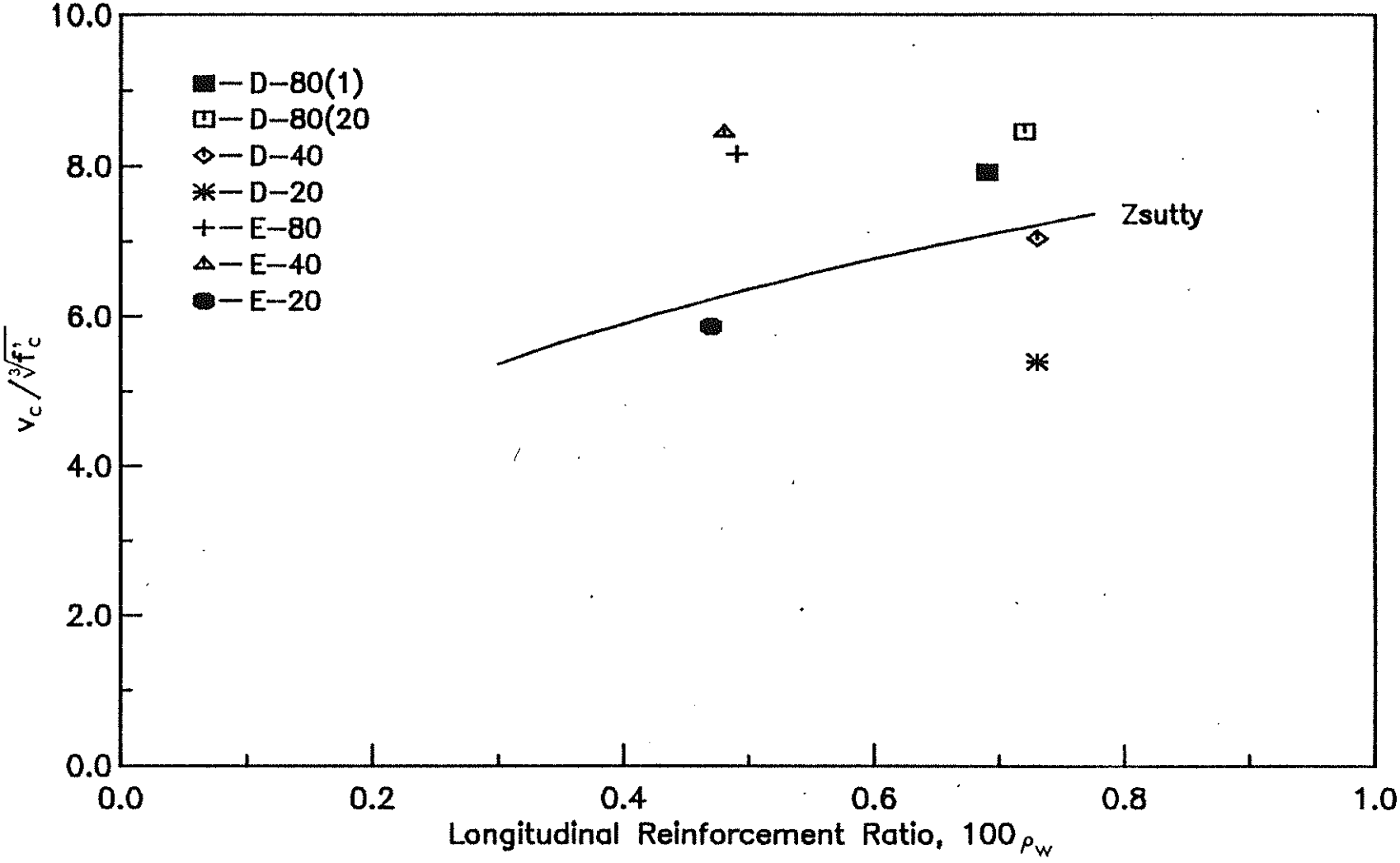

Fig. 3.6 Shear Cracking Stress from Stirrup Strain in the Positive Moment Region

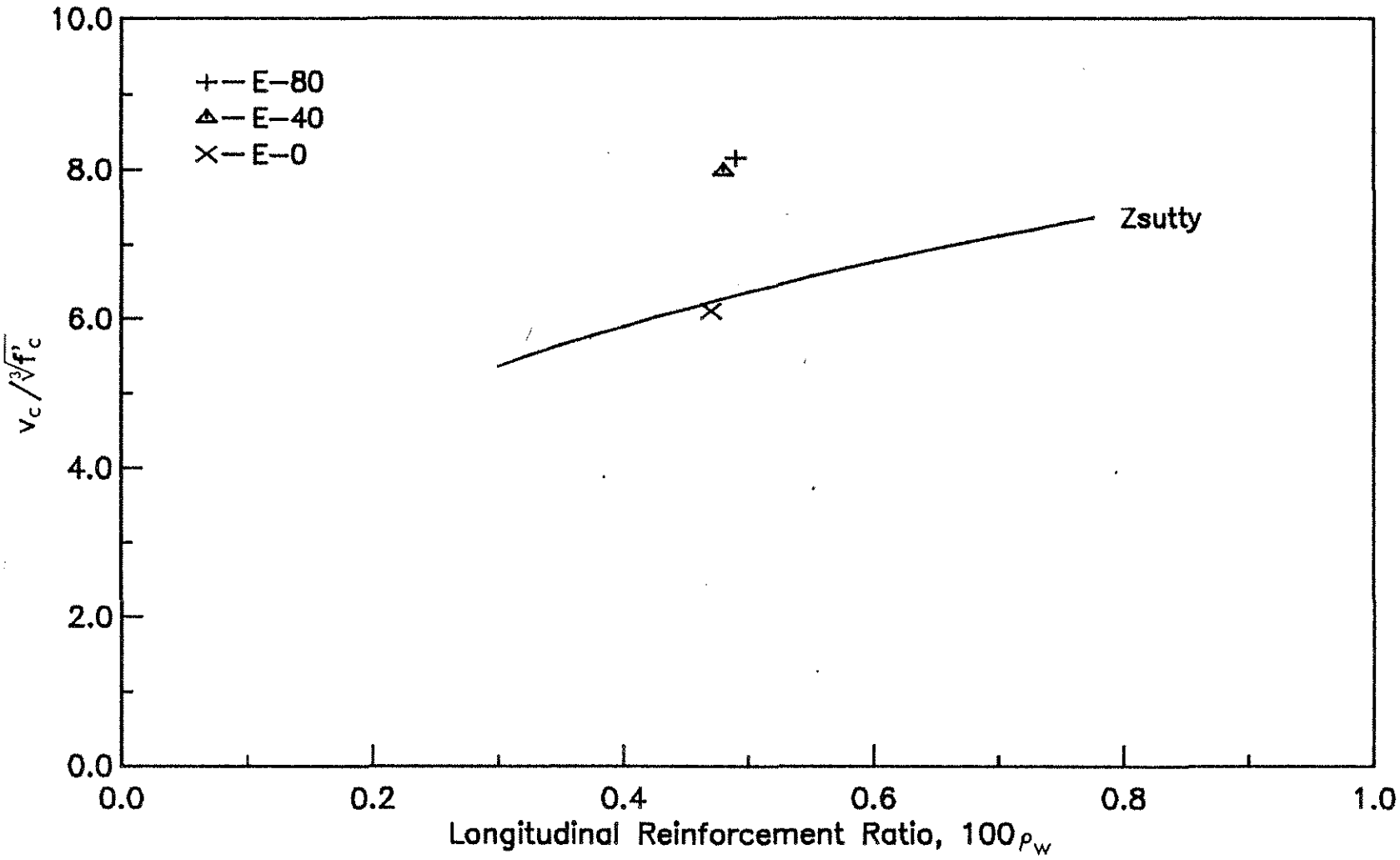

Fig. 3.7 Shear Cracking stress from Depth Increase in the Positive Moment Region

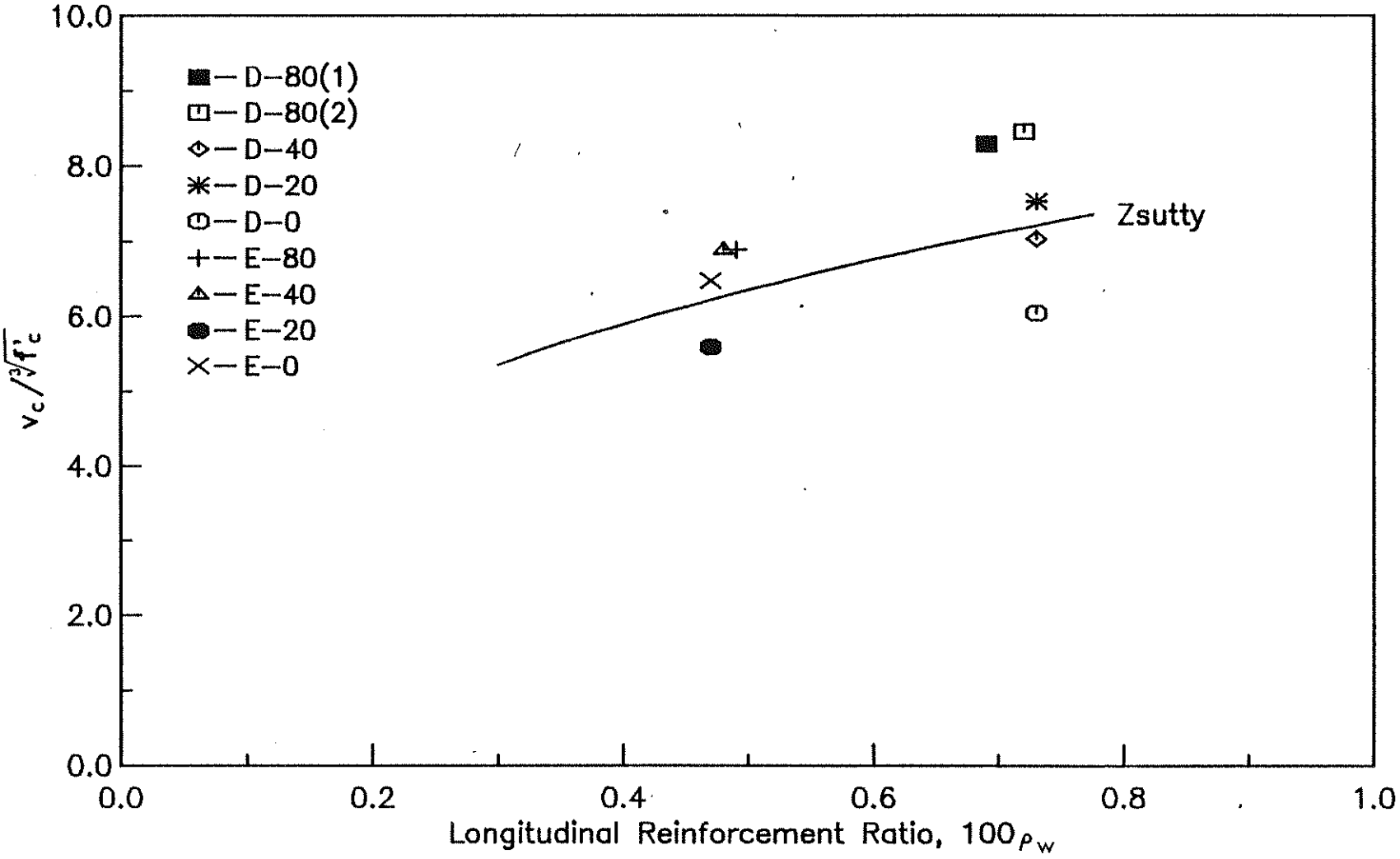

Fig. 38 Shear Cracking Stress from Concrete Strain in the Positive Moment Region

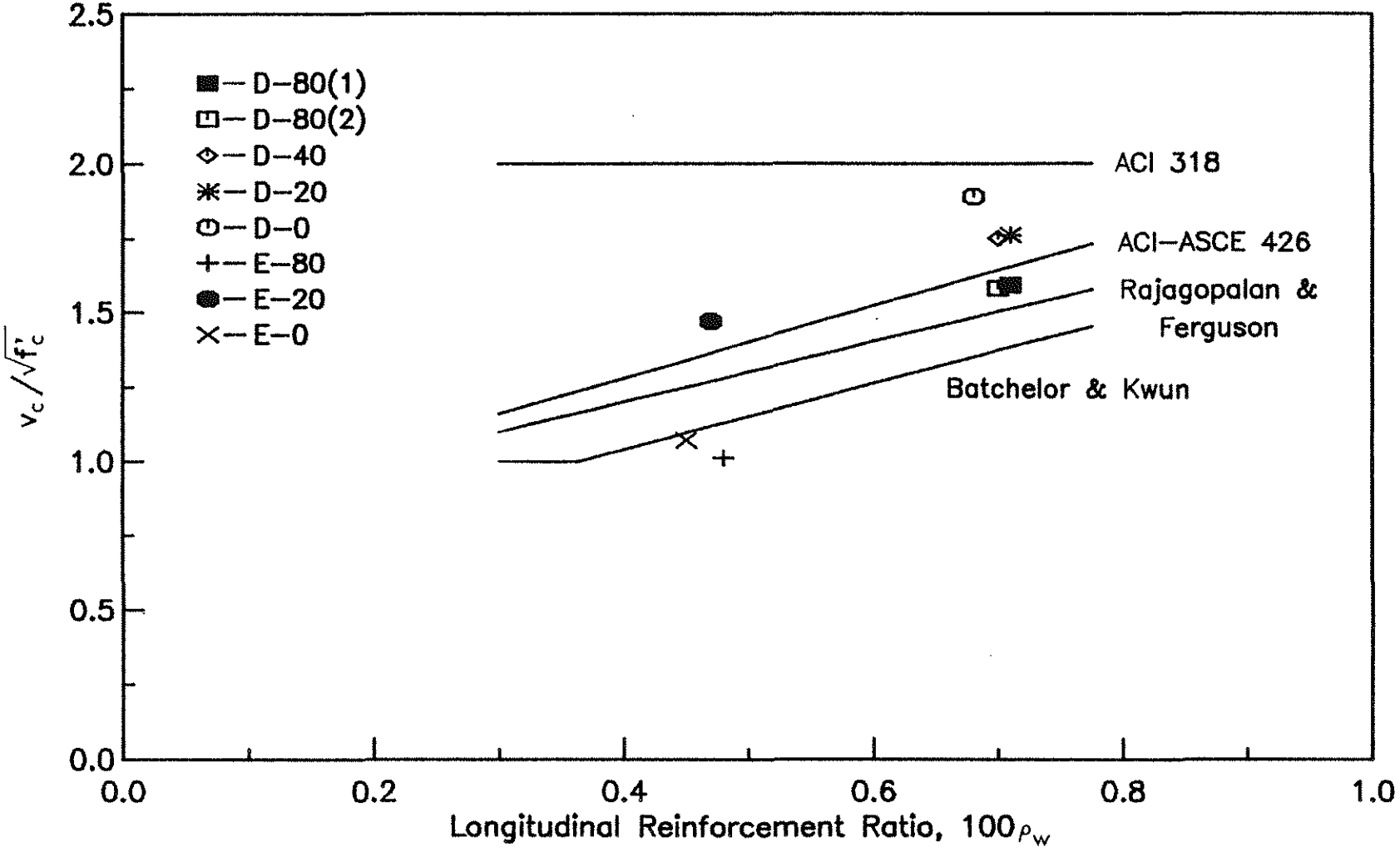

Fig. 3.9 Shear Cracking Stress from Crack Patterns in the Negative Moment Region

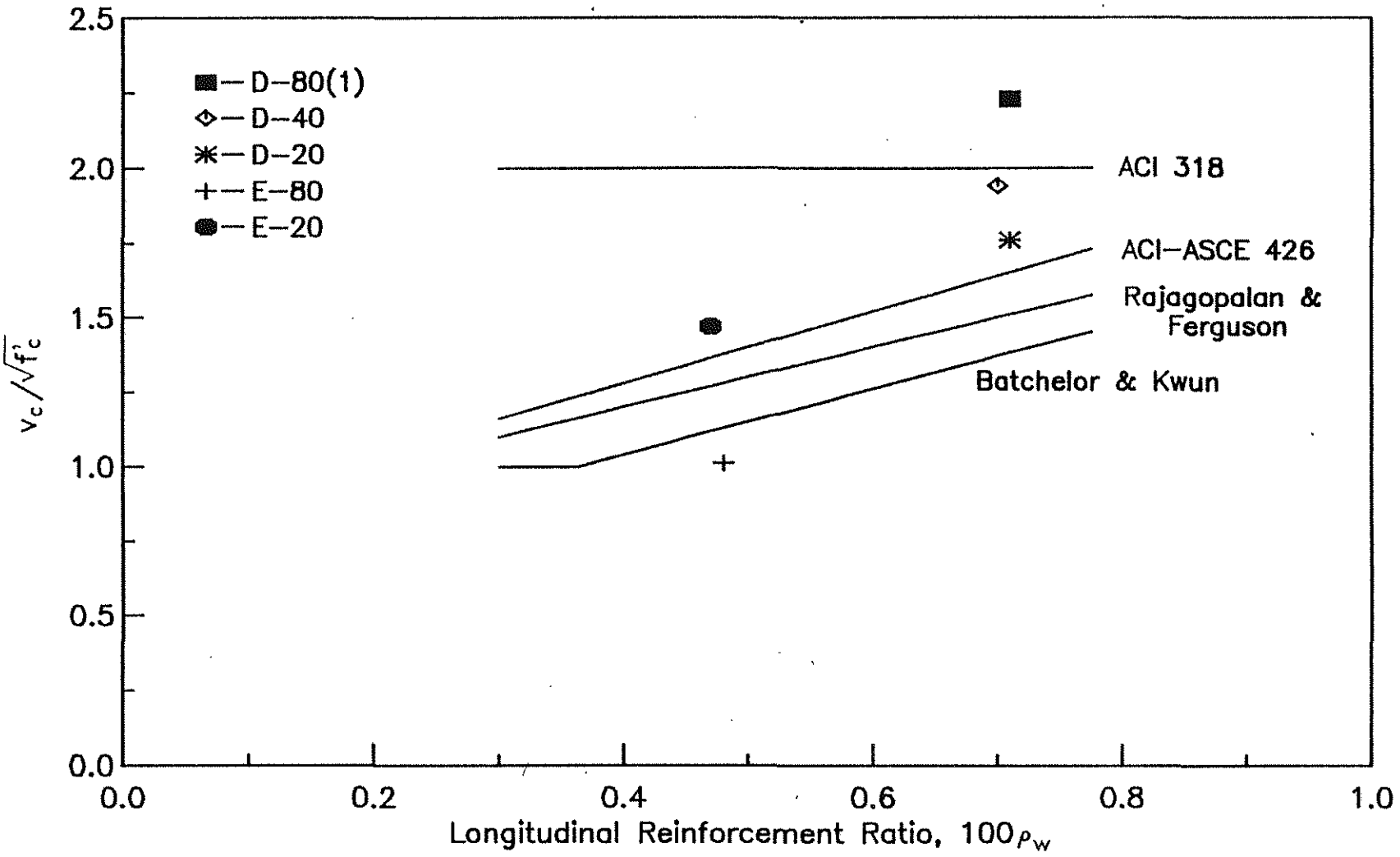

Fig. 3.10 Shear Cracking Stress from Stirrup Strain in the Negative Moment Region

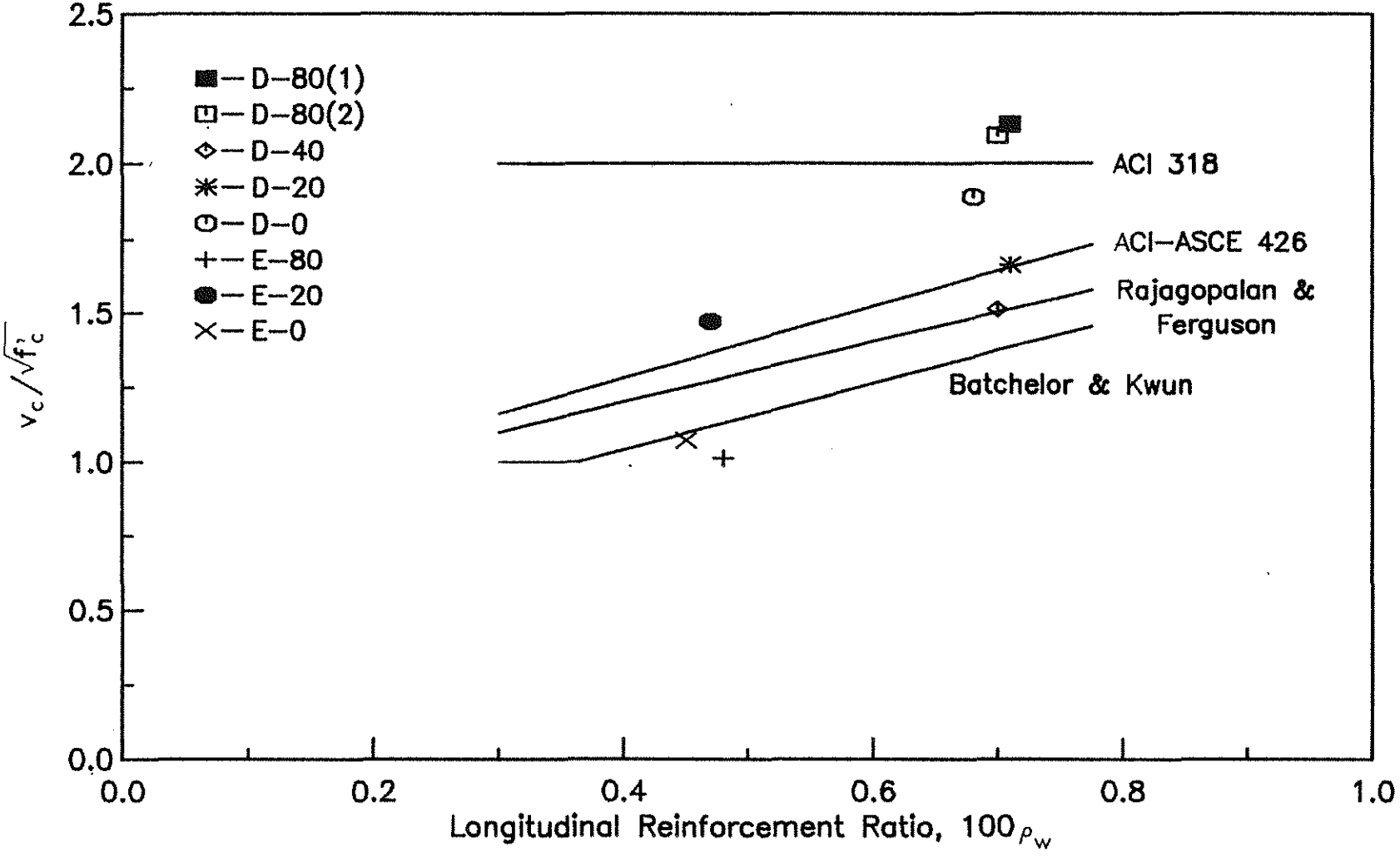

Fig. 3.11 Shear Cracking Stress from Depth Increase in the Negative Moment Region

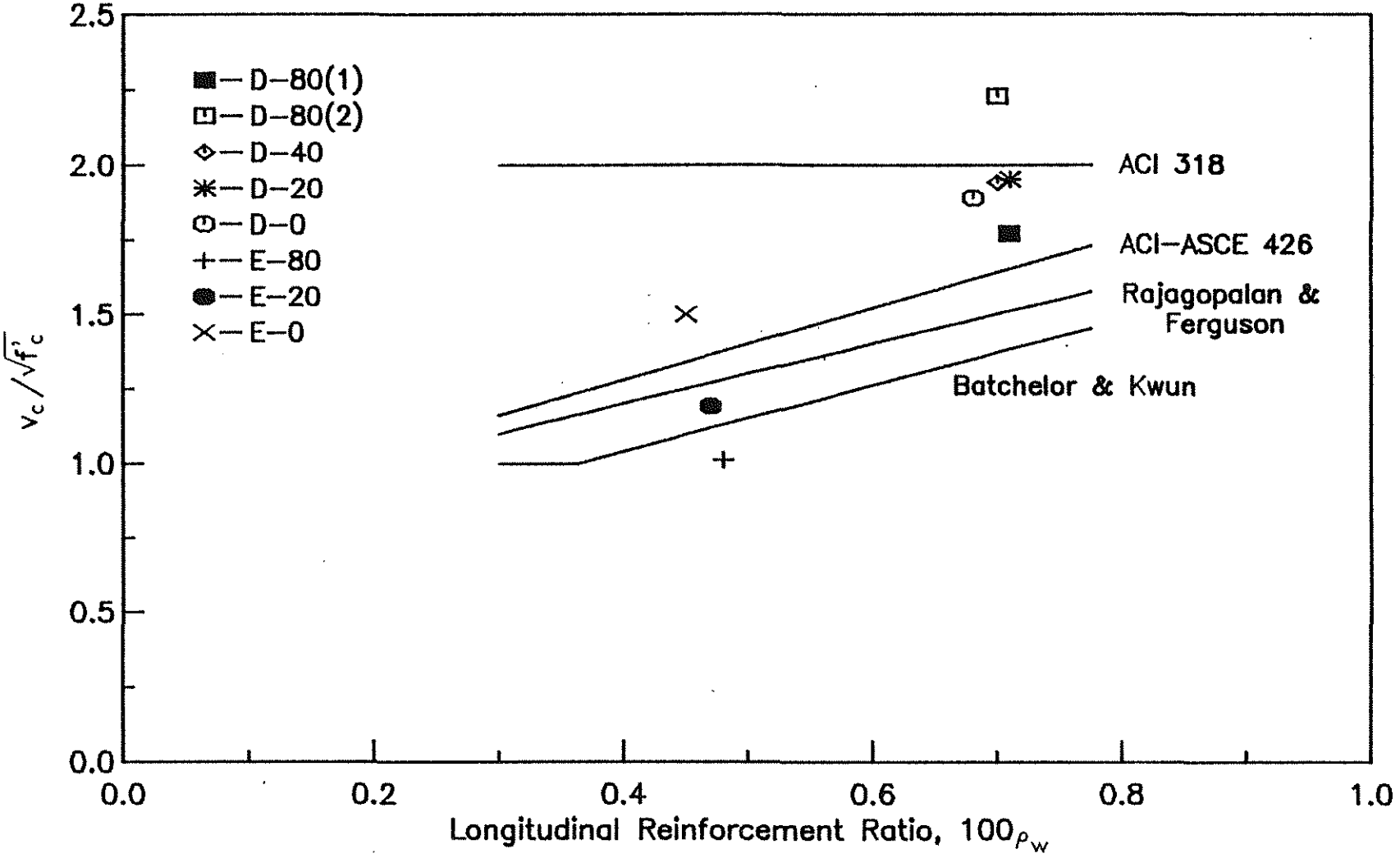

Fig. 3.12 Shear Cracking Stress from Concrete Strain in the Negative Moment Region

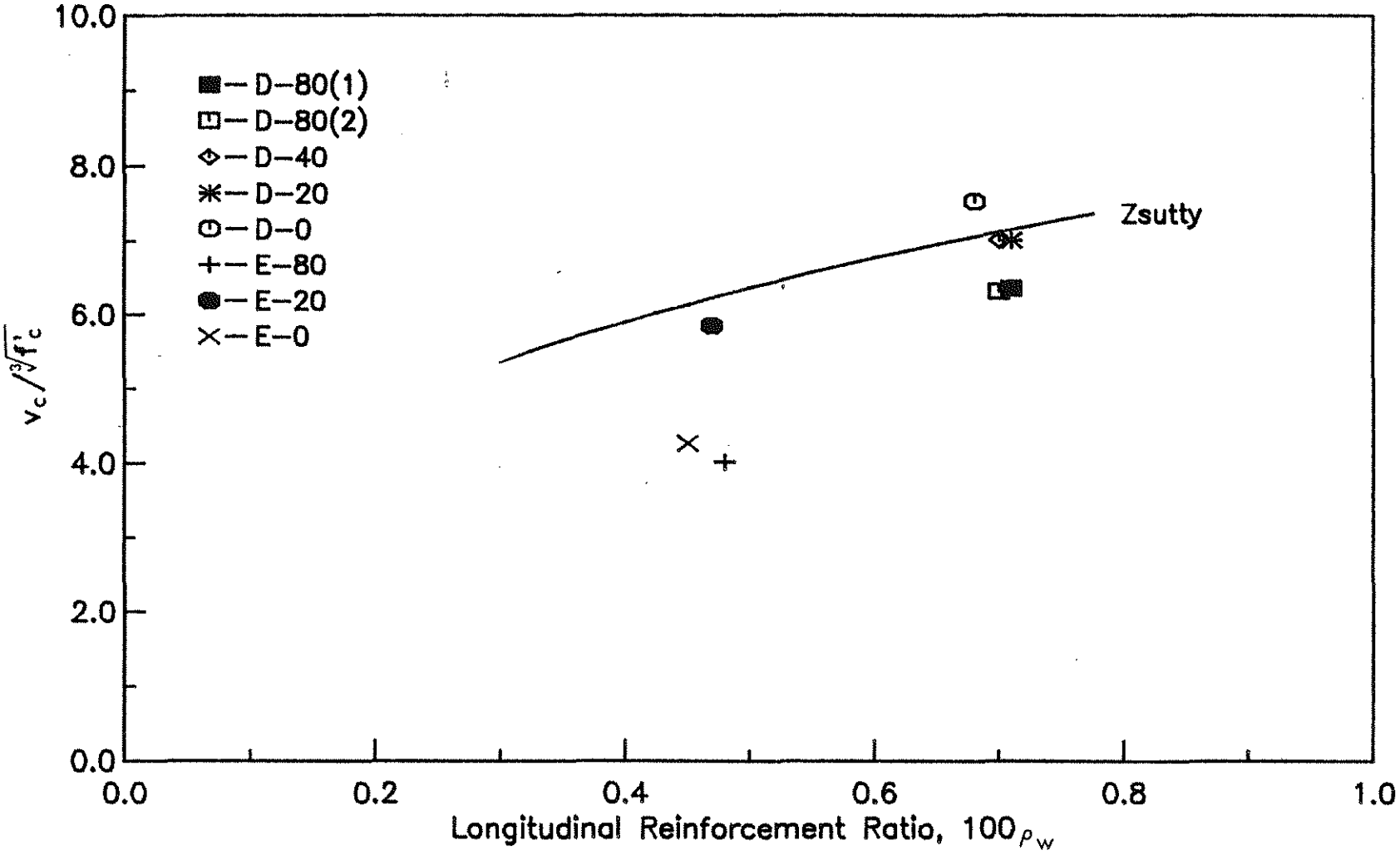

Fig. 3.13 Shear Cracking Stress from Crack Patterns in the Negative Moment Region

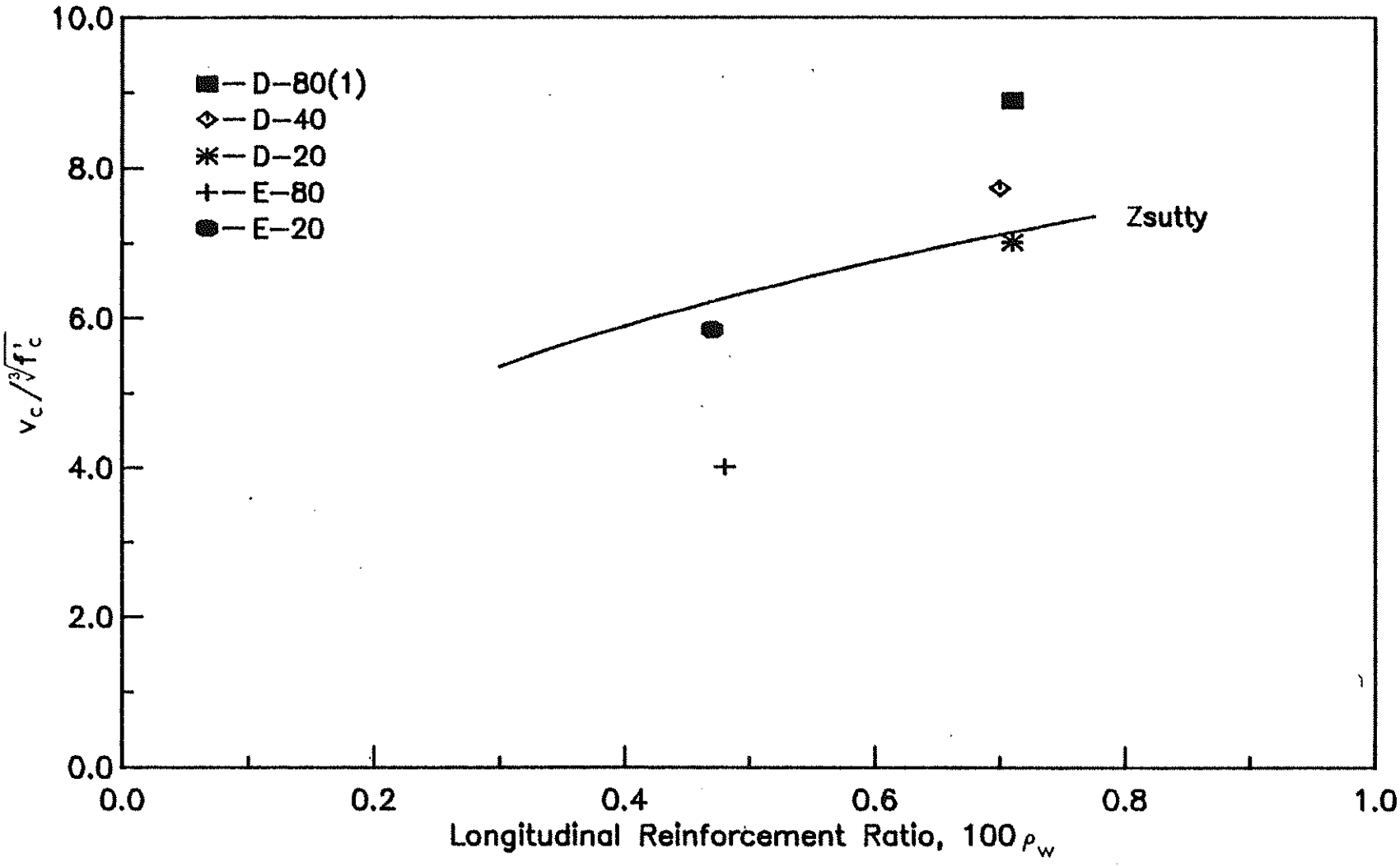

Fig. 3.14 Shear Cracking Stress from Stirrup Strain in the Negative Moment Region

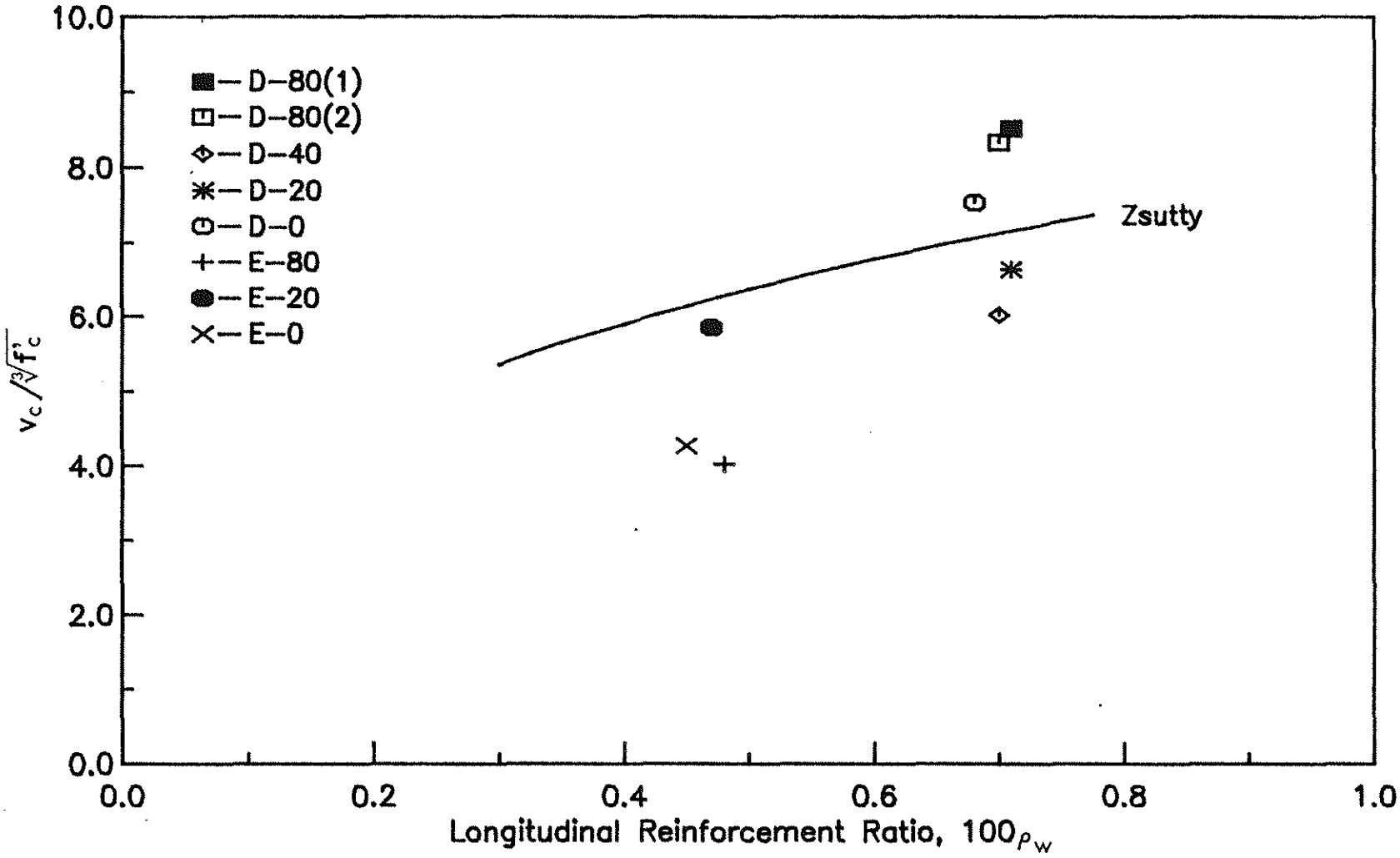

Fig. 3.15 Shear Cracking Stress from Depth Increase in the Negative Moment Region

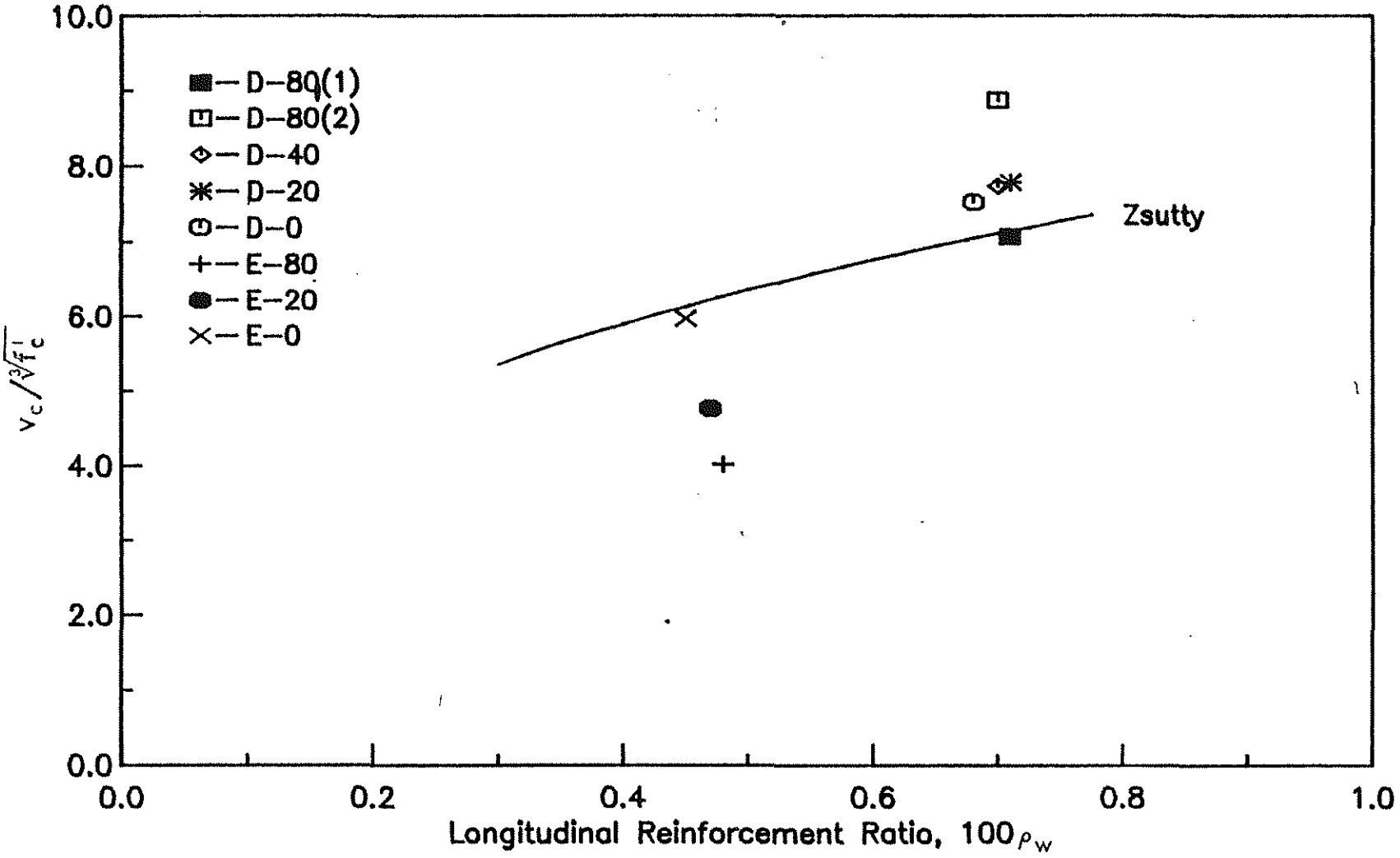

Fig. 3.16 Shear Cracking Stress from Concrete Strain in the Negative Moment Region

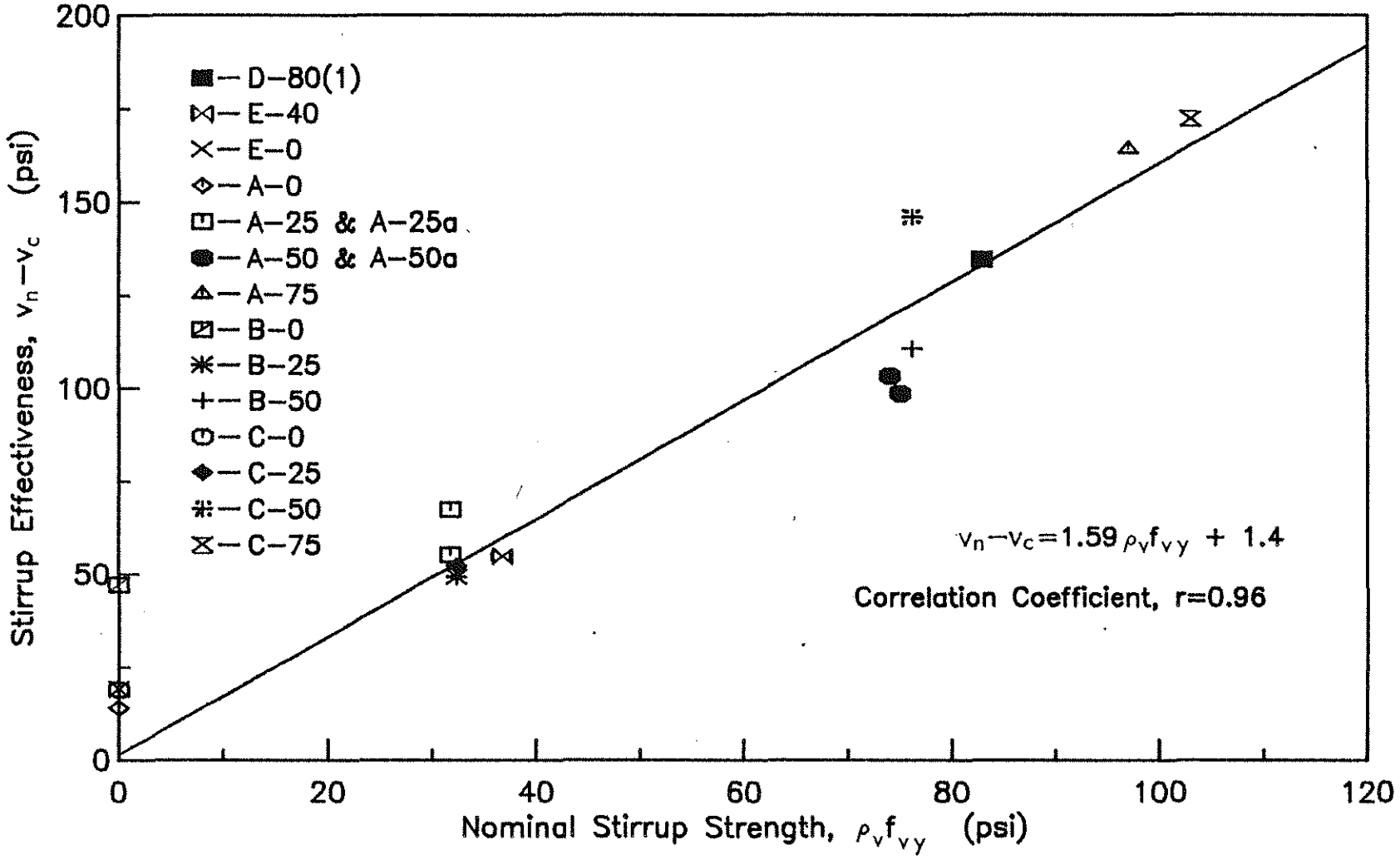

Fig. 3.17 Stirrup Effectiveness in the Positive Moment Region

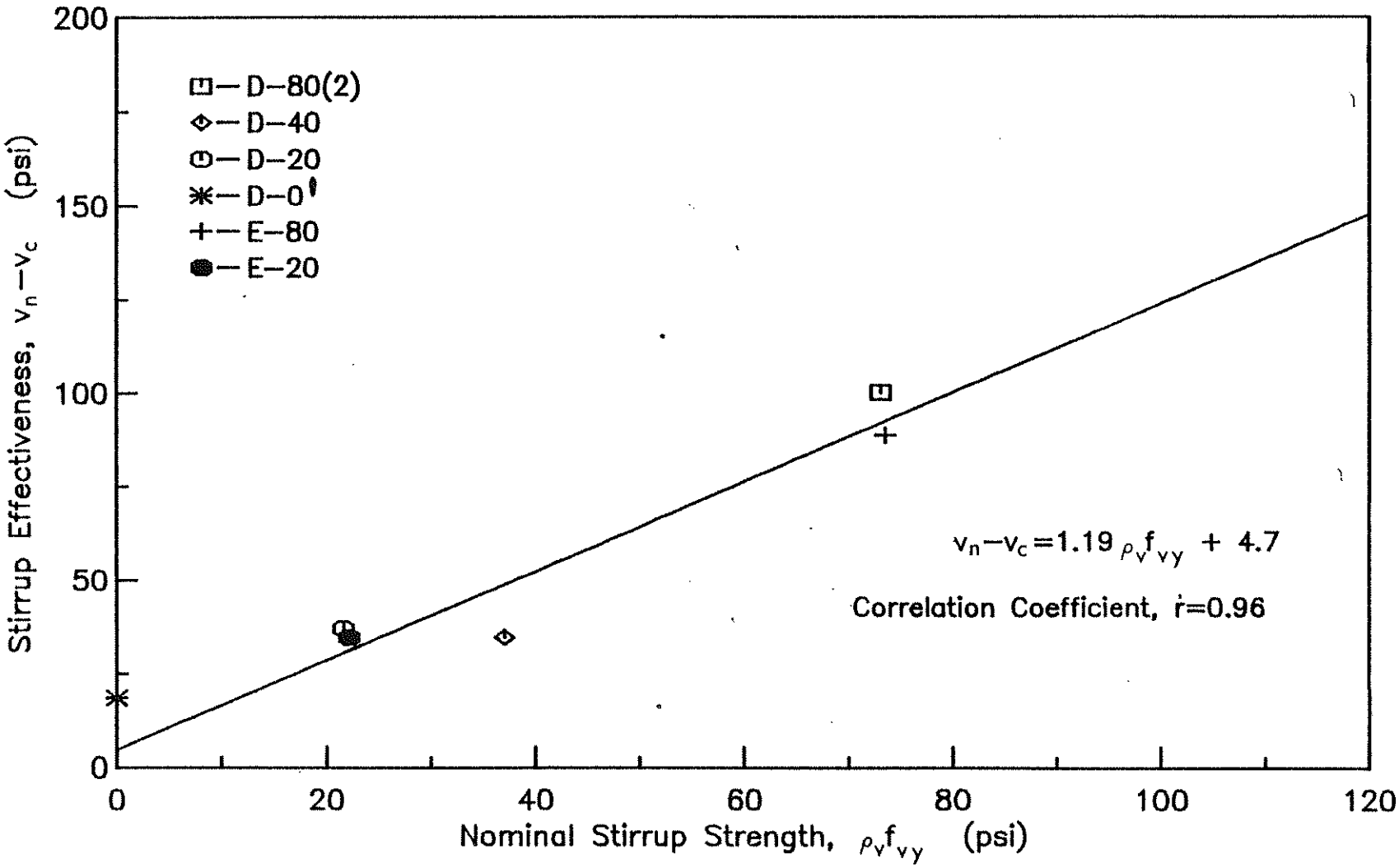

Fig. 3.18 Stirrup Effectiveness in the Negative Moment Region

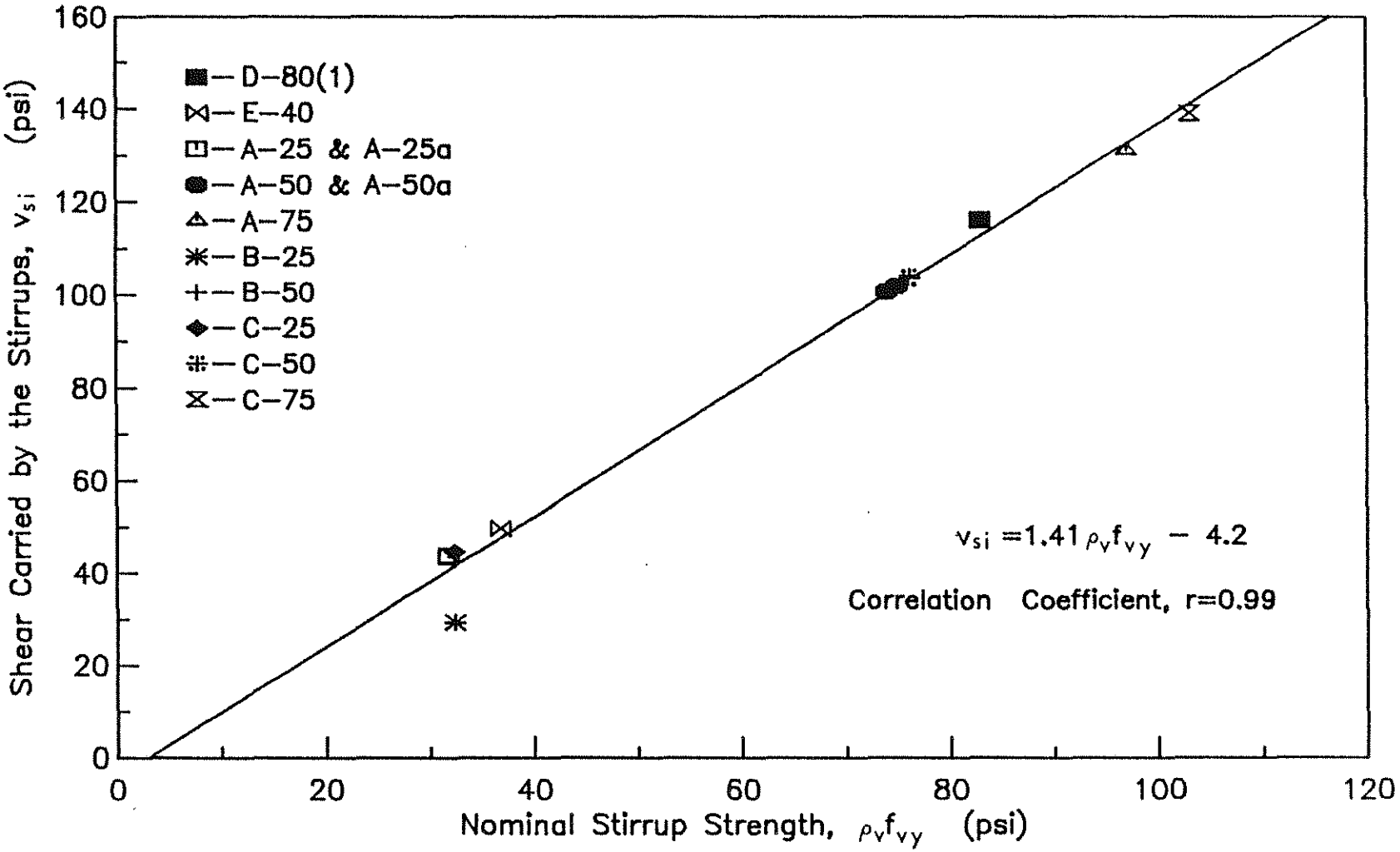

Fig. 3.19 Shear Carried by Stirrups Alone in the Positive Moment Region

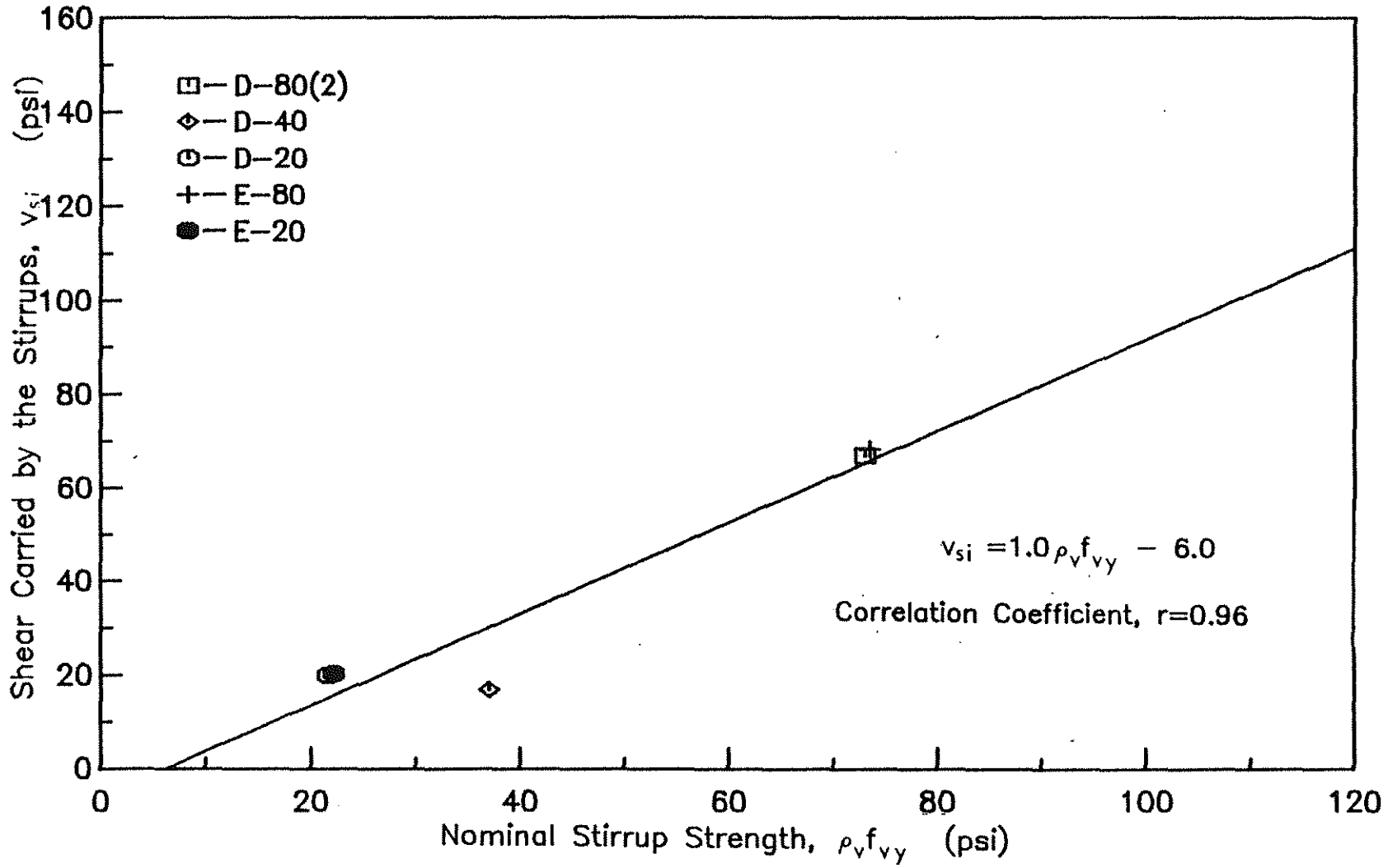

Fig. 3.20 Shear Carried by Stirrups Alone in the Negative Moment Region

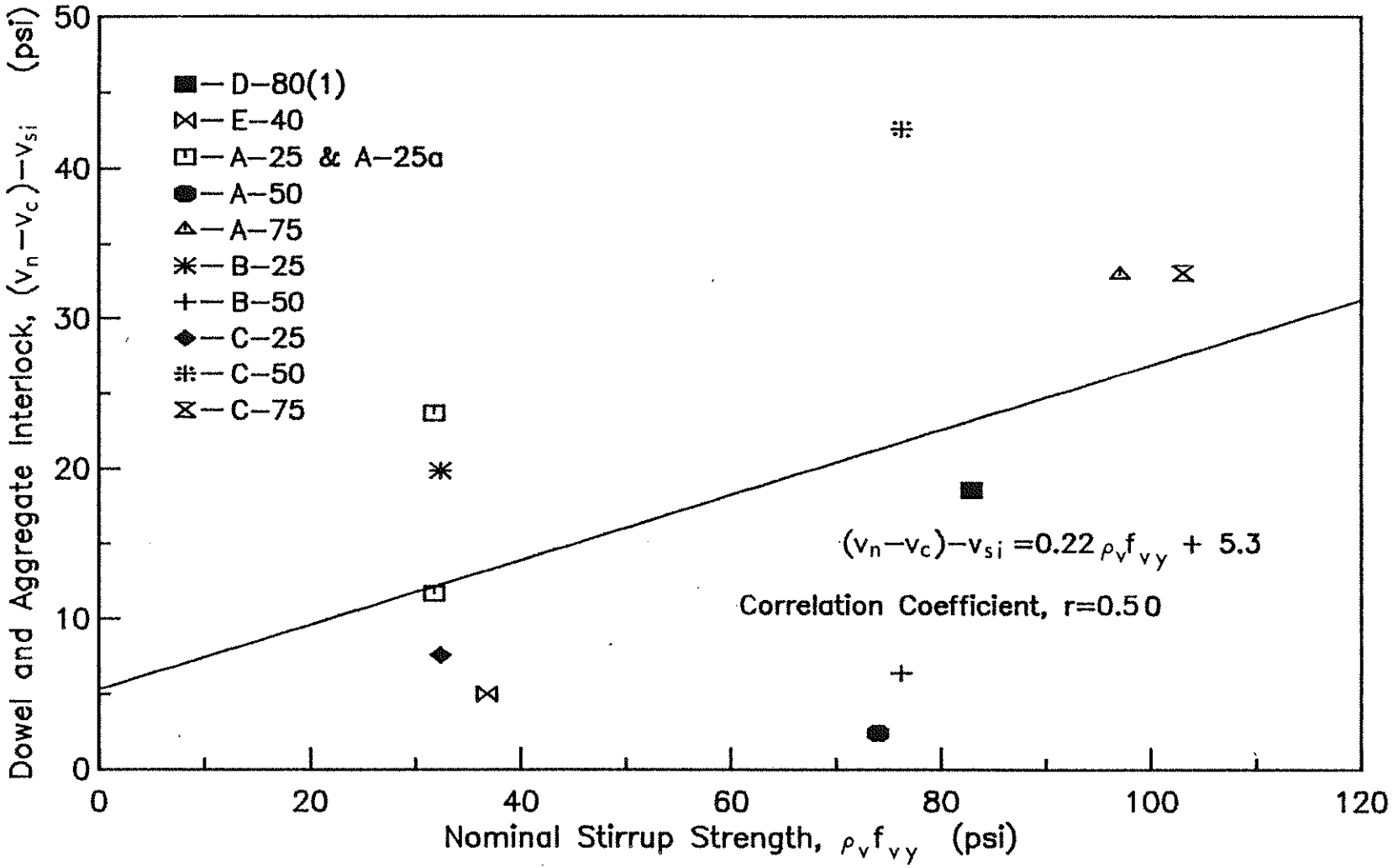

Fig. 3.21 Dowel Action and Aggregate Interlock in the Positive Moment Region

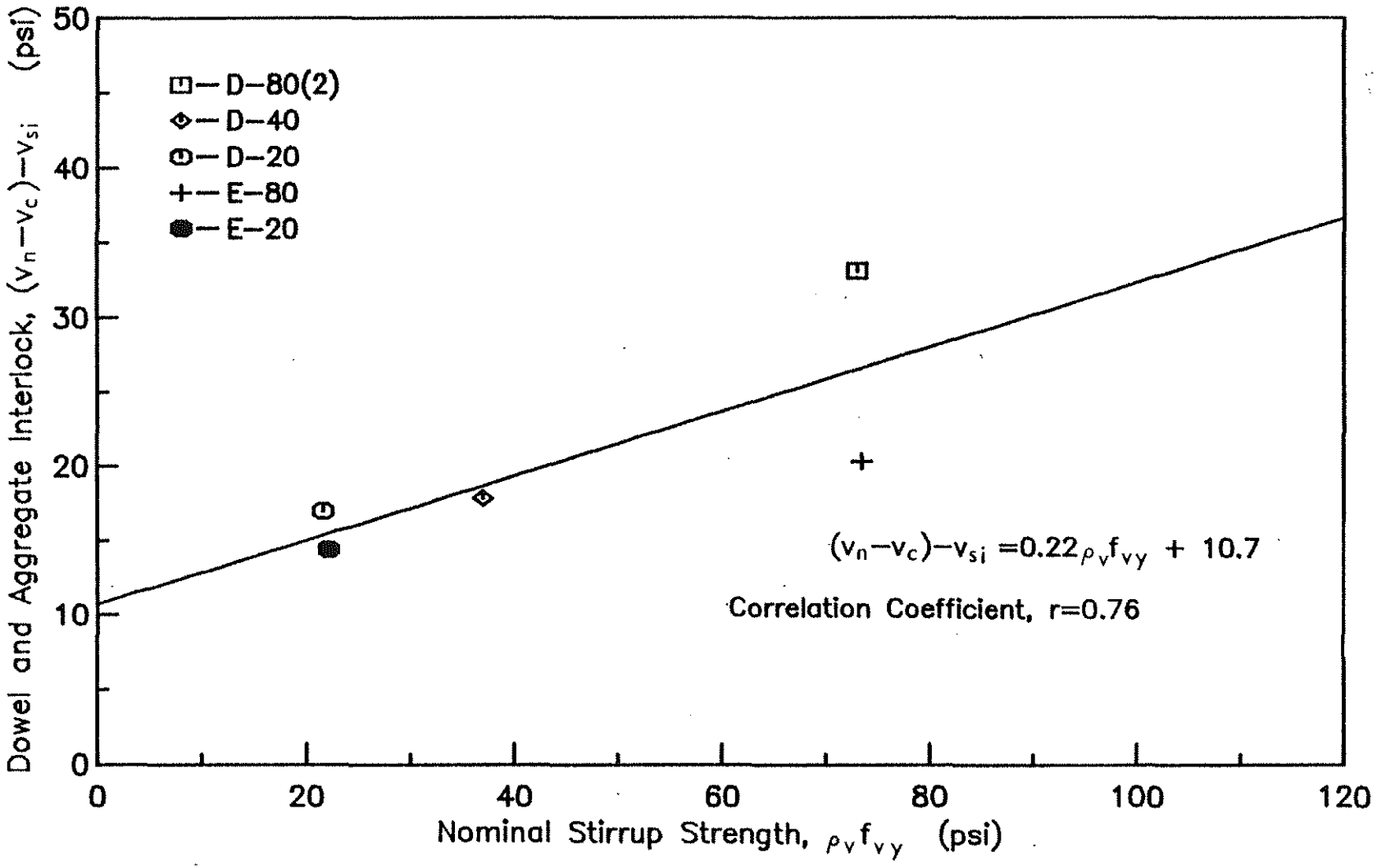

Fig. 3.22 Dowel Action and Aggregate Interlock in the Negative Moment Region

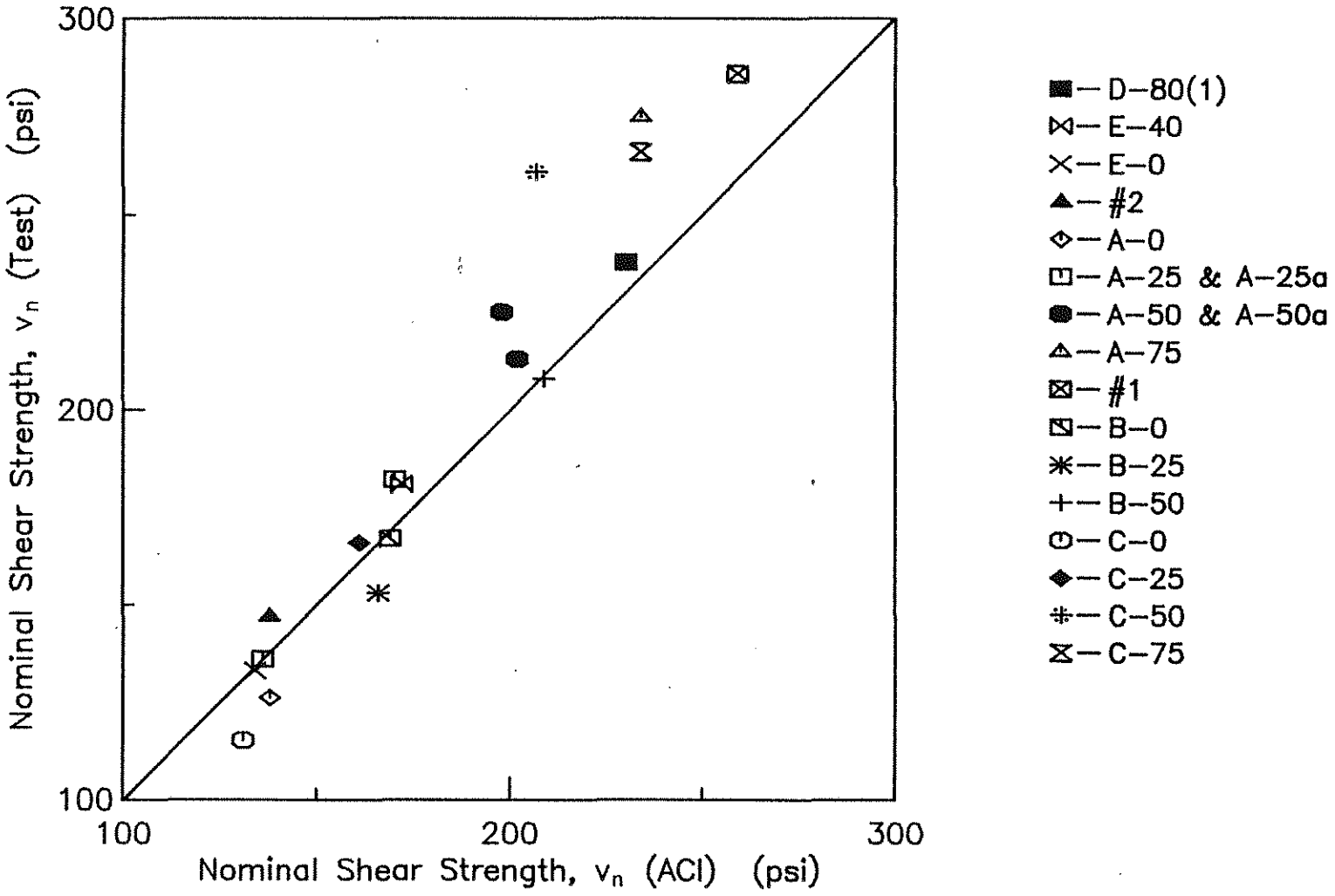

Fig. 3.23a Nominal Shear Strength in the Positive Moment Region, Test versus ACI

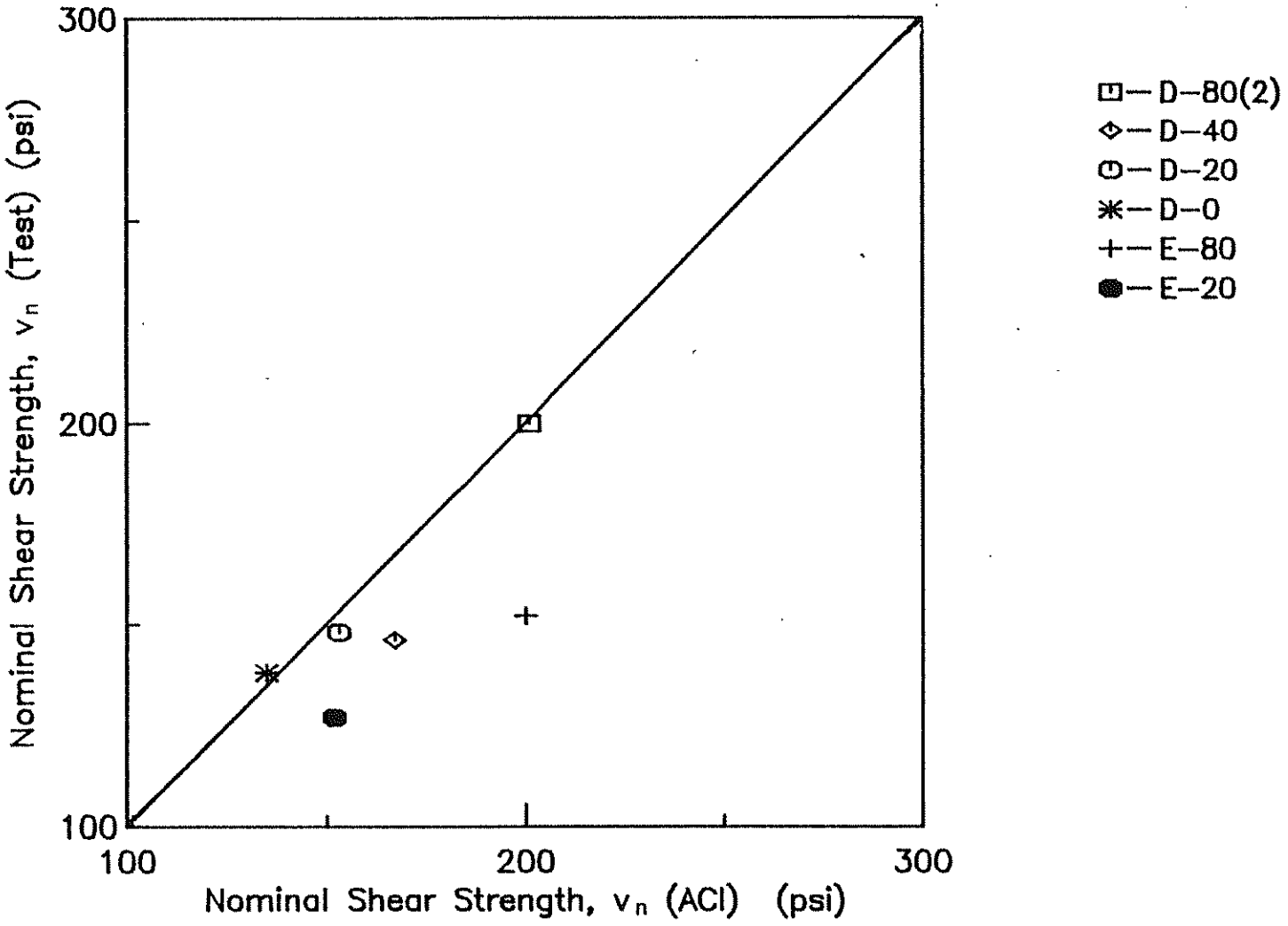

Fig. 3.23b Nominal Shear Strength in the Negative Moment Region, Test versus ACI

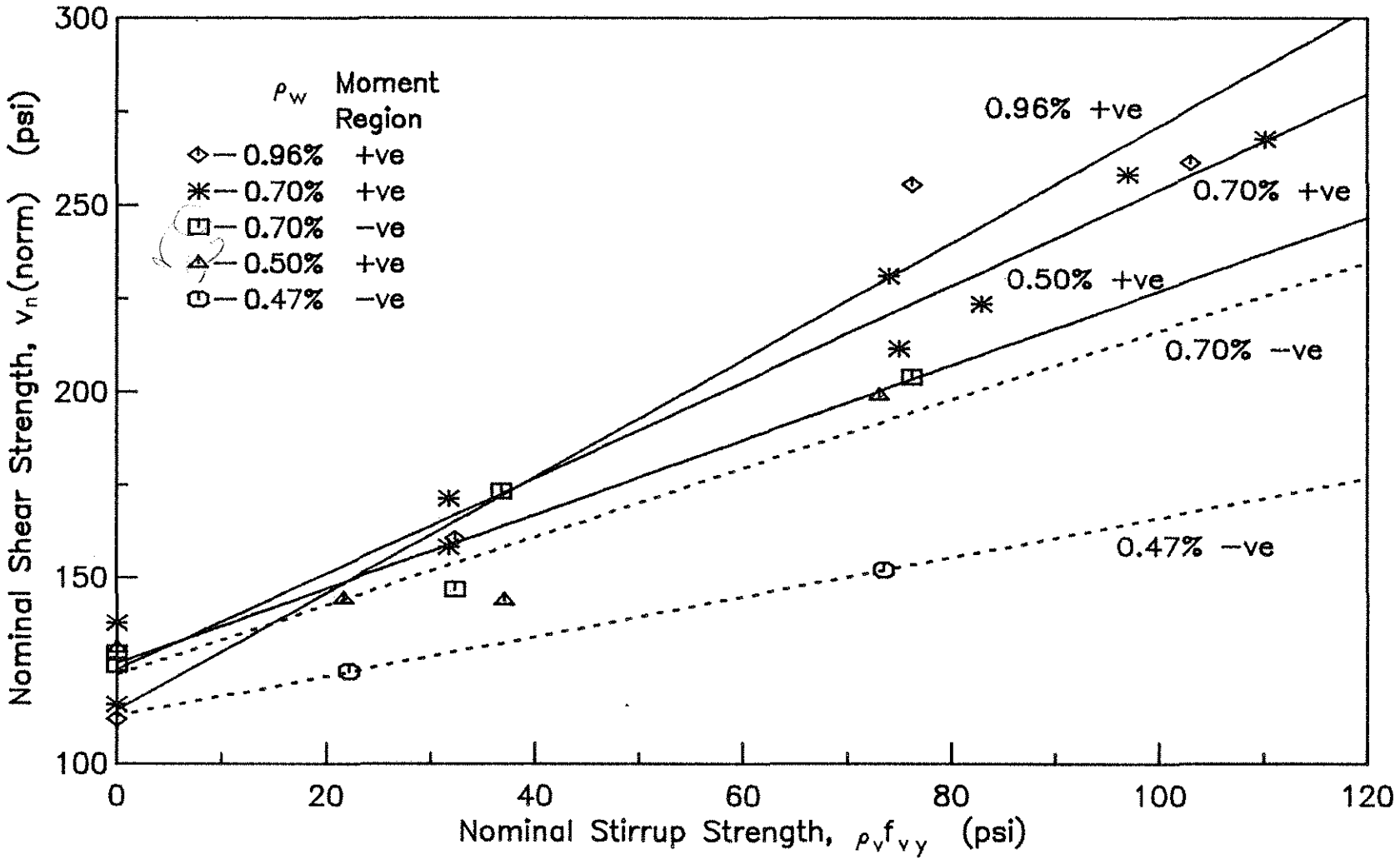

Fig. 3.24 Nominal Shear Strength versus Nominal Stirrup Strength for Beams with Low Reinforcing Ratios (5,20,21)

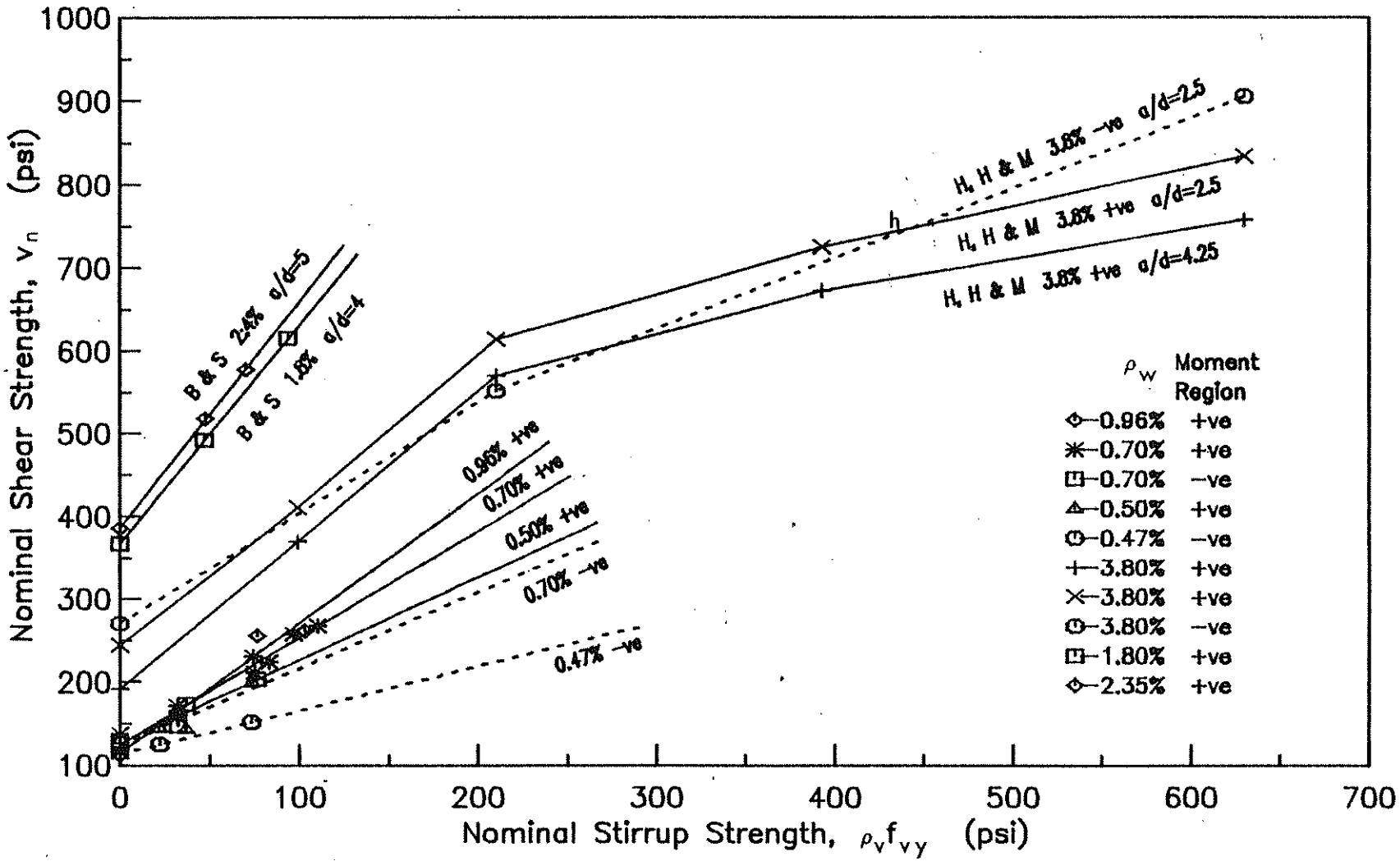

Fig. 3.25 Nominal Shear Strength versus Nominal Stirrup Strength for Beams with Low and High Reinforcing Ratios (5,9,11,20,21)

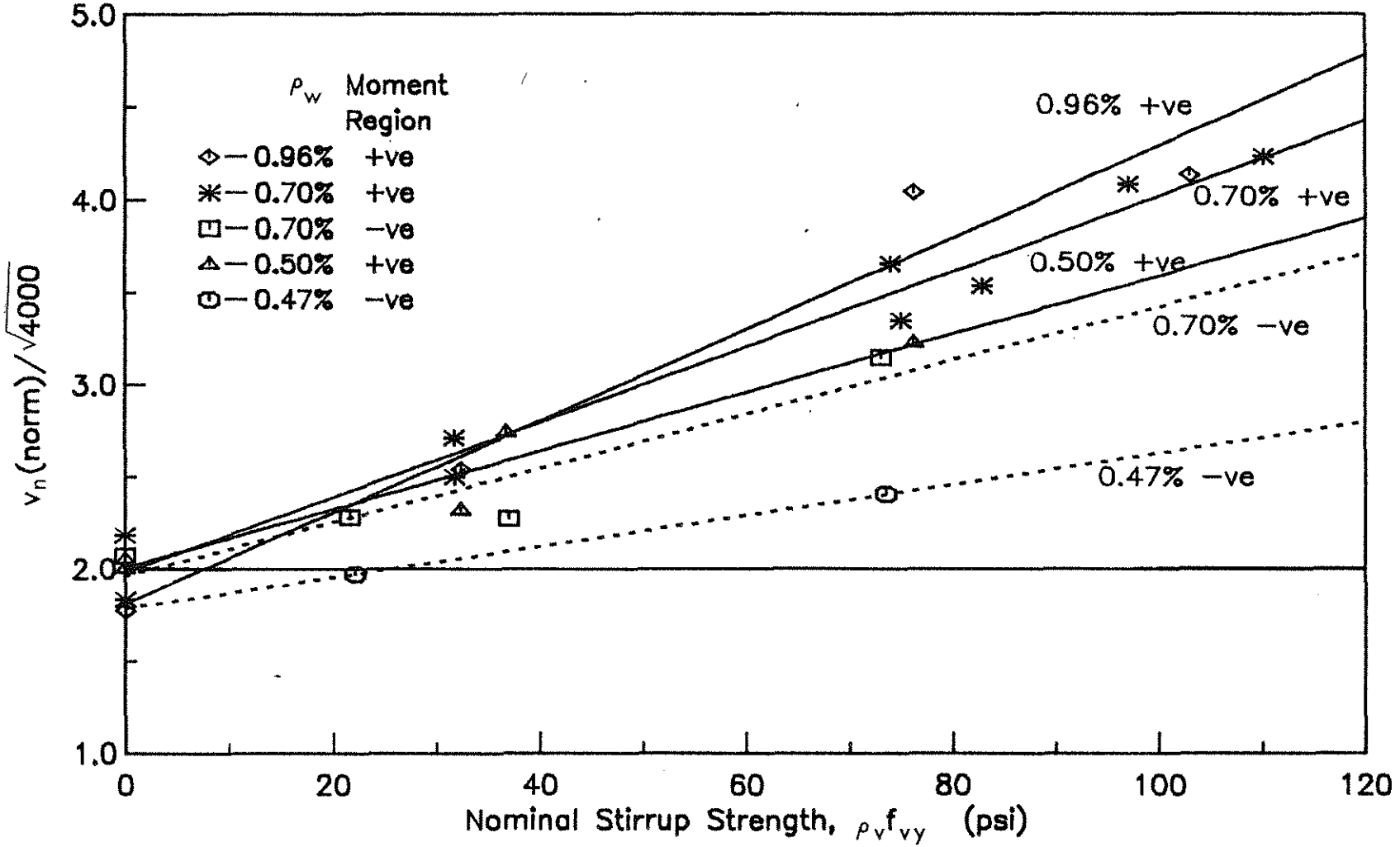

Fig. 3.26 Normalized Nominal Shear Strength versus Nominal Stirrup Strength, Best Fit Lines

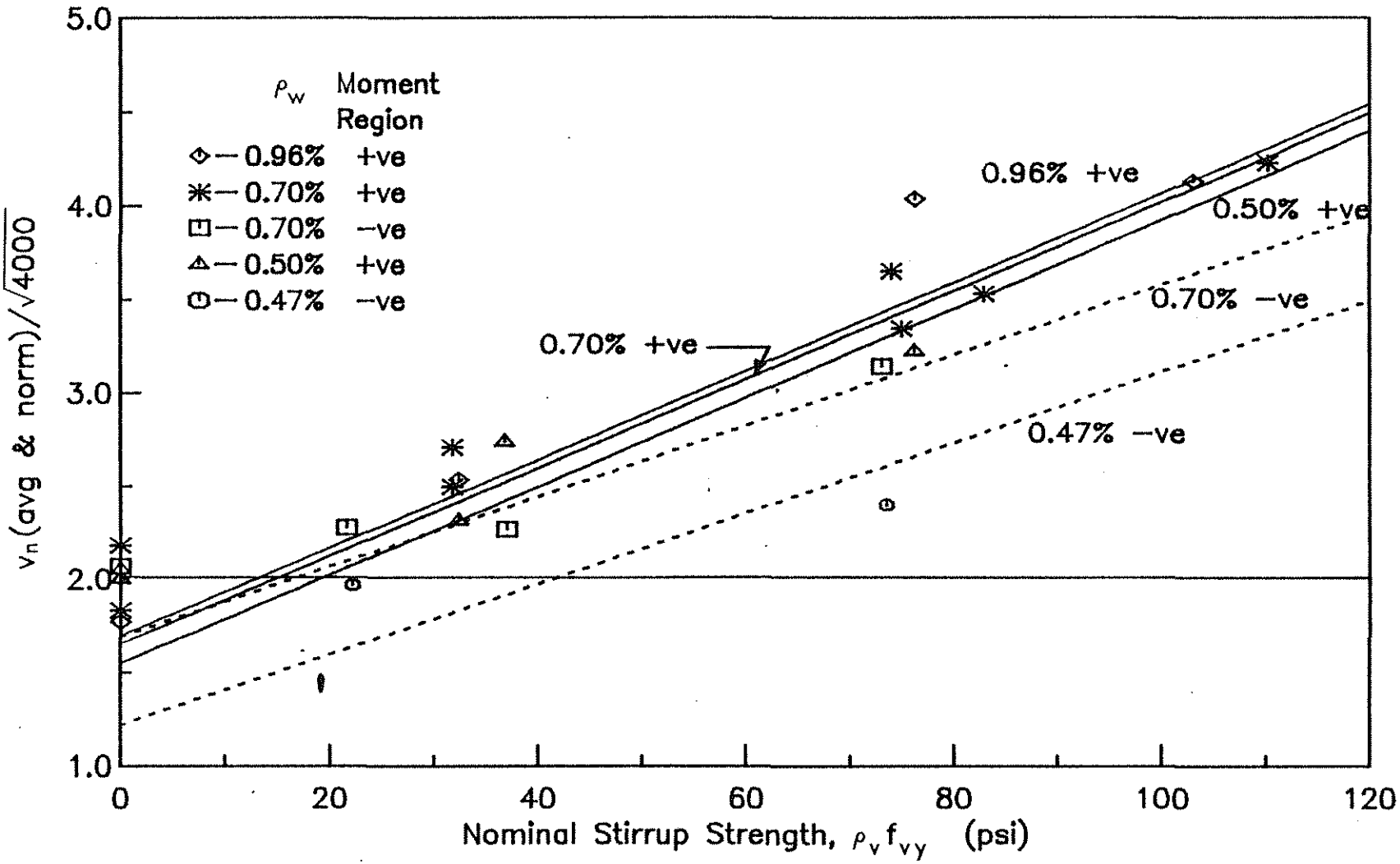

Fig. 3.27 Normalized Nominal Shear Strength versus Nominal Stirrup Strength, Average Stirrup Effectiveness

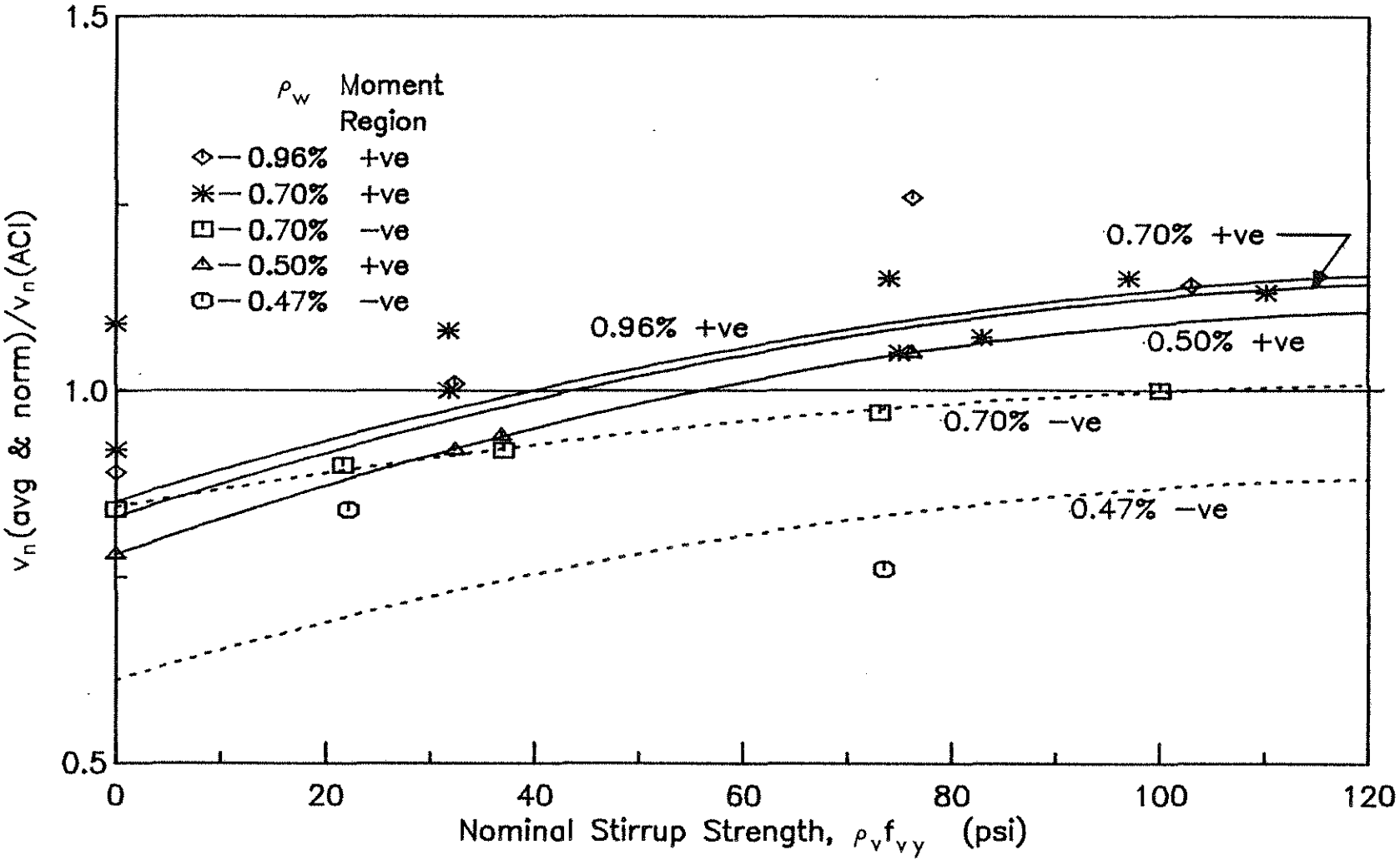

Fig. 3.28 Comparison of ACI Shear Strength Provisions (4) with Normalized Nominal Shear Strength based on Average Stirrup Effectiveness

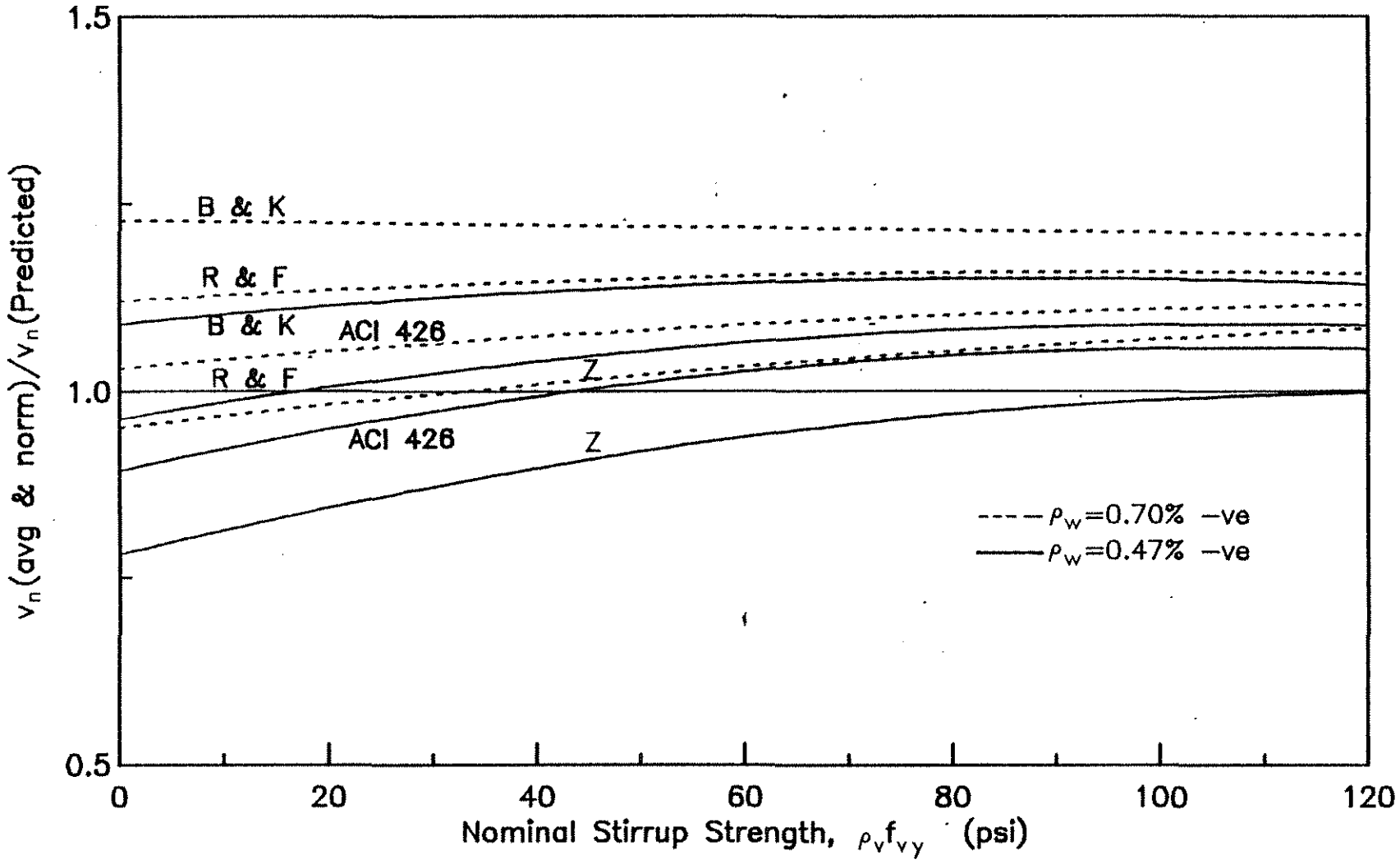

Fig. 3.29 Comparison of Shear Strength Expressions of Other Investigators (3,6,23,26) with Normalized Nominal Shear Strength based on Average Stirrup Effectiveness

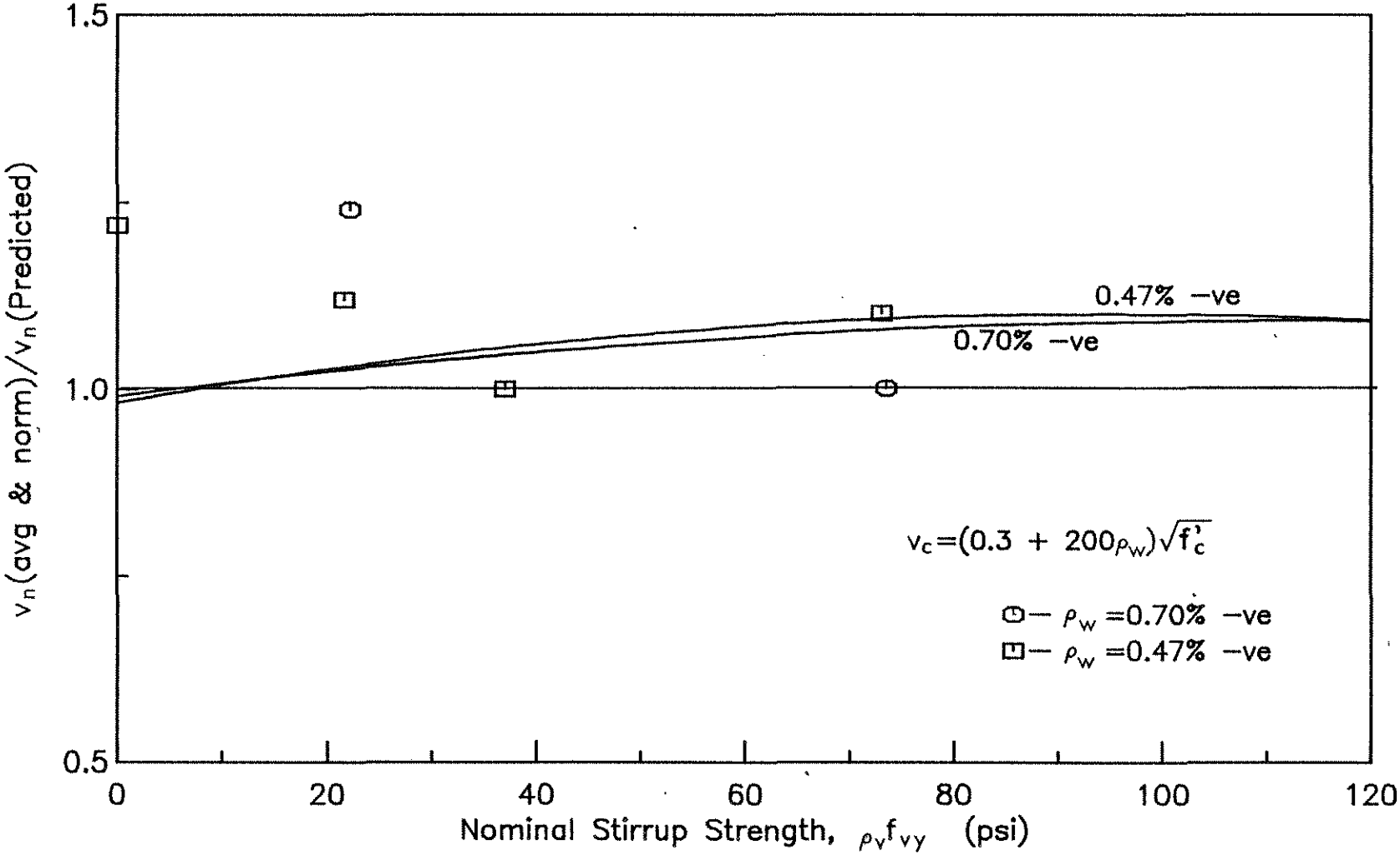

Fig. 3.30 Comparison of Proposed Shear Strength Expression with Normalized Nominal Shear Strength based on Average Stirrup Effectiveness

APPENDIX A

NOTATION

a = shear-span (distance from maximum moment section to zero moment section)

A_s = area of flexural reinforcement

A_v = area of web reinforcement

b_w = web width of T-beam

d = distance from extreme compression fiber to centroid of flexural reinforcement

f'_c = compressive strength of concrete measured on 6 x 12 in. cylinders

f_t = modulus of rupture from 6 x 6 x 22 in. flexural specimens, third point loading on an 18 in. span

f_{vy} = yield stress of web reinforcement

M_u = factored bending moment at section

r = coefficient of variation

s = spacing of stirrups measured in a direction parallel to the longitudinal reinforcement

v_b = basic shear stress (shear stress carried by concrete)

v_c = nominal shear stress carried by concrete (shear stress at diagonal tension cracking = $V_c/b_w d$)

v_n = nominal shear strength = $V_n/b_w d$

v_s = nominal stirrup strength

v_{si} = shear stress carried by stirrups alone

v_u = factored shear stress at section = $V_u/b_w d$

V_c = nominal shear force carried by concrete (shear force at diagonal tension cracking)

V_n = nominal shear strength (Ultimate strength)

V_u = factored shear force at section

NOTATION (continued)

ρ_v = ratio of web reinforcement = $A_v/b_w s$

ρ_w = ratio of flexural reinforcement = $A_s/b_w d$

ϕ = strength reduction factor